NASA Contractor Report 189593

[redacted]

P-121

DEVELOPMENT OF THERMOPLASTIC COMPOSITE AIRCRAFT STRUCTURES

Michael P. Renieri, Steven J. Burpo,
Lance M. Roundy, Stephanie A. Todd,
and H.J. Kim

McDonnell Aircraft Company
St. Louis, Missouri 63166

Contract NAS1 - 18862
March 1992

National Aeronautics and Space Administration

Langley Research Center
Hampton, Virginia 23665-5225

NASA Contractor Report 189593

DEVELOPMENT OF THERMOPLASTIC COMPOSITE AIRCRAFT STRUCTURES

Michael P. Renieri, Steven J. Burpo,
Lance M. Roundy, Stephanie A. Todd,
and H.J. Kim

McDonnell Aircraft Company
St. Louis, Missouri 63166

Contract NAS1 - 18862
March 1992

National Aeronautics and
Space Administration

Langley Research Center
Hampton, Virginia 23665-5225

FOREWORD

The work presented in this report was performed by McDonnell Aircraft Company, St. Louis, Missouri, under Contract NAS1-18862, for the National Aeronautics and Space Administration, Langley Research Center, Hampton, Virginia. Mr. Marvin B. Dow served as Technical Monitor.

Dr. Michael P. Renieri and Steven J. Burpo served as McDonnell Aircraft Company Program Manager and Deputy Program Manager, respectively. Other key contributions to the program were:

Structural Research	Lance Roundy (Lead)
	H. J. Kim
	Skip Ellsworth
Material & Processing	Stephanie Todd (Lead)
	Kelli Corona
Advanced Manufacturing	Glen Redding
	Dave Furdek
Structural Design	Ron Hunt
Tooling	Neal Froeschner
	Jeff Wood
	Russ Krajec
Producibility	Peter Hoffman
	Jay Weatherford
Quality Assurance	Aaron Henson
Product Support	Dave Breihan
Structural Testing	Bruce McIlroy
	Paul McClellan
Planning & Administration	Steve Dominic
Contracts & Pricing	Rick Larsen
Contracts Services	Vicki Stuller

APPENDICES

TABLE OF CONTENTS

1. INTRODUCTION

A major obstacle to widespread use of high performance composites in primary aircraft structures is the high cost of manufacture and assembly. Under NASA's ACT program, McDonnell Aircraft Company investigated cost-effective innovative techniques for the fabrication and joining of primary airframe structure using thermoplastic composite materials. MCAIR is teamed with Douglas Aircraft Company (DAC) under the ACT initiative in a program entitled Innovative Composite Aircraft Primary Structures (ICAPS).

The progression of planned activities in this program followed a classic building block approach: material evaluation, mechanics development, structural element verification, and subcomponent validation. Due to NASA program redirection, efforts were curtailed at the element level. To maintain program continuity, this report summarizes progress through element verification and identifies the subcomponent efforts.

Primary effort on the MCAIR portion of the ICAPS program concentrated on thermoplastic composite developments relative to an advanced fighter fuselage section. While these developments were directed toward an Advanced Short Take-off or Vertical Landing (ASTOVL) aircraft, they are equally applicable to commercial vehicle structure. Efforts in these programs were conducted in design and structural mechanics development, manufacturing concepts development, and structural testing.

In the structural mechanics area attention was focused in two areas. First, the utility of a dissipated strain energy (DSE) technique as an analytical tool was investigated. The DSE formulation is currently under development at the Naval Research Laboratory (NRL) as part of their structural simulator efforts. Secondly, an analytical code to assess the performance of thick composite lugs was developed and verified.

In the manufacturing concepts development area two innovative processes were explored; fiber placement and single diaphragm/coconsolidation (SDCC). Application of these processes to a fuselage upper cover indicated, through a producibility analysis, potential cost savings relative to conventional approaches.

Planned panel manufacturing approach and design concepts, were evaluated through element fabrication. The elements addressed key design issues associated with the fuselage section; fastenerless frame attachment concepts, thick composite lugs, and rolled-formed stiffeners.

Structural verification testing was performed on the element specimens. Pull-off strength tests at ambient and elevated-temperature-wet conditions were conducted on fastenerless frame concepts. To assess the analytical development, thick lug tests were performed under ambient condition for two lug geometries and three laminate configurations.

THIS PAGE INTENTIONALLY LEFT BLANK

2. DESIGN AND STRUCTURAL MECHANICS DEVELOPMENT

2.1 Advanced Fighter Fuselage

The advanced aircraft system selected for the fighter development effort was the Model 4629 ASTOVL design developed by MCAIR under the NASA-Ames sponsored U.S./U.K. ASTOVL Technology Development program. Based on representative fuselage cross-sections of the Model 4629 aircraft, Figure 2.1-1, a generic center fuselage structure was developed as the primary structure demonstration component. While the fuselage structure contains design features particular to advanced ASTOVL aircraft, cost-effective fabrication techniques and innovative design concepts developed in this program demonstrated technology related to all emerging aircraft systems.

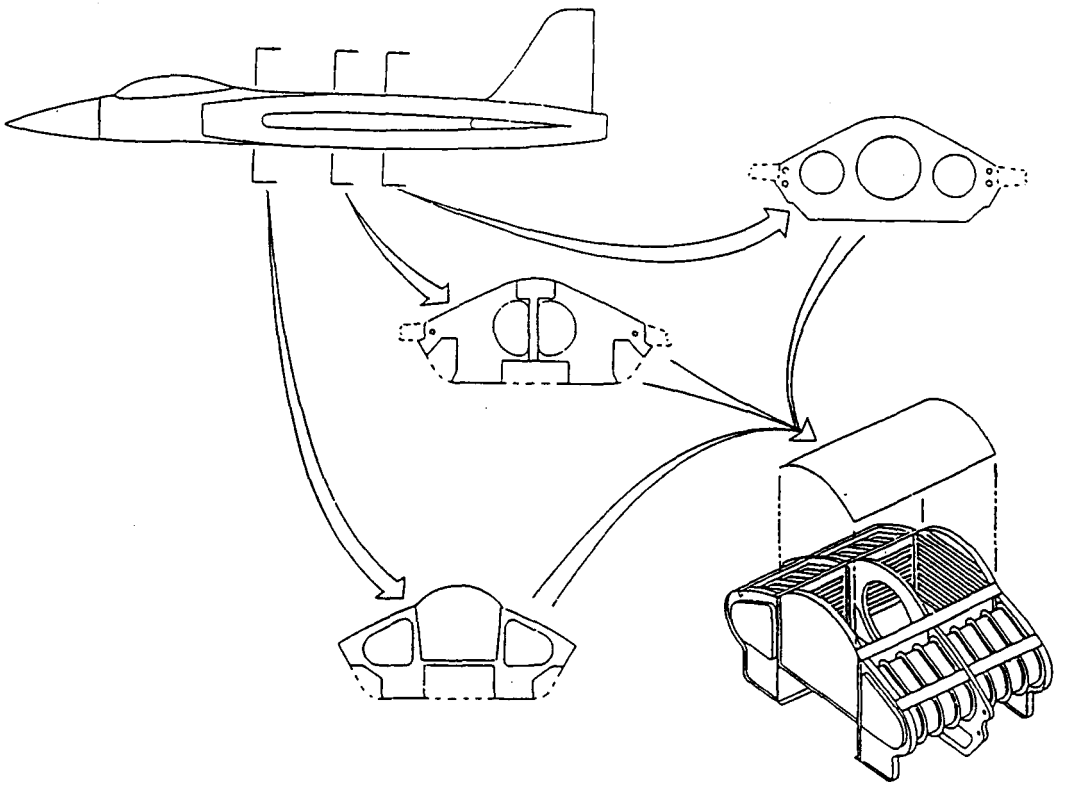

Figure 2.1-1. Generic Fuselage Represented ASTOVL Structure

The generic center fuselage structure, Figure 2.1-2, contains many challenging structural components:

- Upper Cover
- Tank Floor
- Carry-Thru Bulkhead
- Closure Bulkhead
- Keel Webs
- Frames
- Inlet Ducts
- Longerons

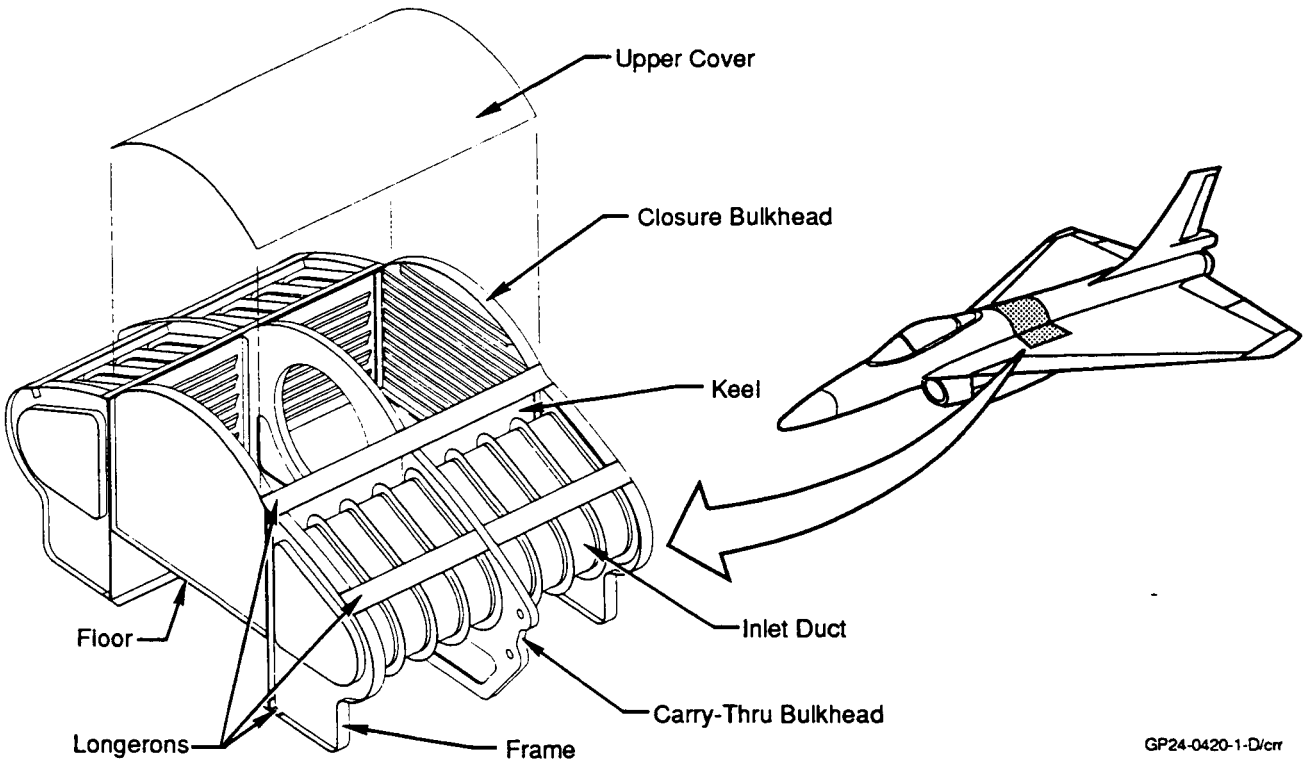

Figure 2.1-2. Generic Fuselage Section Offered a Full Range of Design and Manufacturing Challenges

An upper fuel cell cover, Figure 2.1-3, was selected for investigation since many of its design features and manufacturing approaches would be applicable to the remaining fuselage section. The cover structure ties the upper longerons and bulkheads of the generic fuselage section together and is a primary load carrying component for flight induced structural and fuel cell loading. The cover must be capable of a 255°F (100°C) operating temperature, have a limited number of fasteners on the outer moldline (OML), and resist hydrodynamic ram loading.

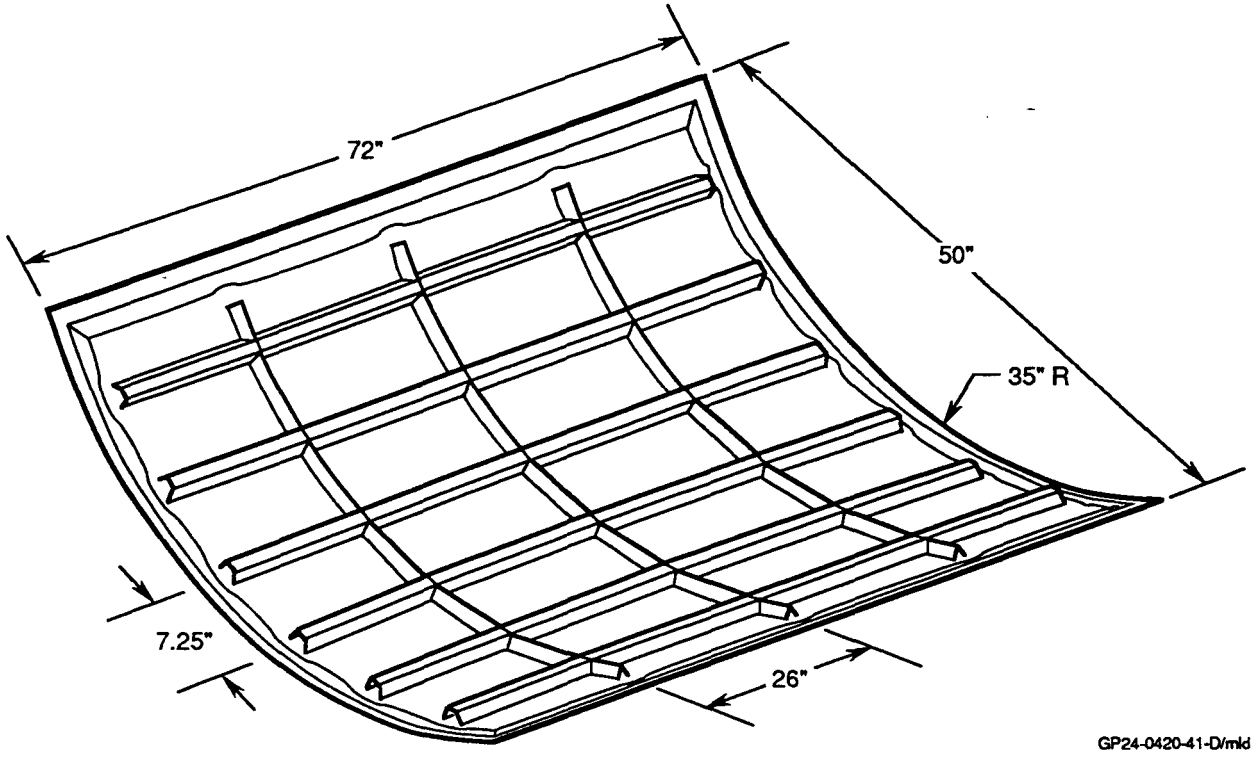

Figure 2.1-3. Upper Fuel Cell Cover Selected for Manufacturing Concepts Development

Conventional methods of analysis were used to develop the upper cover concepts and related subcomponents and elements. In addition to these efforts, a pilot effort was undertaken in conjunction with the Naval Research Laboratories (NRL) to utilize an unique analytical tool, dissipated strain energy (DSE), currently under development.

2.2 Dissipated Strain Energy

Design/analysis enhancement efforts under the ICAPS program were coordinated with the Naval Research Laboratories (NRL) in an effort to validate a developmental material characterization and failure prediction model. The dissipated strain energy (DSE) method has been under development internally at NRL since 1974, primarily through the efforts of Dr. Phil Mast. While the method has continued to evolve, MCAIR and NASA interests in developing a design/analysis tool led to a review of the current methodology and it's capabilities under the ICAPS program.

The DSE method focuses on producing fracture data on fibrous composite materials subjected to different proportions of simultaneously applied general in-plane loads: tension, shear and in-plane bending. For the purpose of generating the fracture data required to fully characterize a material, a computer controlled, in-plane loader previously designed and built at the U.S. Naval Research Laboratories is employed.

The in-plane loader is capable of testing small pre-notched coupons (1" x 0.5") in an automated manner. Specimens of varying cross-ply orientation (+15°, +30°, +45°, and +60°) are tested by gripping one edge in a fixed grip while applying displacement and rotation through a second "floating" grip (Figure 2.2-1). Loading follows a predefined proportional displacement path in order to provide a fixed proportion of the three general in-plane loads. During this displacement controlled loading, the associated forces are measured by the actuators and transformed to an equivalent traction vector at the crack tip which can be associated with transformed displacements for the tip. It then becomes possible to calculate the net energy dissipated in the process by integrating on-line to obtain the total energy imparted, and subtracting the recoverable elastic energy (assumed to be one-half of the displacement and traction dot product). The "fracture load" is defined at the point where a distinctive increase in the dissipative energy is observed. A typical plot of the displacement versus dissipative energy is shown in Figure 2.2-2 which was generated during previous work documented in Reference 1.

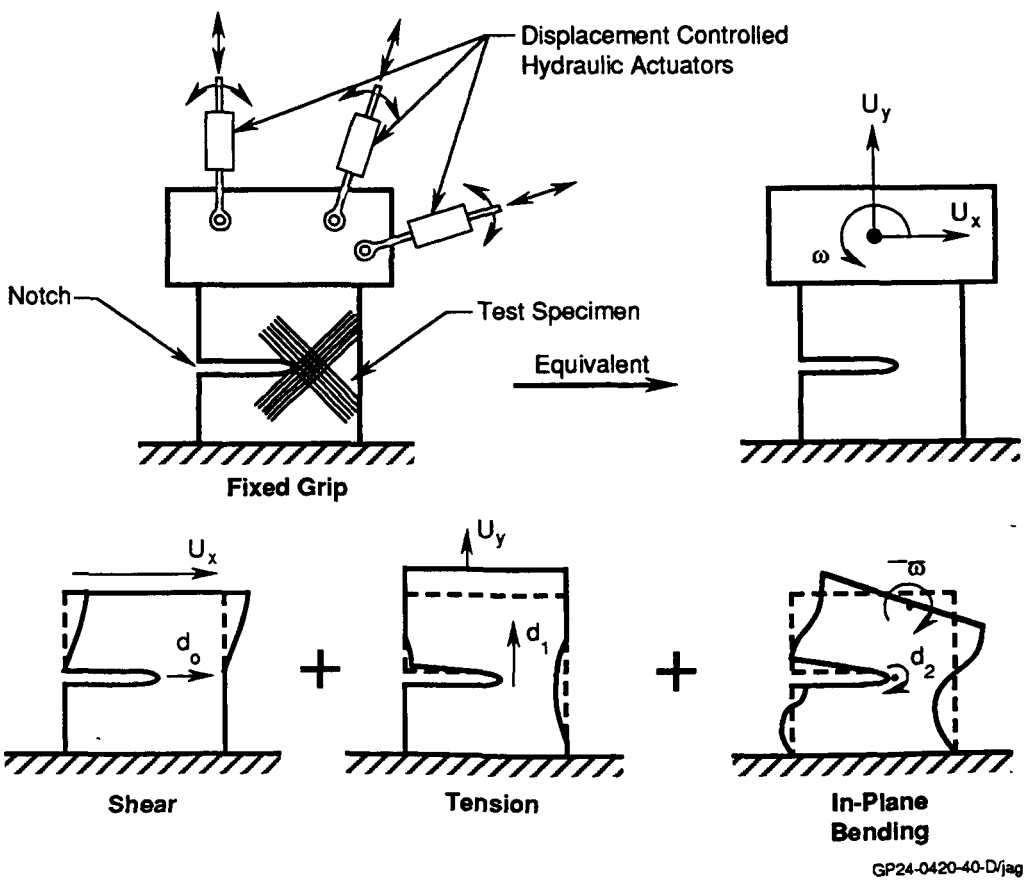

Figure 2.2-1. In-Plane Loading Test Fixture and Proportional Loading Scheme

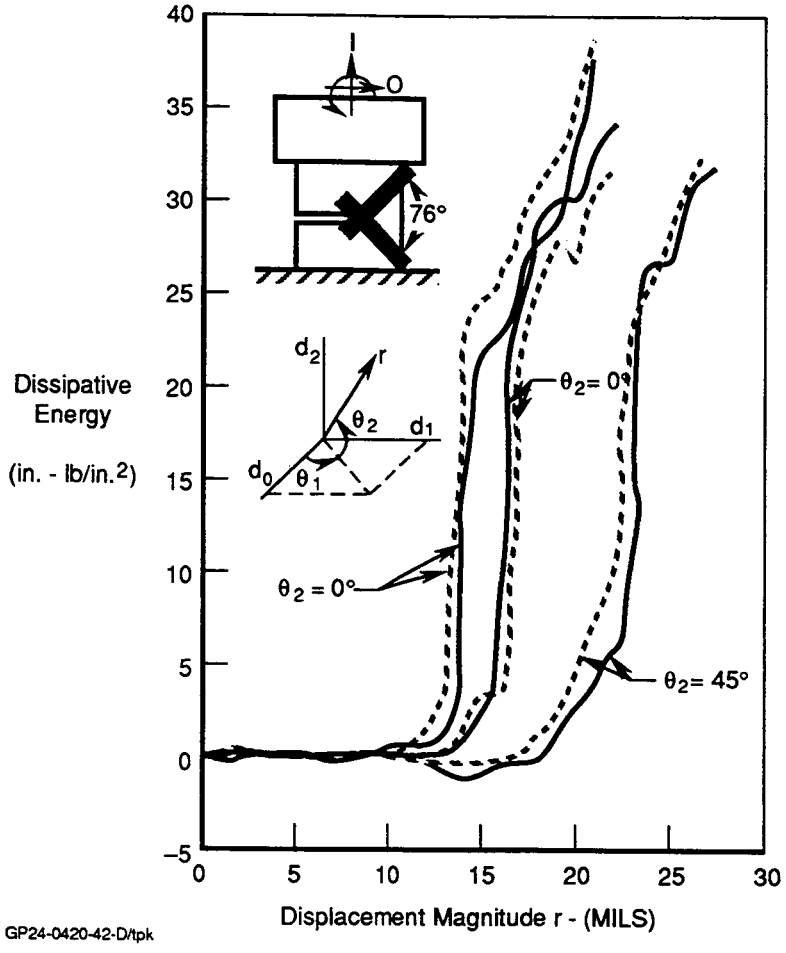

Figure 2.2-2. Cross-Ply Laminate On-Line Testing Results

In order to fully characterize a material through all strain space, 120 coupons of each cross-ply orientation are tested with data being taken at 50 points throughout each loading spectrum. This data can be depicted in the form of strain space failure envelopes, Figure 2.2-3, which depict the "fracture load levels" versus a non-dimensional representation of the proportional loading path.

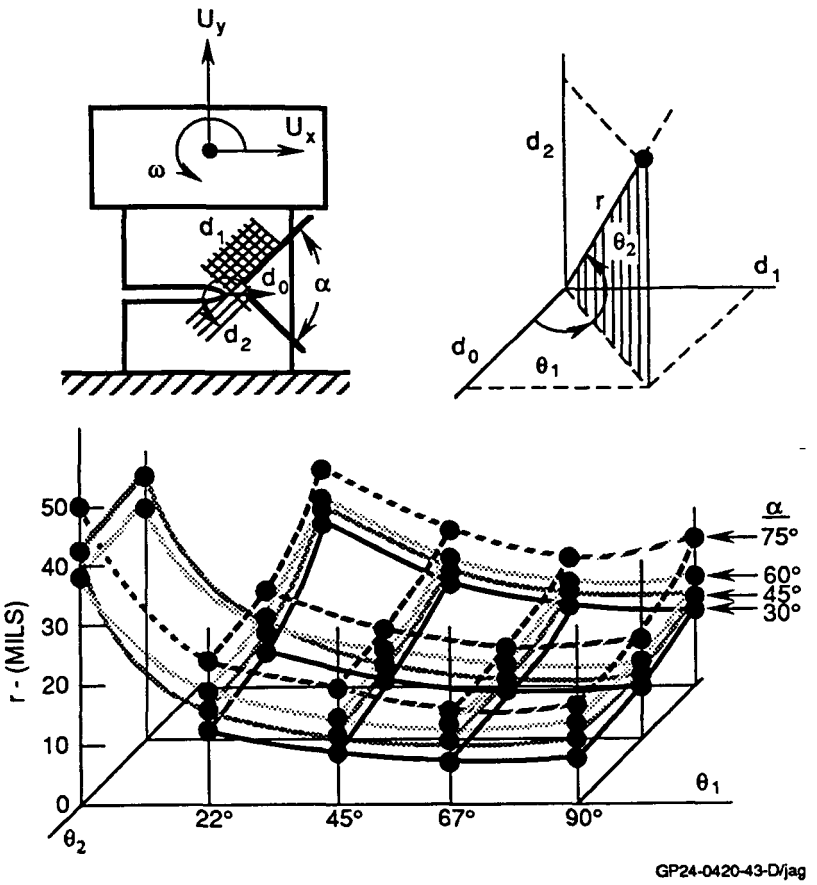

Figure 2.2-3. Representative Strain Space Failure Criteria

In order to assess the validity of the "fracture analysis" which had been proposed by the NRL technique, DSE was to be used to predict the structural response of the upper cover subcomponent to design loads and compared with state of the art (SOTA) techniques and program test results. Mechanical response of the cover structure was to be determined using finite element analysis coupled with lamina nonlinear constitutive parameters which are obtained as part of the DSE effort. Absorbed energy density would be determined over the entire structure and used to determine critical panel areas and subsequently integrated to determine total absorbed energy versus applied load. This relationship could then be used to assess the structural performance and predict eminent structural failure. In addition, the degree of material nonlinearity would be examined to determine whether an iterative scheme should be employed for the final failure predictions.

AS4/PEEK material was characterized using the in-plane loading apparatus. Several material panels of varying cross-ply orientations were fabricated and inspected at MCAIR. NRL performed the final machining of the 1.0" x 0.5" coupons and the necessary notching of each specimen. At the time of testing, some non-critical portions of the test procedure were manually accomplished. This included the loading of the specimen coupon into the test apparatus, and the initiation of the loading sequence. Despite these manual procedures, testing was completed in an expedient manner; 150 specimens were tested within a period of one week.

The in-plane loader data were used to generate several non-linear laminate (cross-ply) constitutive relationships for the AS4/PEEK material. This involved the use of software which had been previously developed at NRL for this purpose. In conjunction with this effort, the coding of a cross-ply-to-lamina and lamina-to-laminate translator was begun. The cross-ply-to-lamina software would allow the cross-ply data to be degenerated into a single lamina constitutive relationship. Lamina data would then be utilized by the lamina-to-laminate module in order to build the necessary constitutive model for any arbitrary stacking sequence.

Concurrent with the NRL activities, the finite element model (FEM) of the curved, stiffened upper cover structure was developed. Modeling of the structure consisted of 1,144 laminated plate elements and included detailed modeling of the hat stiffeners, Figure 2.2-4. The model was analyzed for critical loads including: steady state pull up (SSPU), steady state push down (SSPD), and rolling pull out (RPO), and utilized a static solution (Section 2.4). The data were delivered on magnetic tape to NRL and converted to a parametric-based model for use in the DSE analysis. A cross-ply panel design was generated in order to demonstrate the ability to link the non-linear constitutive model with a FEM run.

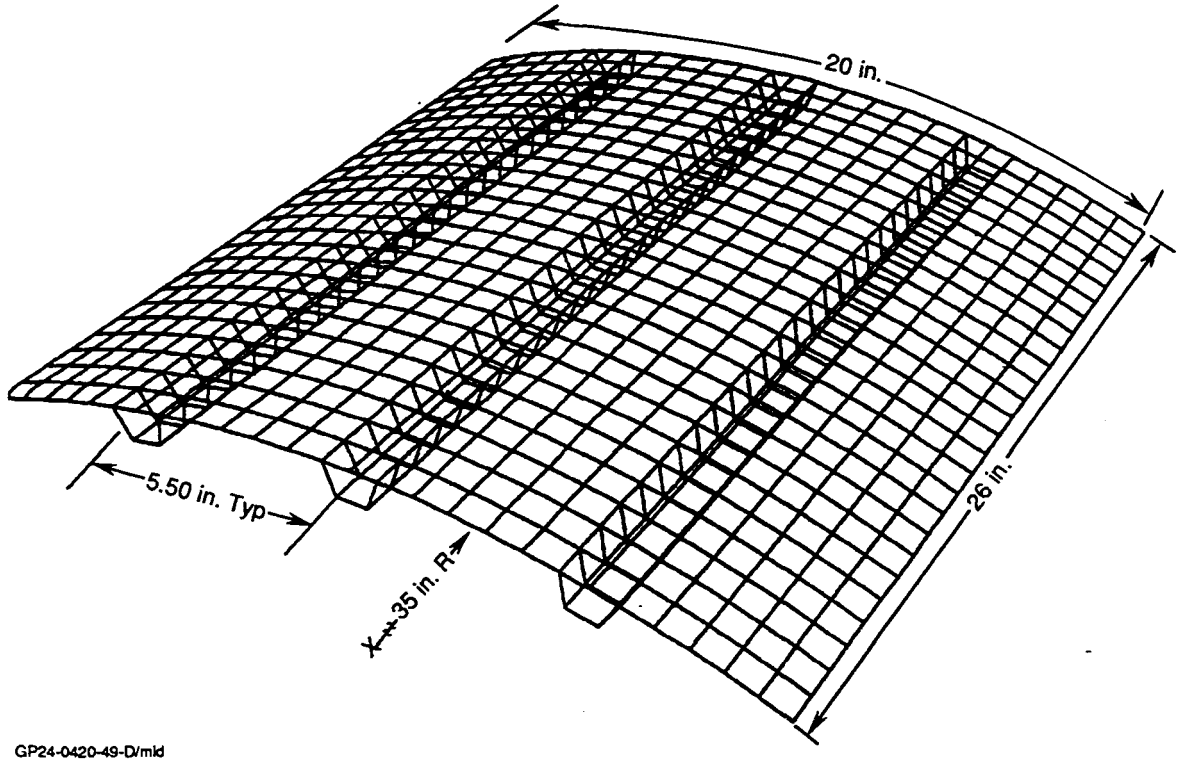

Figure 2.2-4. Upper Cover Finite Element Model for DSE Correlation

A post-processing capability was established linking the DSE analysis with a PATRAN interface. Color contour plots depicting any of the DSE parameters were made available. NRL demonstrated this capability by generating plots for the absorbed energy in the cross-ply panel models, Figure 2.2-5. The DSE technique capabilities of capturing the entire 2-D strain field at any point and represent it by a scaler quantity. In contrast, strain field plots can only depict a single component of the strain state.

ORIGINAL PAGE
COLOR PHOTOGRAPH

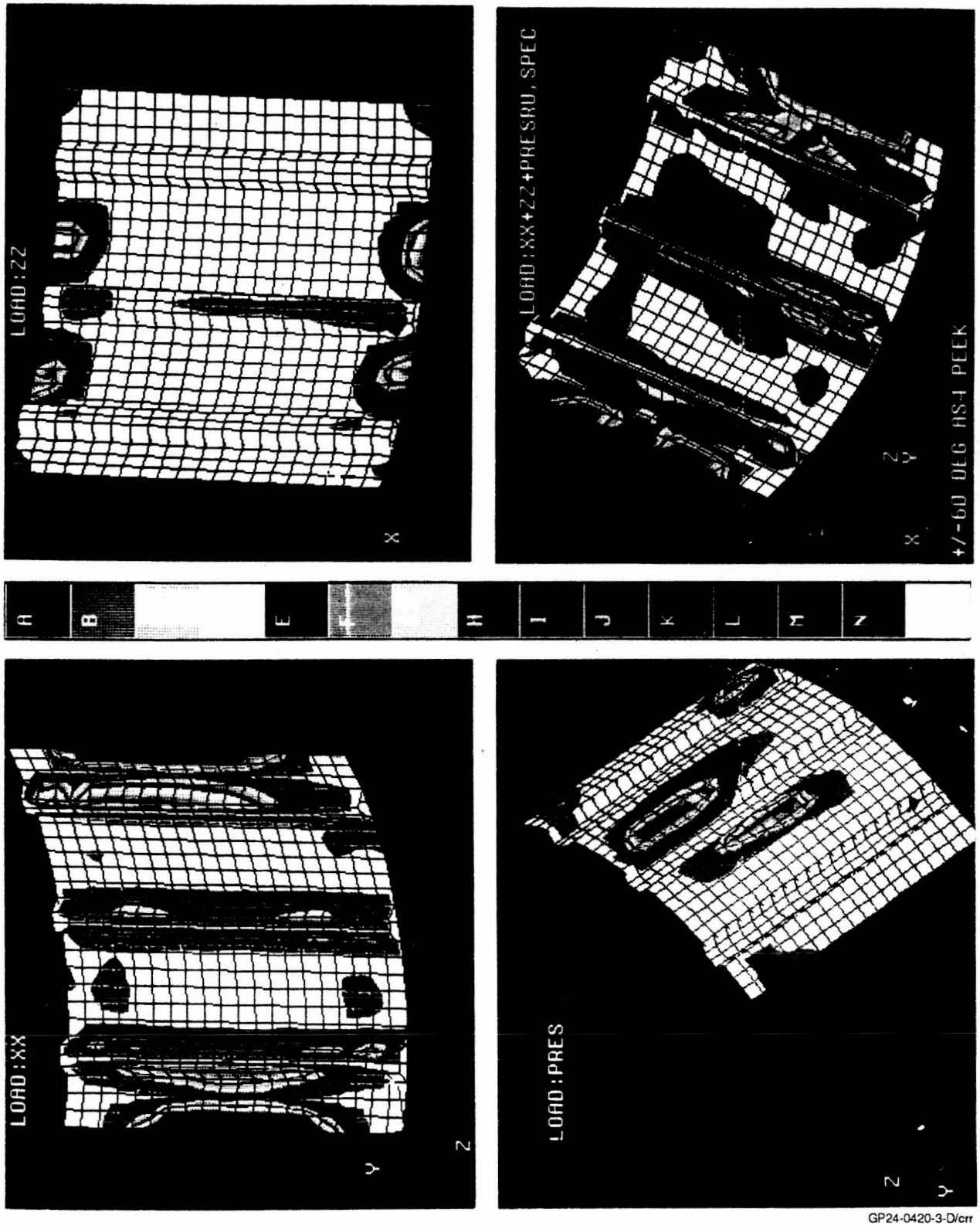

GP24-0420-3-D/crr

Figure 2.2-5. DSE Contour Plots for Upper Cover Structure FEM

INTENTIONALLY BLANK

THIS PAGE INTENTIONALLY LEFT BLANK

A preliminary effort to relate the DSE contours to failure predictions was undertaken within NRL through the modeling of the actual coupon specimens. A FEM model was generated for the cross-ply specimen and subjected to several of the proportional loading schemes used in the material characterization. The orientation and load proportions were chosen based upon some rather unintuitive test results. During the testing several cross-ply coupons failures continually occurred at the back edge of the specimen, away from the notch tip. This failure was consistently produced and can be seen in the C-scans taken from a typical specimen, Figure 2.2-6. A comparison of these NDT results with the DSE color plots for the same configuration and loading condition show excellent correlation, Figure 2.2-7.

THIS PAGE INTENTIONALLY LEFT BLANK

Smoothed Acoustic Images

Load: Compression

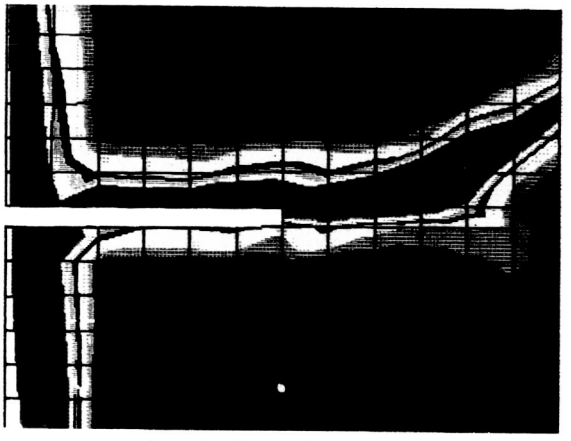

Load: Shear-Tension-Rot

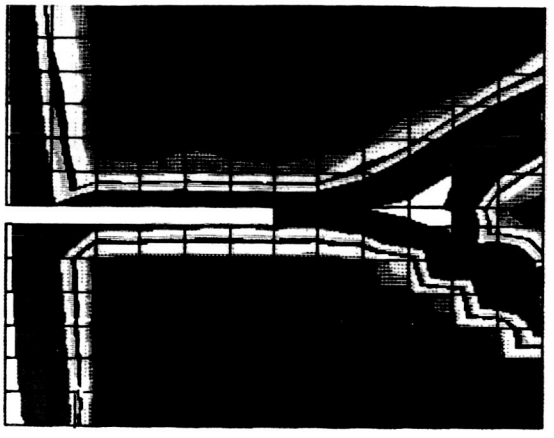

Load: Tension

GP24-0420-2-D/crr

Figure 2.2-6. In-Plane Loader Speciment Post Test C-Scan Results

THIS PAGE INTENTIONALLY LEFT BLANK

Absorbed Energy Images

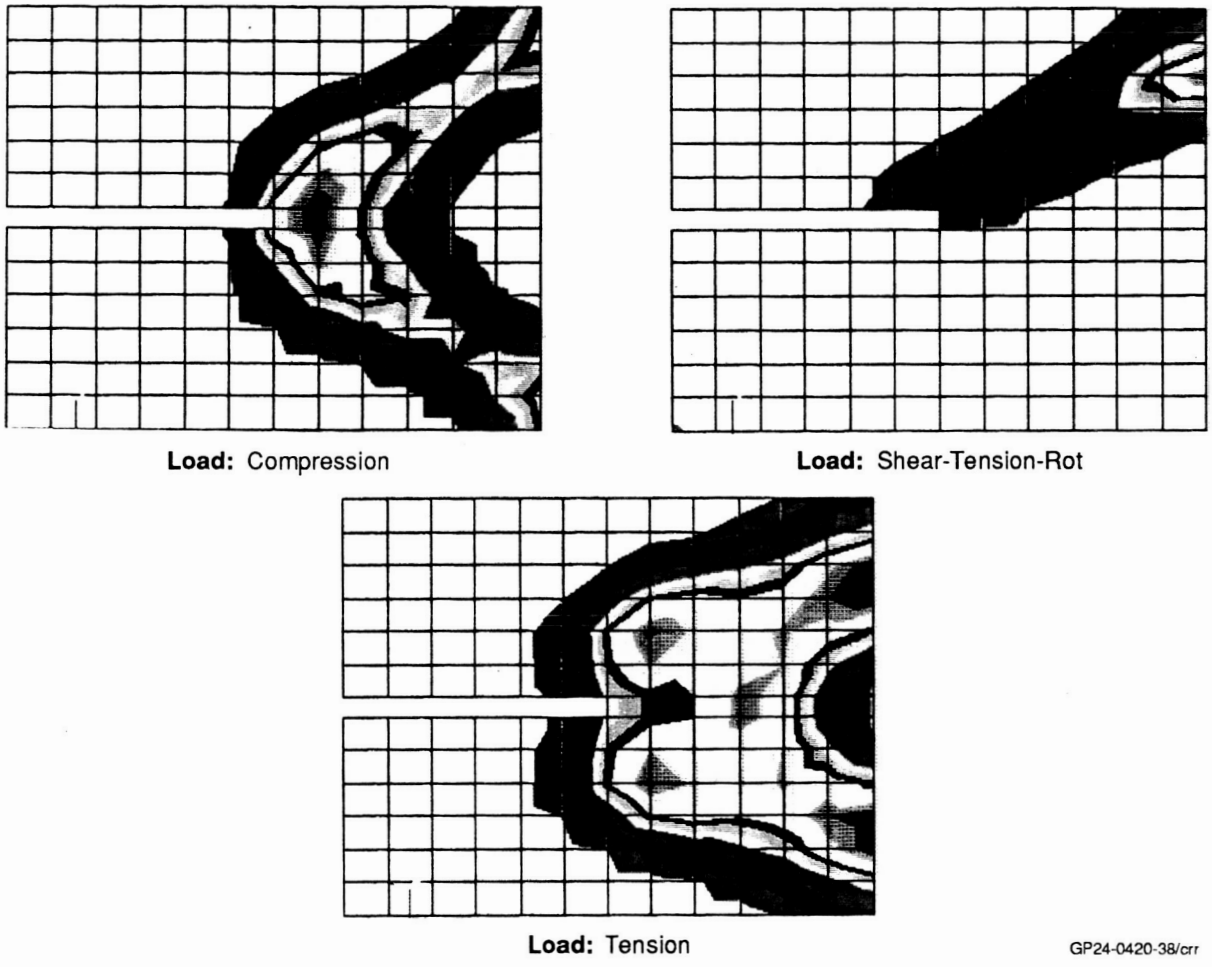

Load: Compression

Load: Shear-Tension-Rot

Load: Tension

GP24-0420-38/crr

Figure 2.2-7. DSE Contours Correlate With NDT Results

ORIGINAL PAGE
COLOR PHOTOGRAPH

THIS PAGE INTENTIONALLY LEFT BLANK

Although efforts on the DSE technique were discontinued due to program redirection, significant progress in understanding and demonstrating the capabilities of DSE was achieved. Summarized below are the conclusions and current state of development at the time of this report:

(a) characterization of AS4/PEEK cross-ply laminates was demonstrated

(b) demonstration of incorporating non-linear constitutive equations into FEM analysis has been accomplished

(c) post-processing capabilities for DSE results were achieved

(d) the potential of DSE as a failure prediction method through NDT and DSE results comparison has been shown

(e) significant progress was made on modules required for lamina and general laminate characterization

(f) a parametric model was established at NRL for stiffened panels with or without curvature

In addition, suggestions for future development and studies related to the Dissipated Strain Energy Technique are provided:

(g) a comparison of the lamina constitutive equations with actual lamina properties has to be completed to gain confidence in this method of "backing out" lamina properties once the module is completed

(h) strength predictions should be carried out on simplified structures first – the coupon specimens provided valuable insight and instilled a great deal more confidence in the method than the original panel cross-ply plots

(i) strength prediction methodology should be more clearly defined

(j) implementation of the non-linear constitutive equations within the FEM analysis and the use of an iterative technique to account for "material softening" still needs to be pursued

2.3 Thermoplastic Fuselage Subcomponent Concepts

The subcomponent design for the fighter development was representative of the fuselage upper cover structure. Design loading requirements were derived from the generic aircraft data for the upper cover and were identically imposed on the subcomponent article. A Design/Manufacturing Integration (D/MI) team was used to establish two design/manufacturing concepts for the subcomponent.

The D/MI engineering team developed over fifty potential panel concepts, Section 3.2.1, for a stiffened skin of single curvature sized for an advanced STOVL aircraft. The cover design was driven mostly by weight and manufacturing considerations. A hat-stiffened skin offered the most weight savings when

compared to other stiffening concepts. This configuration was also found to be less costly to manufacture. Selection of the final concepts was based upon innovativeness in design, manufacturing approaches, applicable material form, low-cost, weight, maintainability, and survivability.

Two design concepts were selected for final development for the fuel tank upper cover. The first design, Figure 2.3-1, contains discrete hat stiffeners with a constant thickness Outer Mold Line (OML) skin. The second design, Figure 2.3-2, contains a constant thickness Inner Mold Line (IML) pan with an OML skin with local pad-ups beneath stiffener locations. The first design was decided upon for its applicability to the Fiber Placement (FP) manufacturing process. The second design was chosen to demonstrate an innovative diaphragm forming concept utilizing a single super-plastic aluminum diaphragm resulting in coconsolidation of IML and OML pans.

The laminate stacking sequence shown in Figure 2.3-3 initially designed for both the FP and SDCC processes was optimized for weight with respect to flight load, buckling and fabrication requirements. IM7/ITX was chosen based on satisfying the temperature requirements of the upper cover. Initial estimates for lamina properties were made from limited data and comparisons with similar fiber-resin systems. Later checks versus test data showed the estimates to be reasonably accurate and no redesign was required. For the diaphragm formed panel a 3/16" slit tape braided sheet was substituted for each pair of +45 and 0/90 adjacent plies. This was utilized to enhance the survivability of the panel to hydrodynamic ram loads, improve its formability, and decrease layup time while maintaining strength and stiffness. This resulted in a slightly different layup from the fiber placed skin, as shown in Figure 2.3-4.

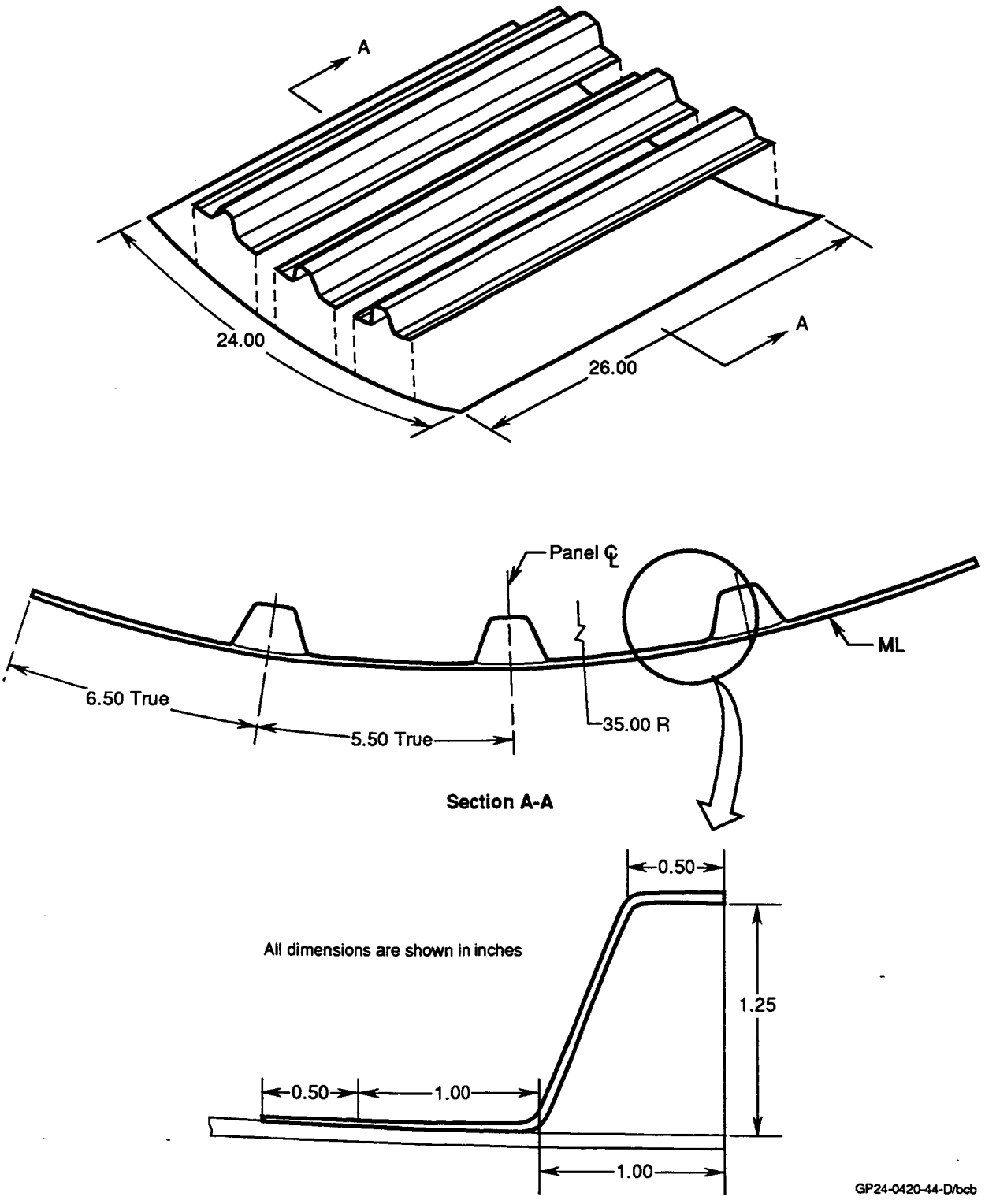

Figure 2.3-1. Subcomponent Design Concept Employing Fiber Placement/Roll Formed Hats

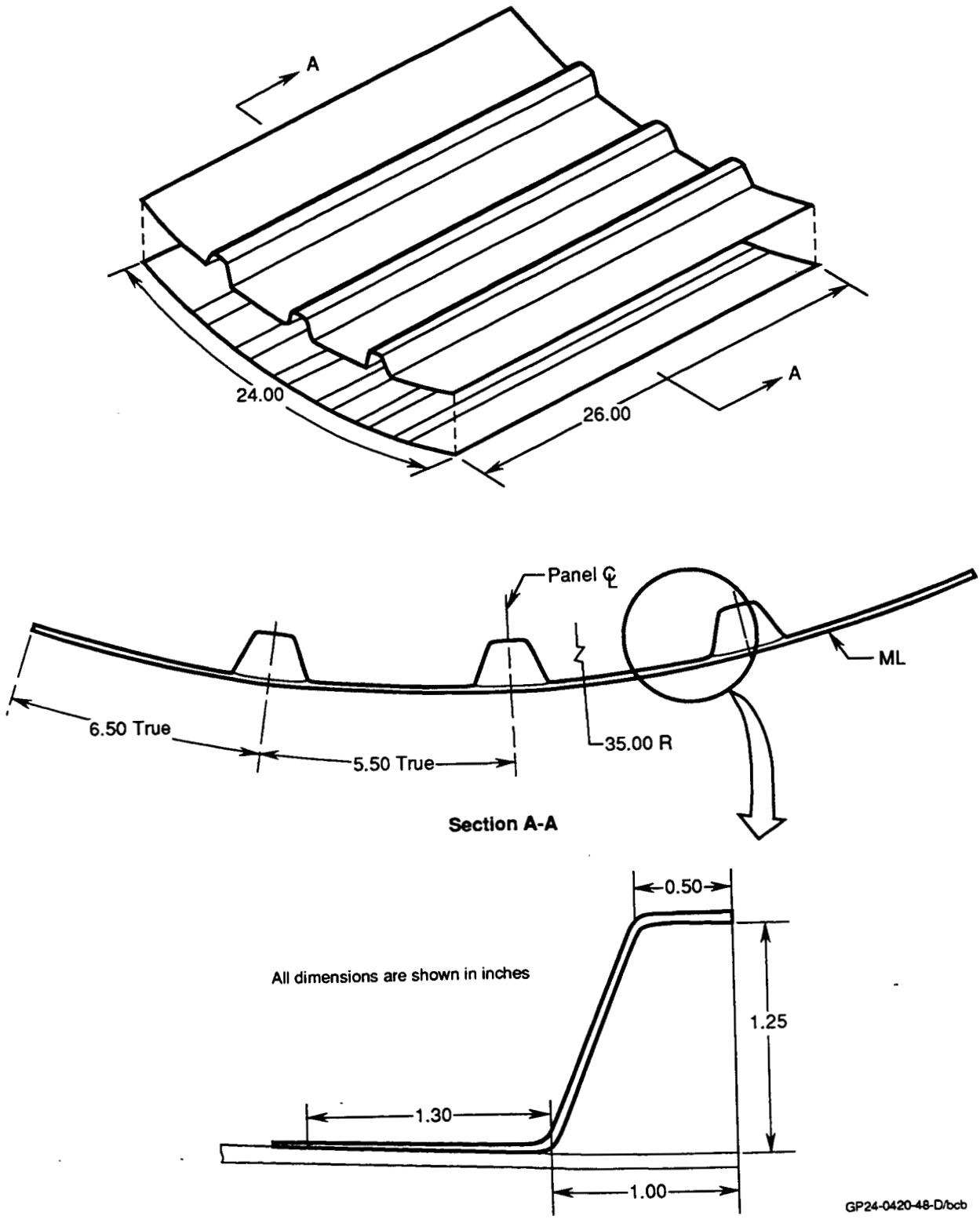

Figure 2.3-2. Subcomponent Design Concept Employing Single Diaphragm Co-Consolidation

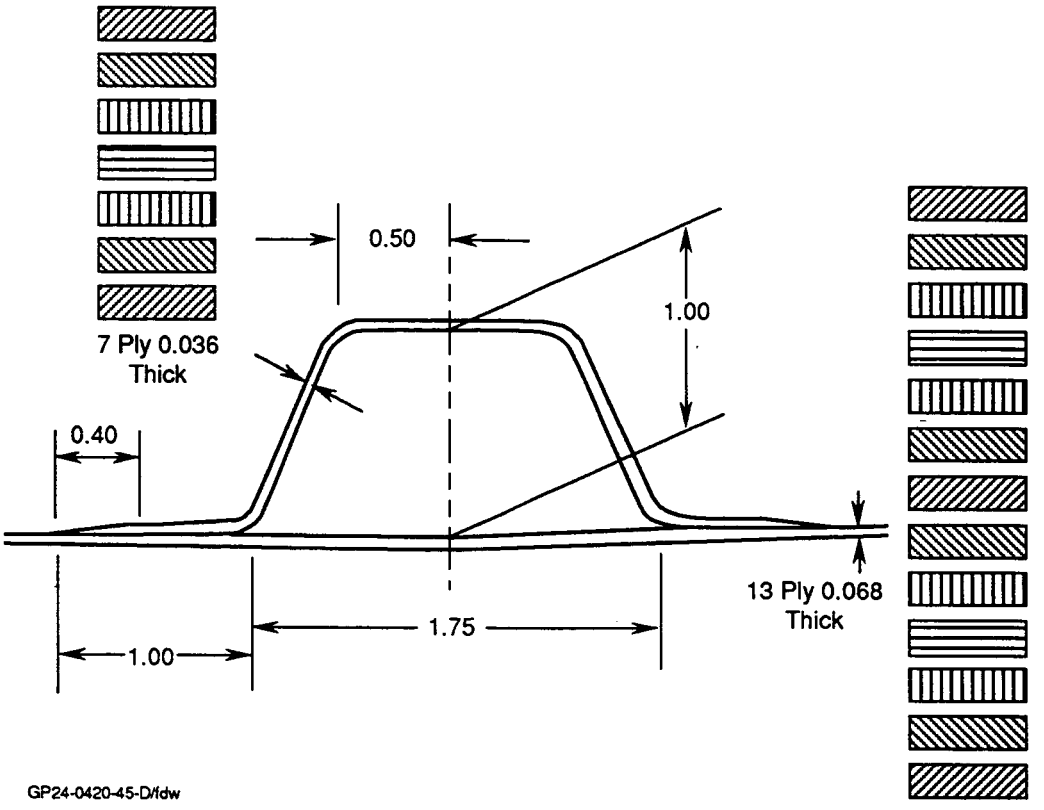

Figure 2.3-3. Fiber Placed Skin and Roll Formed Hat Laminated Design

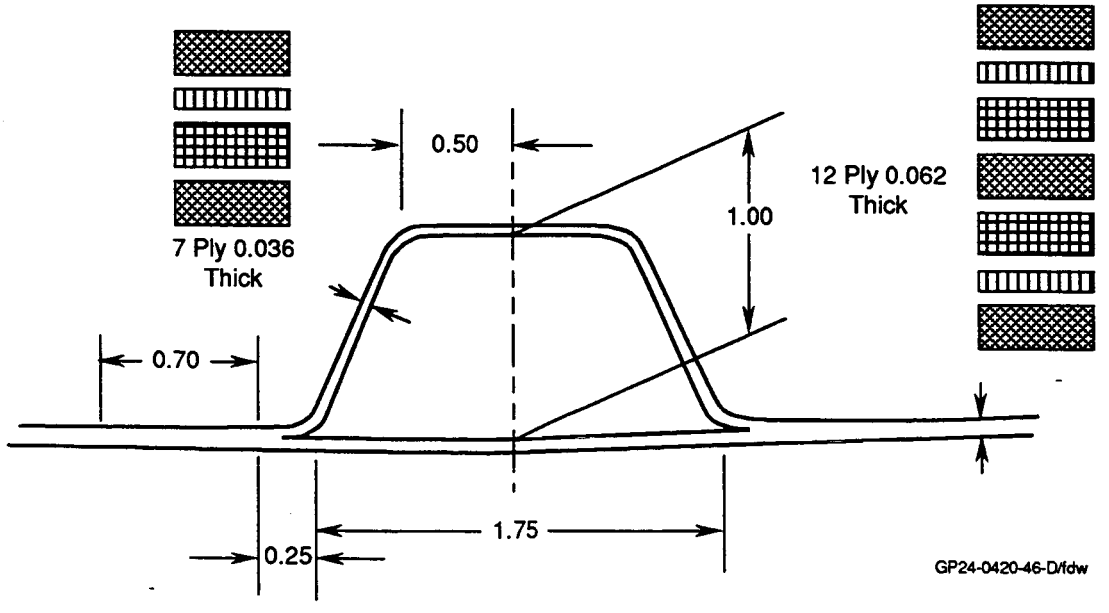

Figure 2.3-4. Single Diaphragm Co-Consolidation Laminate Designs

Design loads for the upper fuselage skin panel were determined from MCAIR's Advanced STOVL Model 4629 configuration. Maneuvering flight conditions represented by these loads: a 9g symmetric steady state pull-up (SSPU) for down bending, a -3g steady state push-down (SSPD) for up bending, and a 7.2g rolling pull-out (RPO) for combined vertical and lateral loads. All flight conditions are at sea level and 0.95 Mach. In addition, a 22.0 psi (ultimate) fuel pressurization load condition was included in the design requirements. Ultimate loads are presented in Figure 2.3-5, and include a 1.5 factor of safety.

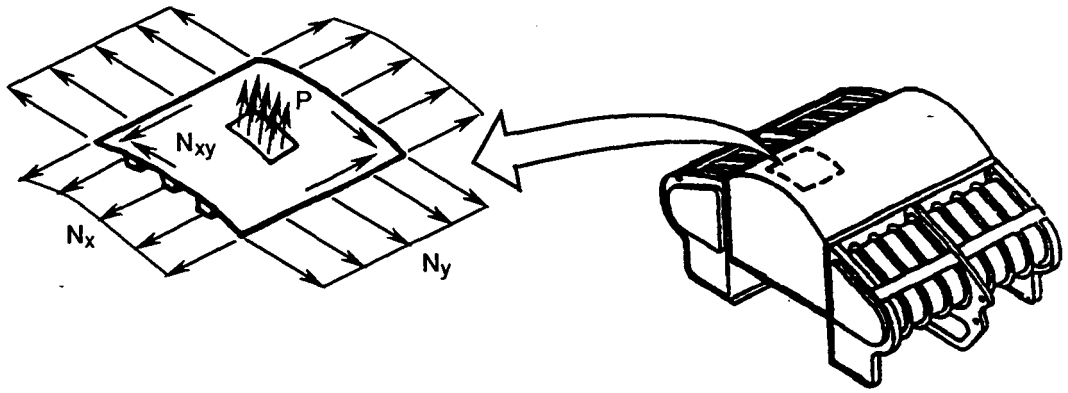

Ultimate Loads

Condition	Nx (lb/in.)	Ny (lb/in.)	Nxy (lb/in.)	P (psi)
SSPU, 0.95 Mach, SL, 9.0 g	2,500	±100	0	1.0
SSPD, 0.95 Mach, SL, –3.0 g	–800	±100	0	5.0
RPO, 0.95 Mach, SL, 7.2 g	2,000	±100	±500	5.0
Fuel System Over Pressure Malfunction	0	0	0	22.0

GP24-0420-47-D/mld

Figure 2.3-5. Design Ultimate Loads Used for ASTOVL Upper Cover Analysis

The cover structure FEM was utilized to examine the effects of combined loads and determine static deflections. Panel stability was initially analyzed for its buckling response with the SS8 Anisotropic Curved Panel Analysis Program (Reference 2). Skin buckling design requirements were established from typical fighter aircraft designs with composite moldline skins and stated that buckling was to occur at 120% of design limit load.

In addition to satisfying all static and buckling response requirements, both designs were reviewed by dynamics personnel to verify their ability to tolerate the severe acoustic environment inherent in STOVL aircraft. Certification of the survivability of the designs was also demonstrated through the analysis of hydrodynamic ram phenomena on the panels. Figure 2.3-6 is a typical contour map of the laminate strains generated during hydrodynamic ram. The map was prepared using the hydrodynamic analysis code ERAM (reference 3 and 4). The impact event corresponds to an encounter with a 14.5 mm armor piercing incendiary (API) round with the impact location centered within a stiffener bay. The results of this analysis showed the survivability of the upper cover design.

ORIGINAL PAGE
COLOR PHOTOGRAPH

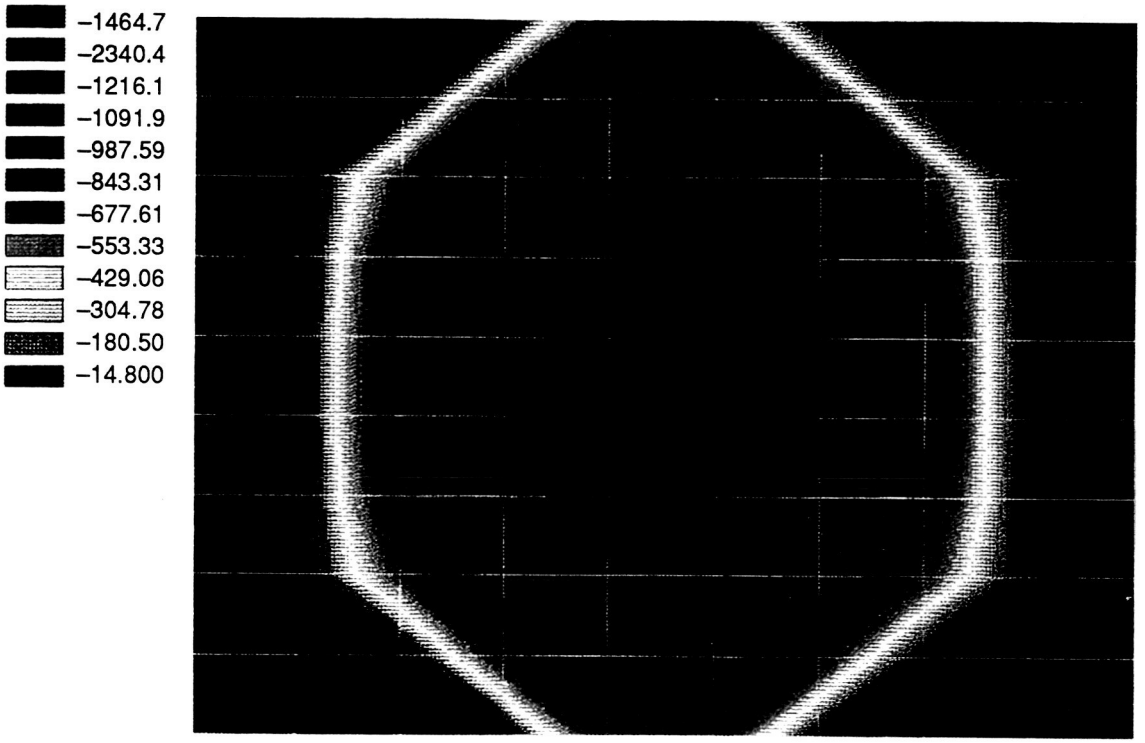

GP24-0420-37/crr

Figure 2.3-6. Hydrodynamic Ram Analysis Results for 15.5 mm API Round

THIS PAGE INTENTIONALLY LEFT BLANK

2.4 Thermoplastic Fuselage Element Concepts

As a first phase in the building block approach to the production of a full-scale fighter fuselage section, element components were selected for design, analysis, and structural validation. Elements were sought which would address key areas of the innovative composite design including structural design, analysis, and manufacturing development. In addition, the elements were to be representative of key components in the future subcomponent development. Analysis methodologies were sought to improve the currently available structures technologies. Implementation of these methods was continually targeted at providing a state of the art design tool.

Two structural areas of particular interest in the fuselage structure were identified by the D/MI team, Figure 2.4-1. Stiffener to skin joints were selected because of:

- expected increases in structural performance through optimal design for pull-off and shear-transfer loading
- decreased costs through manufacturing innovations in the form of single diaphragm cocon-solidation (SDCC)
- potential for low-observable applications, reduced weight, and reduced assembly due to the fastenerless design associated with SDCC
- current MCAIR developments for the analysis of stiffener pull-off strengths and comparative test data

Thick composite lugs were selected identified as the second element for evaluation because of:

- expected increases in structural performance through optimal design for pin-bending effects and through-the-thickness loading effects
- decreased costs through the validation of water-jet-cutting of thick composites for initial and final trim
- opportunity to develop a useful design/analysis tool for the evaluation of highly loaded and out-of-plane loading of thick composites

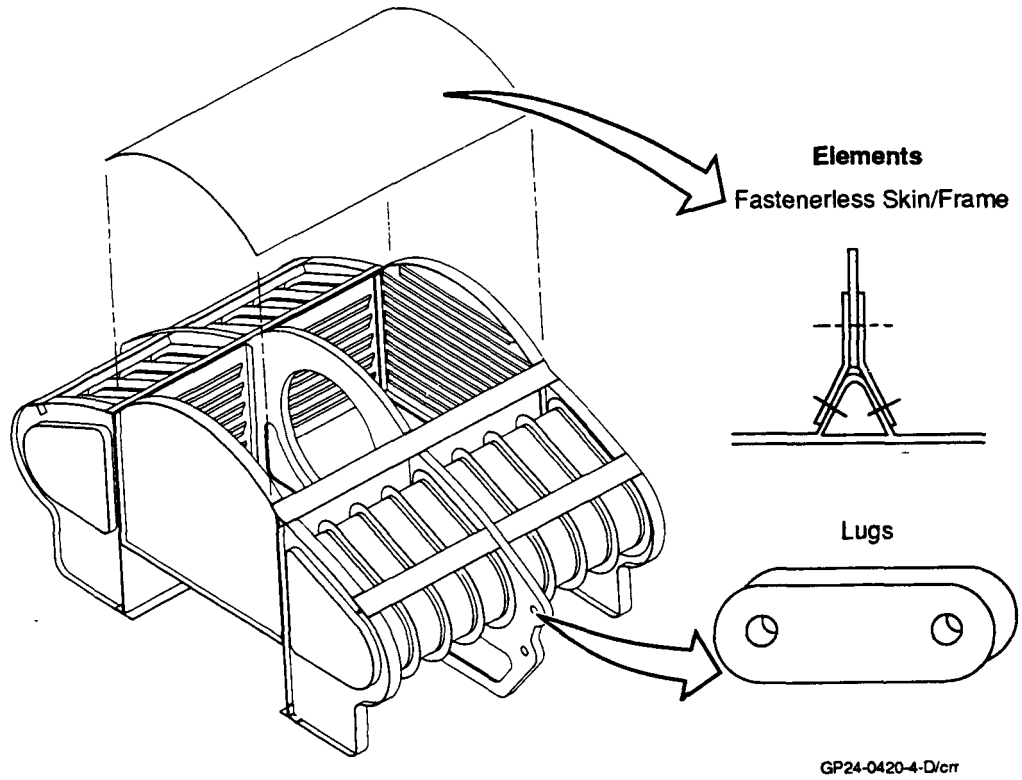

Figure 2.4-1. Structural Elements Pursued During Building Block Approach

2.4.1 **Lug Elements** – In aircraft structures, single-pinned joints (i.e., lugs) play a key role in the transmission of large loads between major structural components. The use of composite materials for these highly loaded structures has the potential for substantial weight reductions.

The design of lug elements was not focused on identifying an optimal design for application to the fuselage structure and loading being considered. Instead, the designs were chosen to provide a fairly comprehensive set of test cases to which analytical developments could be compared. This form of building block approach was adopted due to the complexities involved in the design of both lugs and thick composite sections.

The design of thermoplastic lug test articles focused on providing specimens which could validate the most critical portions of the analysis. Pin bending effects and a study of the different failure modes were targeted by the D/MI team as the primary areas of concern. Means were sought to separate these design variables and maintain constancy for all other design parameters.

Previous efforts determined that ply stacking sequences can affect the pin bending response of a lug. By varying the through-the-thickness stiffness distribution of the laminate, peak stresses could be reduced, thereby minimizing pin bending effects. In order to explore this potential for increased performance and to validate the methodology's ability to predict it, three lug layups were chosen which resulted in different pin bending responses while maintaining nearly identical in-plane response. This goal was

accomplished by varying the stacking sequence of the six sublaminates used in the manufacture of each lug. Maintaining the in-plane response was necessary to allow for an investigation of the other design parameter, failure mode.

Failure mode of the composite lugs was expected to depend on lug geometry. Lug geometries were chosen to provide two distinct modes of failure based on a metallic analysis using smeared in-plane properties for the composite lugs. External geometries on all the lugs were held constant (W=3.5"), while the hole diameter was varied to 1.0" or 1.75". This resulted in different W/D ratios (3.5 and 2.0 respectively), and was expected to result in bearing failures in 50% of the specimens, while the remainder would experience net-section failures. A summary of the lug designs used for analysis correlation is shown in Figure 2.4.1-1.

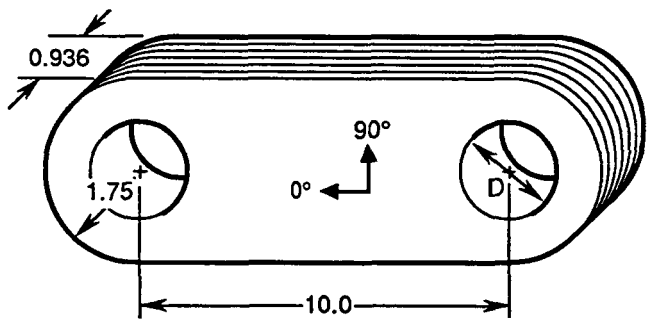

Note: All dimensions are inches

Lug Specimens	Quantity	Hole Diameter (in.)	Sublaminate Stacking Distributrion*			Effective Layup
			Sublaminate 1	Sublaminate 2	Sublaminate 3	
Static 1	4	1.00	(47/40/13)	(47/40/13)	(47/40/13)	(47/40/13)
Static 2	3	1.00	(47/40/13)	(34/53/13)	(60/27/13)	(47/40/13)
Static 3	4	1.00	(60/27/13)	(47/40/13)	(20/67/13)	(42/45/13)
Static 4	4	1.75	(47/40/13)	(47/40/13)	(47/70/13)	(47/40/13)
Static 5	4	1.75	(47/40/13)	(34/53/13)	(60/27/13)	(47/40/13)
Static 6	4	1.75	(60/27/13)	(47/40/13)	(20/67/13)	(42/45/13)

* Sublaminate stacking sequences are as follows: (47/40/13): $[0_2/45_2/90_2/-45_2/0_2/45/0/-45/0_2]s$
(34/53/13): $[45_2/0_2/-45_2/90_2/45_2/0_2/-45_2/0]s$
(60/27/13): $[0_2/45/0_2/-45/0_2/45/0_2/-45/90_2/0]s$
(20/67/13): $[45_2/0/-45_2/90/45_2/0/-45_2/90/45/0/-45]s$

GP24-0420-50-D/des

Figure 2.4.1-1. Configuration and Stacking Sequence of Lug Test Specimens

The analysis development pursued under this program was a compromise between two existing methods of composite analysis which employ the finite element method (FEM):

1) laminated plate elements based on classical lamination theory, which are easily modeled and provided quick solutions but are unable to handle thickness effects associated with composites, and

2) three dimensional solid anisotropic elements which allow for complete generality, but are computationally exhaustive

To provide a useful design tool, a compromise between these existing techniques was utilized. A subparametric laminated solid element, previously developed in Reference 5, was incorporated into an analysis package tailored for the analysis of lug sections. The element formulation utilized was originally used to study through-the-thickness stress fields that develop during low velocity impact events. Choice of this element was based on its excellent correlation to experimental results for the dynamic response of laminated plates during lateral impact.

The element geometry is defined by four nodes that specify the x, y positions of the edges of a right prism, and stacking sequence of the laminate under consideration, Figure 2.4.1-2. Twelve degrees of freedom as specified at each node: the translation in each coordinate direction (3 degrees of freedom), and the partial derivatives of each translation with respect to each coordinate (9 degrees of freedom). Stacking sequence effects are accounted for by explicitly integrating the strain energy density through the thickness of the element.

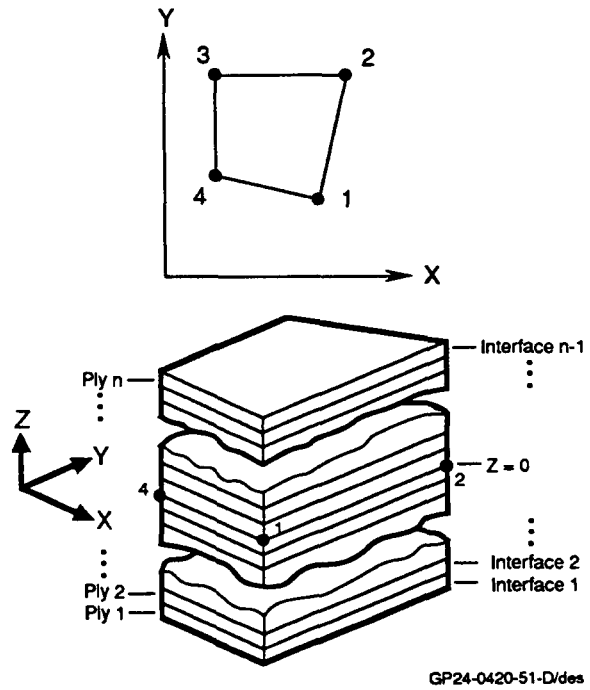

Figure 2.4.1-2. Subparametric Laminated Solid Element

To account for pin bending effects, both lug and pin were modeled. Typical meshes for the lug and pin for actual testing specimens are shown in Figure 2.4.1-3. The generation of these models was relatively simple, since the geometry is defined in only two (x, y) dimensions. The lug-pin contact was modeled by coupling lug and pin displacements in the radial direction. The converged displacement field is then used to perform a laminate analysis on an element by element basis. Averaged strains in a ply are calculated by integrating the strain field over the area of the element and through the portion of the element thickness associated with that ply. These strains are then used to calculate average ply and interface stresses within the element. Since all six stress components are available, it was desirable to use a failure criteria that account for interactions between these components. Hence, for predicting failure within a ply, modified Hashin's failure criteria (Reference 6) were used. These failure criteria account for distinct modes of failure for both the fiber and matrix.

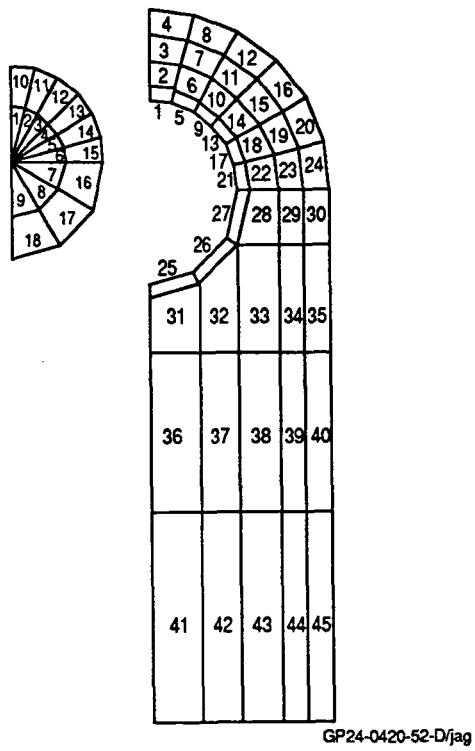

Figure 2.4.1-3. Lug and Pin Models for FATLAM Analysis

The analysis methodology developed in support of the lug designs involves the use of two programs: Failure Analysis of Thick Laminates (FATLAM) and Static Analysis of FATLAM (STAFLM). FATLAM is used to generate and condense the stiffness matrices for the lug and pin, and to perform a ply-by-ply laminate analysis on the lug after a static displacement solution has been found. STAFLM performs the iterative lug/pin contact analysis, utilizing the stiffness matrices provided by FATLAM. A computational schematic is shown in Figure 2.4.1-4 with an outline of the analysis procedure following.

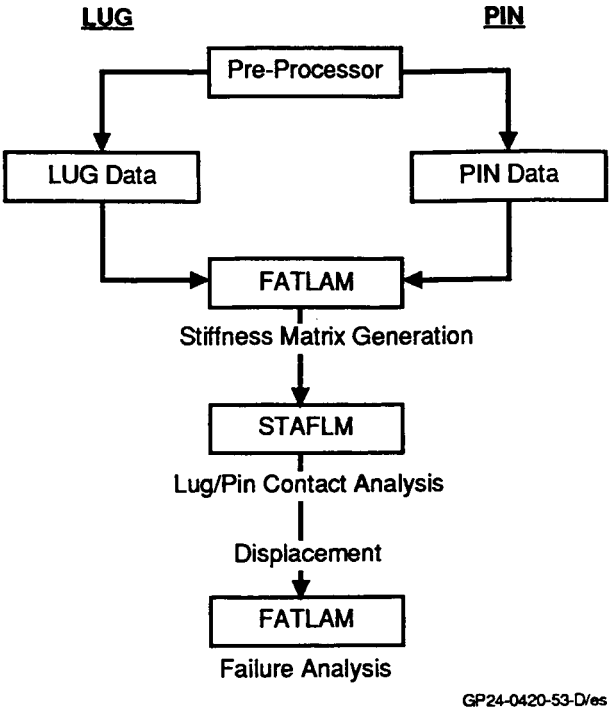

Figure 2.4.1-4. Computational Schematic for Lug Analysis

A two dimensional lug model is generated using any available preprocessor. Boundary conditions are imposed on model symmetry. Degrees of freedom at the hole are specified as master degrees of freedom for the model. FATLAM is then run to generate the stiffness matrix for the complete lug in terms of these master degrees of freedom. Several additional files are generated which contain information about the boundary conditions, lamina properties, and the relationship between degrees of freedom at the hole and all other degrees of freedom. A two dimensional model of the pin is generated following the same procedure as that for the lug. Master degrees of freedom for the pin are defined for degrees of freedom which correspond to those of the lug and where loads will be applied.

The lug and pin substructures are coupled with contact/gap elements in STAFLM. Since the models have been condensed to include only the nodes at which contact is possible, the iterative contact problem runs very quickly. The output from STAFLM includes a binary file that contains the displacement solution for the master degrees of freedom. Finally, ply-by-ply failure analysis is performed by FATLAM employing this solution. Documentation and examples for the analysis can be found in Appendix 1. Comparisons with test results are summarized in Section 4.1. A 2-D analysis option was added to the existing 3-D finitie element program in order to reduce run times for initial evaluations. Input files for the 3-D analysis are not altered to run 2-D analysis; unused degrees of freedom are simply ignored. This 2-D option should provide an economic tool for preliminary studies since only a few minutes of CPU time are required.

2.4.2 Frame Elements – Several key issues were addressed during this phase of the building block approach. For the frame attachment elements, designs were sought which would be directly applicable to the subcomponent article and identified manufacturing methods. Key parameters in the design were investigated for their effect on strength and stiffness of the proposed designs. Implementation of new analysis techniques were targeted for use in the determination of failure loads and modes for design assessment and test prediction. And finally, potential joining methods for final frame attachments were identified.

A fastenerless moldline Y-frame attachment design was selected because it suited the diaphragm forming coconsolidation technique. The design was also anticipated to generate substantially greater strengths for pull-off and shear transfer due to the increased interlaminar shear and tension strengths associated with semicrystalline thermoplastic composites. The design therefore exploited both the mechanical and manufacturing strengths of the thermoplastic material system.

Design of the frame elements was carried out concurrently with efforts for subcomponent design (Section 2.3). Final configurations closely followed the panel designs in order to provide comparative test results. The layup consisted of identical outer-moldline (OML) and Y-section (IML) laminates: [+45/90/0/90/+45]. The inner and outer skin were to be coconsolidated during the diaphragm forming process. This initial element design resulted in a thinner skin section beneath the Y-frame than in the bay areas. The only design variable addressed thoroughly was the attachment angle of the two Y-frame legs. This geometric parameter controls the ratio of shear to flat-wise tension loading at the frame/skin interface. A 45° and 60° angle of incidence were established based upon initial parametric evaluations. Although initial analysis was unable to show a distinct difference in failure mode for these two geometries it did identify differences in the failures loads associated with each. The final designs incorporating the SDCC manufacturing method and the differing leg angles are shown in Figure 2.4.2-1.

In order to establish a baseline comparison, blade elements were also designed and analyzed. The blade configuration, Figure 2.4.2-2, incorporates back-to-back angle laminates which are identical in layup to the Y-section legs. The OML skin was chosen to be equivalent to the "bay skin" used in the Y-section, [+45/90/0/90/+45]s. This design yields a substantially stiffer skin section beneath the frame attachment, but it was chosen in order to maintain the critical stacking sequence in the corner radius and provide an identical skin laminate for the testing. The effects of this design on test results are detailed more fully in Section 4.2.

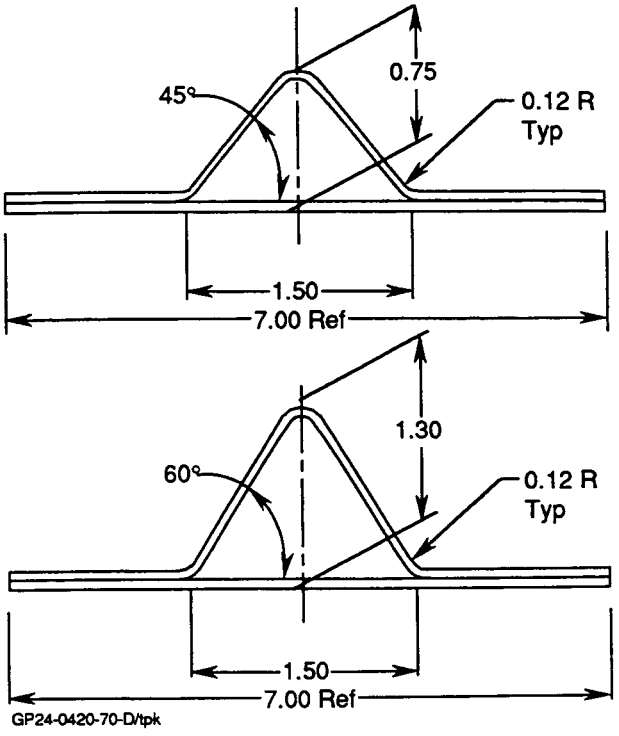

Figure 2.4.2-1. SDCC Fastenerless Frame Attachment Geometries

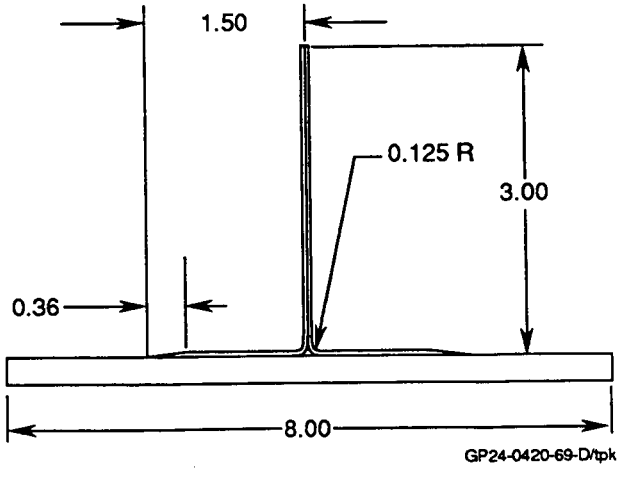

Figure 2.4.2-2. Baseline Co-consolidated Blade Design Configuration

Analysis of the frame designs for the pull-off testing was made using a specialized finite element package developed under MCAIR IRAD efforts. The Simplified Stiffener Analysis Model (SSAM) employs beam and membrane elements to model the skin and interface respectively (Figure 2.4.2-3). A quadratic failure criteria is then utilized to assess the normal and shear stresses which arise in the interface. This methodology was shown to provide excellent correlation to pull-off modeling of adhesively bonded hats (Figure 2.4.2-4) in Reference 7.

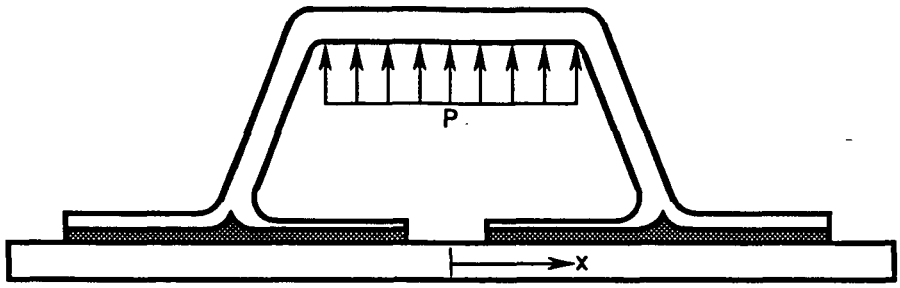

Hat Stiffener Under Direct Pull Off Load

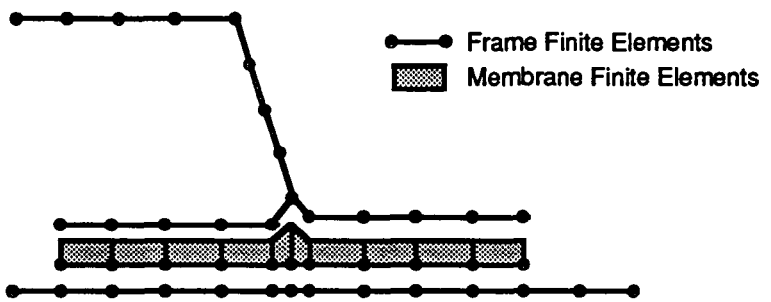

Simplified Finite Element Idealization of a Hat Section

GP24-0420-54-D/es

Figure 2.4.2-3. Simplified Stiffener Analysis Method (SSAM) Modeling

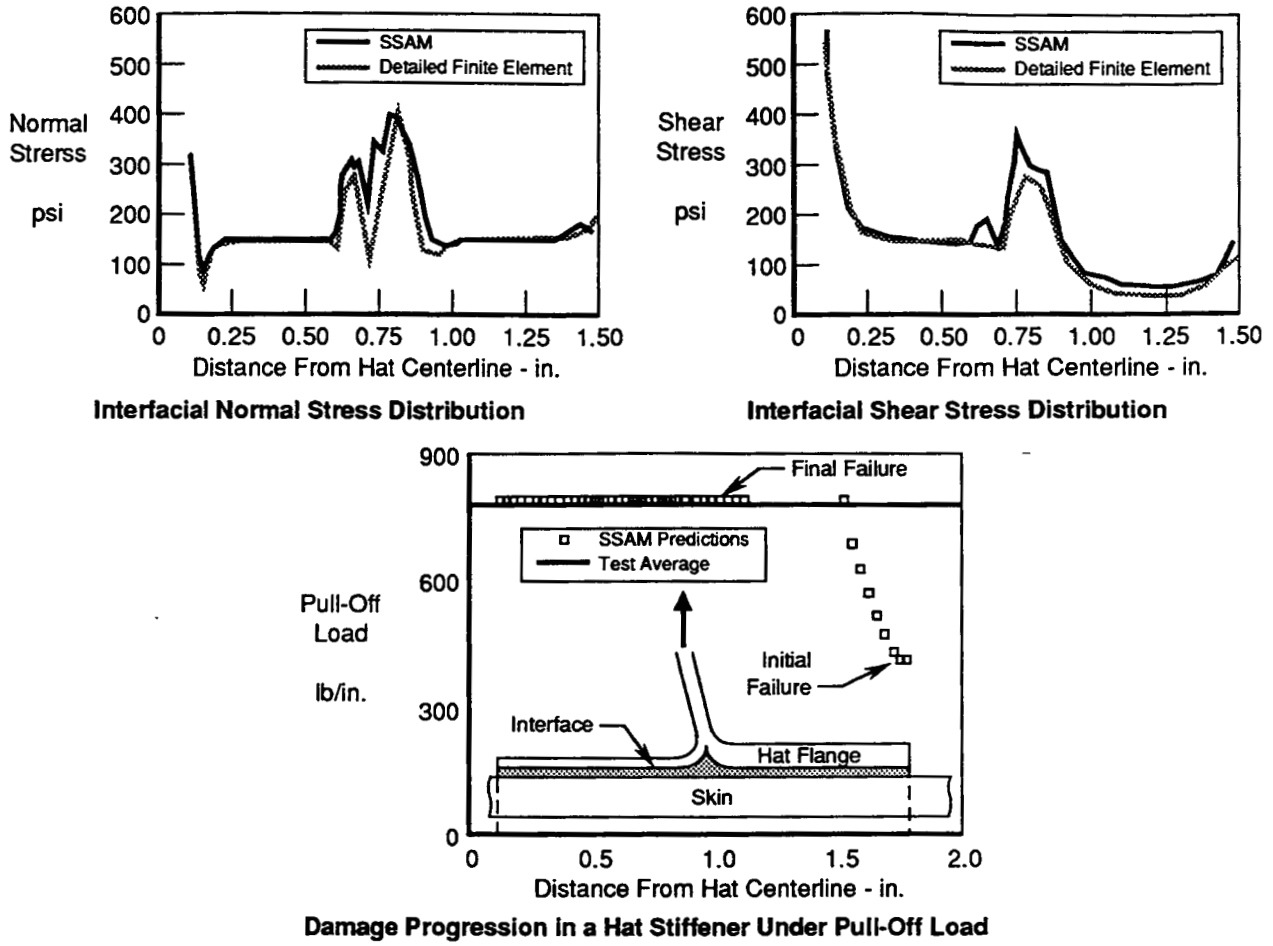

Figure 2.4.2-4. SSAM Correlation Study for Hat Pull-Off Testing

Due to the parametric representation used to define model geometry the method is not restricted to hats; analysis of the Y and blade sections was accomplished without difficulty. The modeling of the interface was the primary issue to be addressed in using the code to analyze coconsolidated structure. For typical bonded joints a scrim can be used to accurately control the thickness of the bondline; however, in the coconsolidation process a distinct bondline is not present. Initial attempts at modeling the bondline as a pure resin layer showed some thickness dependent variations in the calculated strains and failure loads. Examination of several photomicrographs taken during the initial manufacturing attempts for the SDCC process showed no distinctive separation in the upper and lower ply packs. For the purpose of setting test load limits a conservative analysis was used and initial results compared relative strength magnitudes only. The nominal thickness chosen for the original analysis was 0.0026 (50% ply thickness).

Finally, potential attachment concepts proposed for the frames were amorphous bonding, resistance joining, induction welding, adhesive bonding, coconsolidation, and mechanical fastening. Although the frame attachment design and testing was focused on assessing the coconsolidation process through pull-off testing, other potential attachments were assessed. Additional Y-frame elements were fabricated through the induction welding of the OML and Y-section laminates. The frame geometry was obtained by diaphragm forming the IML skin in the absence of an OML skin. The two skins were then joined employing the induction welding technique. These additional frame specimens were subjected to similar pull-off tests to assess their relative strength. The results of these tests are reported in Section 4.2.

THIS PAGE INTENTIONALLY LEFT BLANK

3. MANUFACTURING CONCEPTS DEVELOPMENT

3.1 Material Selection

3.1.1 Baseline Materials – The material chosen was based on temperature requirements, solvent resistance, component design, manufacturing approaches, and processing ease. Due to the 255°F design requirement, the baseline thermoplastic resin system selected was ITX (intermediate temperature crystalline), which has service capability to 300°F. ITX processing temperature and pressure ranges are 700°-750°F and 100-150 psi, respectively, processing conditions similar to ICI's APC-2 (PEEK) system. Amorphous systems were not considered due to their poor resistance to solvents such as jet fuel.

The fiber selected was IM7, an intermediate modulus fiber produced by Hercules. In addition, AS4/APC-2 was selected for early forming studies due to immediate availability and to verify analytical predictions for thick composite lugs. A summary of IM7/ITX and AS4/APC-2 mechanical properties is presented in Figure 3.1.1-1.

	AS-4/APC2		IM7/ITX	
Elastic Constants	RTD	ETW	RTD	ETW
E_1^t (msi)	18.5	18.5	23.5	23.4
E_1^c (msi)	18.4	18.4	21.2	21.1
E_2^t (msi)	1.37	1.30	1.32	1.17
E_2^c (msi)	1.51	1.41	1.51	1.46
n_{12}	0.35	0.35	0.30	0.30
G_{12} (msi)	0.74	0.49	0.79	0.70
Strength Allowables	RTD	ETW	RTD	ETW
F_1^t (ksi)	240	135	353	257
F_1^c (ksi)	185	125	159	105
F_2^t (ksi)	9.9	8.1	12.0	9.3
F_2^c (ksi)	31.0	17.2	31.0	22.6
F_s (ksi)	27.1	18.3	27.1	23.1-
F_{bru} (ksi)	99.5	70.0	99.0	72.0

Figure 3.1.1-1. IM7/ITX and AS4/APC-2 Mechanical Properties

3.1.2 New Resin Evaluation – Under this task, emerging thermoplastic resins were screened for state-of-the-art resin advancement. TPI was chosen, with NASA concurrence, based on it's high Tg of 485°F and good mechanical properties for further evaluation . The high Tg was expected to translate into a minimum service temperature of 400°F, significantly extending the temperature range of structural

thermoplastics. The resin was produced by Mitsui Toatsu and the prepreg was supplied by BASF in powdered form. Preliminary mechanical properties received from BASF are shown in Figure 3.1.2-1.

Typical Composite Properties

	RT Dry	350°F Wet	400°F Wet	–65°F	Unit	Test Method
0° Properties						
Compression Strength	160				KSI	ASTM D695
Compression Modulus	25.7				MSI	
Flexural Strength	213	132	116		KSI	ASTM D790
Flexural Modulus	21.8	21.7	20.9		MSI	
Tensile Strength	361				KSI	ASTM D3039
Tensile Modulus	24.6				MSI	
90° Properties						
Tensile Strength	8.9				KSI	ASTM D3039
Tensile Modulus	1.1				MSI	
+/– 45° Properties						
In Plane Shear Strength	18.8		13.2		KSI	SACMA SRM 7-88
In Plane Shear Modulus	0.58		0.40		MSI	
Compression After Impact						
Ultimate Stress	36.6				KSI	SACMA SRM 2-88
Modulus	8.4				MSI	
Strain to Failure	4,385				µin./in.	
Impact Energy	1,478				in. - lb/in.	
Edge Delamination						
Strength-First Failure	44.2				KSI	NASA 84592
Strength-Ultimate	86.4				KSI	
Open Hole Compression						
Strength	38.2		28.4		KSI	SACMA SRM 3-88
Modulus	8.8		7.7		MSI	
Strain to Failure	0.438		0.359		µin./in.	
Open Hole Tension						
Strength	65.3			65.3	KSI	SACMA SRM 5-88
Modulus	9.3			9.4	MSI	
Strain to Failure	0.701			0.687	µin./in.	

Fiber volume 58%
Fiber area/weight 145 g/m ^{2}

GP24-0420-58-D/bcb

Figure 3.1.2-1. Mechanical Properties of IM8/TPI (BASF Data)

The program objectives were to determine mechanical, environmental, and damage tolerance properties of the material. Also the processing capabilities for the low cost fabrication methods of fiber placement and diaphragm forming were to be established. Initially, panels were received from BASF for mechanical testing. With the exception of lower 0° compression strength, results were equivalent to the values supplied by BASF, Figure 3.1.2-2.

Test Type	Temp °F	Ultimate Strength psi	Initial Modulus psi x 10E6	Shear Strength psi	Shear Modulus psi x 10E6
0 Tensile	RT 420 D 420 W	120,800 99,300 96,500	22.6 23.1 23.6		
0 Tensile	-65 RT	389,700 363,100	25.9 25.3		
90 Tensile	RT 420 D 420 W	9,480 5,290 2,730	1.11 0.877 0.561		
±45 Inplane Shear	RT 420 D 420 W			23,100 14,600 14,300	0.611 0.376 0.215
Interlaminar Shear (SBS)	-65 RT 420 D 420 W			14,200 11,200 4,430 1,590	- - - -

GP24-0420-56-D/mld

Figure 3.1.2-2. Mechanical Properties of IM8/TPI

Five pounds of powdered, unidirectional IM8/TPI were obtained. IM7 fiber was preferred, but only prepreg containing IM8 fiber was available. Five panels, varying in thickness from 6 to 25 plies, were laid-up for material characterization. All panels were autoclave consolidated.

The panels were laid-up directly on the project plate due to the difficult handling characteristics of the material. Typically, material is laid-up on a flat plate and transferred to a project plate. However, when transfer was attempted the plies slipped. Spraying each ply with deionized water before laying the next ply kept the plies from shifting during lay-up. The panels were then dried at 200°F for one hour to remove the added water. The panels were consolidated using the processing cycle recommended by BASF, Figure 3.1.2-3.

All of the panels were poorly consolidated, especially the 25 ply panel. Panels and prepreg were analyzed using thermal mechanical analysis (TMA) to determine the cause of poor consolidation. BASF recommended a longer drying cycle of two hours and 50°F higher, or 250°F. They also recommended that the drying cycle be performed in the autoclave as part of the processing cycle. McDonnell Douglas Research Laboratories (MDRL) recommended an intermediate hold at 520°F to remove volatiles that might be forming. The cure cycle was modified to incorporate these recommendations.

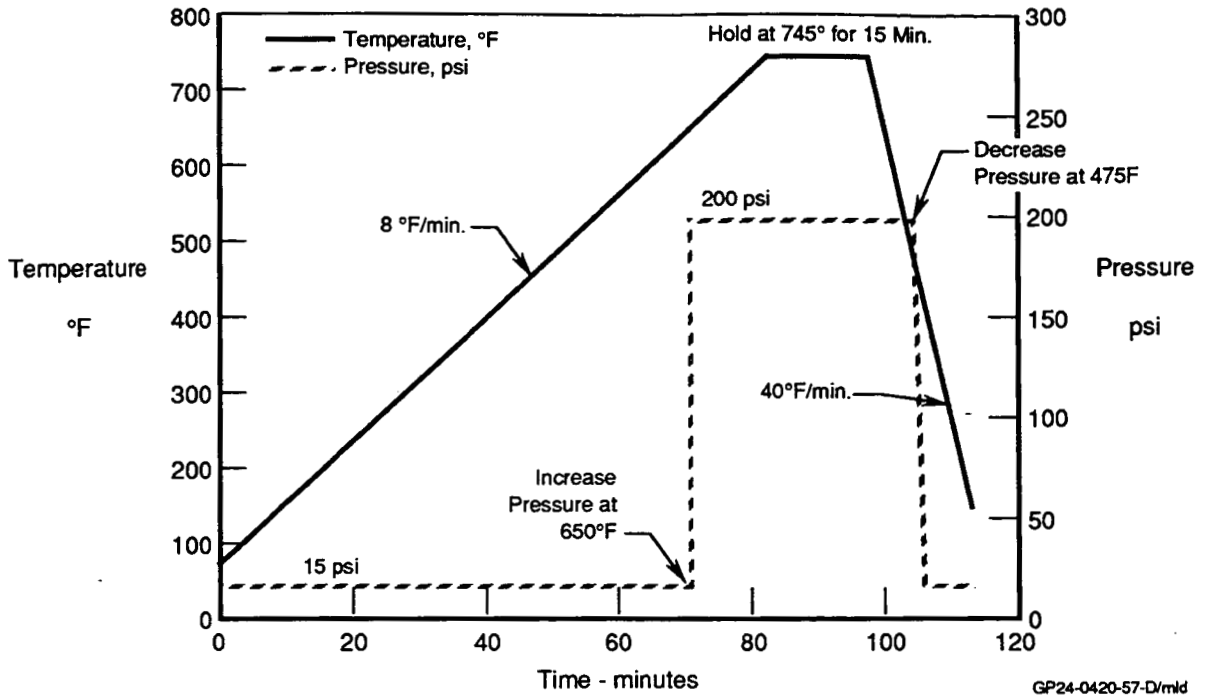

Figure 3.1.2-3. Processing Parameters for IM8/TPI

The modified cure cycle was used to reconsolidate 4 of the 5 panels fabricated. One panel, the 8 ply panel, was scrapped due to severe material distortion, and a new panel was substituted. The reconsolidated panels were better, but were still not of acceptable quality.

BASF stated that they were also unsuccessful in consolidating thick panels and the powdered version of TPI was being discontinued. Therefore, the processing development of powdered TPI was halted.

3.2 Process Selection

3.2.1 Trade Study – A trade study to determine optimal manufacturing concepts to produce innovative and cost-effective fuselage cover structure with a high potential for use of these concepts on the remaining fuselage section was performed. The baseline cover designs were used to evaluate manufacturing processes and a numerical evaluation analysis was utilized to select two manufacturing approaches. Following is a description and results of the analysis.

Concepts for Manufacturing Processes, Design Options, Material Forms, and Joining Techniques were developed. These concepts were inserted into several two-dimensional selection arrays as illustrated in Figure 3.2.1-1. Concepts were eliminated based on the following rationale.

Manufacturing Process	Structural Details							
	Stiffeners						Skin	Fillets
	Z	J	T	Hat	I	C		
Roll Form	x	x	x	x	x	x		x
Fiber Placement						x	x	
Diaphragm Form	x		x	x		x	x	x
Thermoform	x		x	x		x	x	x
Pultrude	x	x	x	x	x	x		x
Autoclave	x	x	x	x	x	x	x	x
Comp. Mold	x	x	x	x	x	x	x	x

Material Forms	Manufacturing Process						
	Roll Form	Fiber Place	Diaph'm Form	Thermo-form	Pultrude	Auto-Clave	Comp. Mold
Uni-Tape	x	x	x	x	x	x	x
Woven Preform (1)	x		x	x	x	x	x
Braided (2)	x		x	x	x	x	x
Commingled (3)	x		x	x	x	x	x
Quadrax (3)	x		x	x	x	x	x
Tow		x					
Chopped Fiber							x
Preconsolidated Sheet	x		x	x		x	x

Assembly Techniques
Coconsolidation
Amorphous Bond
Adhesive Bond (4)
Ultrasonic Bond
Resistance Join (5)
Fasteners (6)

Not a viable process

x Candidate processes

Processes considered for Upper Cover structure

Notes:

1. Bulking problems
2. No advantage over other material systems
3. Alternate to uni-tape material applications
4. Insufficient strength due to surface preparation
5. Technology immature
6. Added weight, potential leak path

Figure 3.2.1-1. Viable Manufacturing Processes, Material Forms, and Assembly Techniques Were Selected as Candidates for the Upper Cover

MANUFACTURING PROCESSES ELIMINATION RATIONALE:

Pultrusion – Pultrusion was considered for stiffener fabrication, but was eliminated when compared to roll-forming. Pultrusion and roll-forming currently have the same limitations, constant cross section and/ or constant curvature. Based on observations of part quality between the two processes, roll-forming appeared to be a more desirable technology for higher pressure consolidation.

DESIGN CONCEPT ELIMINATION RATIONALE:

"Z" and "C" Stiffeners – These stiffeners were eliminated because they experience severe out-of-plane effects due to burst pressure and hydrodynamic ram loads. These stiffeners do not allow for attachment flange tailoring to reduce peel stresses.

"T" Stiffener – The evaluation team concurred that the "T" type design, lacking a flange, would not have sufficient stiffness to provide bending rigidity under pressure loads. Adding a flange results in either a "J" or "I" type stiffener. In addition it is more cost-effective to fabricate a "J" or "I" stiffener.

MATERIAL FORMS ELIMINATION RATIONALE:

Chopped Fiber – This material was considered only for compression molding fillets. In addition, chopped fiber for these applications provides a desirable method of utilizing scrap thermoplastic composite materials. Inherent weakness in strength and stiffness prevent the use of this material in other primary structural areas.

Braided Preform – Braided preforms were eliminated because they lack the design adaptability of woven preforms. In addition, braided laminates are weaker than woven laminates.

JOINING CONCEPT ELIMINATION RATIONALE:

Resistance Bonding – The resistance bonding technique has manufacturing potential. However, resistance bonding at the time of process selection was not considered production worthy nor was it expected to be production worthy in time for subcomponent fabrication.

Fasteners – Utilization of fasteners is a proven assembly technique that represents very little innovativeness and risk. Fasteners were not a primary assembly technique, but fasteners would be resorted to if the higher risk more innovative concepts did not prove to be flight worthy.

The arrays shown in Figure 3.2.1-1 were then utilized to determine potential cover concepts. All potential candidates were compiled for numerical evaluation, Figure 3.2.1-2.

	Skin	Stiffener	Assembly	Comments
1	Fiber Place	Roll Form "J"	Co-Consolidate	Co-Consolidate During Fiber Placement
2	Fiber Place	Roll Form "J"	Amorphous	
3	Fiber Place	Roll Form "J"	Ultrasonic	
4	Fiber Place	Roll Form Hat	Co-Consolidate	Co-Consolidate During Fiber Placement
5	Fiber Place	Roll Form Hat	Amorphous	
6	Fiber Place	Roll Form Hat	Ultrasonic	
7	Fiber Place	Roll Form "I"	Co-Consolidate	Co-Consolidate During Fiber Placement
8	Fiber Place	Roll Form "I"	Amorphous	
9	Fiber Place	Roll Form "I"	Ultrasonic	
10	Fiber Place	Thermoform Hat	Co-Consolidate	Co-Consolidate During Fiber Placement
11	Fiber Place	Thermoform Hat	Amorphous	
12	Fiber Place	Thermoform Hat	Ultrasonic	
13	Diaphragm Form	Roll Form "J"	Co-Consolidate	Co-Consolidate in Autoclave
14	Diaphragm Form	Roll Form "J"	Amorphous	
15	Diaphragm Form	Roll Form "J"	Ultrasonic	
16	Diaphragm Form	Roll Form Hat	Co-Consolidate	Co-Consolidate in Autoclave
17	Diaphragm Form	Roll Form Hat	Amorphous	
18	Diaphragm Form	Roll Form Hat	Ultrasonic	
19	Diaphragm Form	Roll Form "I"	Co-Consolidate	Co-Consolidate in Autoclave
20	Diaphragm Form	Roll Form "I"	Amorphous	
21	Diaphragm Form	Roll Form "I"	Ultrasonic	
22	Diaphragm Form	Thermoform Hat	Co-Consolidate	Co-Consolidate in Autoclave
23	Diaphragm Form	Thermoform Hat	Amorphous	
24	Diaphragm Form	Thermoform Hat	Ultrasonic	
25	Diaphragm Form	Diaphragm Form	Co-Consolidate	Co-Consolidate During Diaphragm Form
26	A/C Consolidate	Roll Form "J"	Co-Consolidate	Co-Consolidate in Autoclave
27	A/C Consolidate	Roll Form "J"	Amorphous	
28	A/C Consolidate	Roll Form "J"	Ultrasonic	
29	A/C Consolidate	Roll Form Hat	Co-Consolidate	Co-Consolidate in Autoclave
30	A/C Consolidate	Roll Form Hat	Amorphous	
31	A/C Consolidate	Roll Form Hat	Ultrasonic	
32	A/C Consolidate	Roll Form "I"	Co-Consolidate	Co-Consolidate in Autoclave
33	A/C Consolidate	Roll Form "I"	Amorphous	
34	A/C Consolidate	Roll Form "I"	Ultrasonic	
35	A/C Consolidate	Thermoform Hat	Co-Consolidate	Co-Consolidate in Autoclave
36	A/C Consolidate	Thermoform Hat	Amorphous	
37	A/C Consolidate	Thermoform Hat	Ultrasonic	
38	Thermoform	Roll Form "J"	Co-Consolidate	Co-Consolidate in Autoclave
39	Thermoform	Roll Form "J"	Amorphous	
40	Thermoform	Roll Form "J"	Ultrasonic	
41	Thermoform	Roll Form Hat	Co-Consolidate	Co-Consolidate in Autoclave
42	Thermoform	Roll Form Hat	Amorphous	
43	Thermoform	Roll Form Hat	Ultrasonic	
44	Thermoform	Roll Form "I"	Co-Consolidate	Co-Consolidate in Autoclave
45	Thermoform	Roll Form "I"	Amorphous	
46	Thermoform	Roll Form "I"	Ultrasonic	
47	Thermoform	Thermoform Hat	Co-Consolidate	Co-Consolidate in Autoclave
48	Thermoform	Thermoform Hat	Amorphous	
49	Thermoform	Thermoform Hat	Ultrasonic	

GP24-0420-59-D/rdm

Figure 3.2.1-2. Candidate Upper Cover Concepts

The numerical evaluation criteria was determined as follows by averaging inputs from the evaluation team:

Criteria	Weight Factor
Innovativeness	10
Cost	8.5
Risk (Manufacture)	4.5
Supportability	6
Survivability	6.5
Weight	5.5

Each of the above criteria was given a rating of 1 to 10 for each of the potential concepts. The weighting factors were applied to these values with the top ten concepts shown in Figure 3.2.1-3.

Of the top four concepts, three were basically the same with various shaped, roll-formed stiffeners coconsolidated to a fiber placed skin. The hat-section concept was selected on the basis of manufacturing cost, structural integrity, and supportability.

The second concept selected involved an innovative diaphragm forming manufacturing process. This concept incorporates coconsolidation into the diaphragm forming process to provide an innovative, one-step process for forming of a stiffened skin.

Concept	Skin	Stiffener	Assembly	Comments	Score (1)
7	Fiber Place	Roll Form " I "	Co-consolidate	Co-con during F. P.	2615
1	Fiber Place	Roll Form " J "	Co-consolidate	Co-con during F. P.	2599
4	Fiber Place	Roll Form Hat	Co-consolidate	Co-con during F. P.	2531
19	Diaphragm Form	Roll Form " I "	Co-consolidate	Co-con in Autoclave	2491
13	Diaphragm Form	Roll Form " J "	Co-consolidate	Co-con in Autoclave	2466
10	Fiber Place	Thermoform Hat	Co-consolidate	Co-con during F. P.	2440
38	Thermoform	Roll Form " J "	Co-consolidate	Co-con in Autoclave	2428
44	Thermoform	Roll Form " I "	Co-consolidate	Co-con in Autoclave	2427
25	Diaphragm Form	Diaphragm Form	Co-consolidate	Co-con during D. F.	2417
16	Diaphragm Form	Roll Form Hat	Co-consolidate	Co-con in Autoclave	2416

Selected Concepts for Upper Cover Subcomponent Verification.
Stiffener Selection for Fiber Placement Concept Still in Evaluation.

Notes:

1. See breakdown in figure below.

Concept	Innovative-ness	Cost	Risk	Scale-up	Support-ability	Surviv-ability	Weight	Total
7	680	434	207	324	436	242	293	2615
1	680	417	207	324	429	242	300	2599
4	675	425	209	324	306	281	311	2531
19	570	459	234	264	423	245	296	2491
13	570	459	216	264	416	245	296	2466
10	600	425	212	306	299	283	315	2440
38	490	429	257	294	423	239	296	2428
44	490	429	257	294	429	239	289	2427
25	690	442	194	204	267	314	308	2417
16	565	468	236	264	293	283	308	2416

Figure 3.2.1-3. Concepts for Upper Cover Structure Were Selected Using a Design/Manufacturing Integration Approach

3.2.2 Producibility Analysis – A producibility analysis, Reference 8, was performed to determine the cost-effectiveness of the selected processes compared to thermoset composite and metallic approaches. The analysis was conducted on the fuel cover design and included the hat-stiffened skin and local peripheral build-ups for direct comparison to subcomponent cost tracking.

The thermoplastic composites were considered for three approaches: the two selected for this effort, (single diaphragm coconsolidation (SDCC) and fiber placement) and manual lay-up. A titanium superplastic formed diffusion bonded (SPF/DB) design and a manual lay-up of toughened bismaleimide (BMI) were used for comparison.

SDCC employs a pressure box to consolidate the outer skin while at the same time forming and consolidating the inner stiffened pan. Fiber placement, uses a tow placement process over preformed hat stiffeners recessed into a fiber placement tool. The manual lay-up approach used unidirectional and comingled material forms.

The baseline toughened BMI thermoset composite (TSC) design utilized rubber mandrels and female tooling to produce a cocured structure. In addition, the TSC design included stitching of the stiffeners to increase stiffeners-to-skin interface strength. A titanium superplastic formed/diffusion bonded design was the metal option. Diffusion bonding allows the economical creation of high performance hat stiffened skins without fasteners.

The analysis explored the impact of component complexity on producibility and cost. Two levels of complexity were considered. The fuel cell cover is a single curved component. A producibility analysis of this generic cover was established to serve as a baseline. A complex, doubly curved version of the cover was also considered since OML fighter skins are typically complex surfaces.

High processing temperatures for thermoplastic composites (750°F, 385°C) imposed two major fabrication constraints; (1) flexible rubber mandrels (for hat stiffener tooling) can not be used since they are unable to survive the processing temperatures and, (2) high temperature tooling is required instead of aluminum tooling. The influence of these constraints for both recurring and non-recurring costs were considered. Each fabrication approach listed above was evaluated in order to identify the best technique.

Recurring component costs were generated by summing material and labor costs for each step of process plans for each fabrication approach. Labor costs were burdened to include equipment/facilities costs. Non-recurring costs took into account tooling expenses including any duplicate tooling required to produce the theoretical rate of 85 ship sets per year (600 aircraft total). Cost comparisons for this study were normalized; the least expensive simply curved approach is set equal to one with the cost of other options appropriately ratioed.

The cost study results for both complex and simply curved components showed that the SDCC approach was most cost-effective for the cover due to flat ply collation and short cycle times, Figure 3.2.2-1. TPC fiber placement was the next most cost-effective approach due to automated processing of the skin. Although TPC's are difficult to manually lay-up, this process is less expensive than TSC manual lay-up due in part to the stitching required with TSC in order to increase hat pull off strength. Titanium SPF/DB and TSC were close in recurring cost due to the labor intensive operations required for these approaches. As expected, the recurring cost of fabricating complex structure was consistently higher then simple structure.

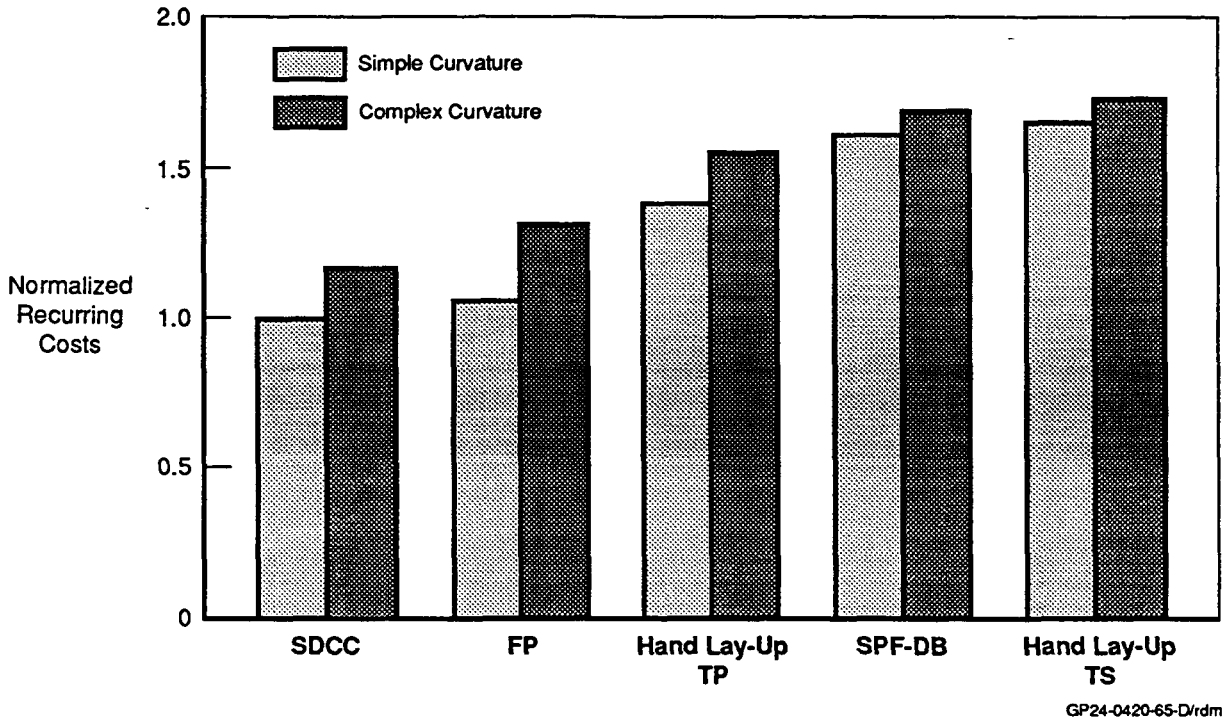

Figure 3.2.2-1. Recurring Cost Comparisons Indicate Potential Cost Savings for Selected Manufacturing Approaches

Non-recurring costs (tooling) for the fabrication approaches showed that duplicate tooling requirements for TSC and TPC manual lay-up increases their respective tooling costs to a level comparable to the other fabrication approaches, Figure 3.2.2-2. Even with duplicate tooling, non-recurring costs for simply curved TSC and TPC are the least expensive options. Five-axis machining requirements for tooling on complex curved manual lay-up TSC and TPC approximately doubles their respective non-recurring costs. Although press forming and fiber placement tooling costs are identical for simply curved applications, a substantial cost increase is incurred in press forming versus fiber placement costs for complex curvature. This increase is attributed to difficult machining requirements (five-axis) for not only the press forming tool but also for the associated pressure box. High temperature matched metal steel tools must be supplied for the titanium SPF/DB approach resulting in the highest tooling costs of any approach.

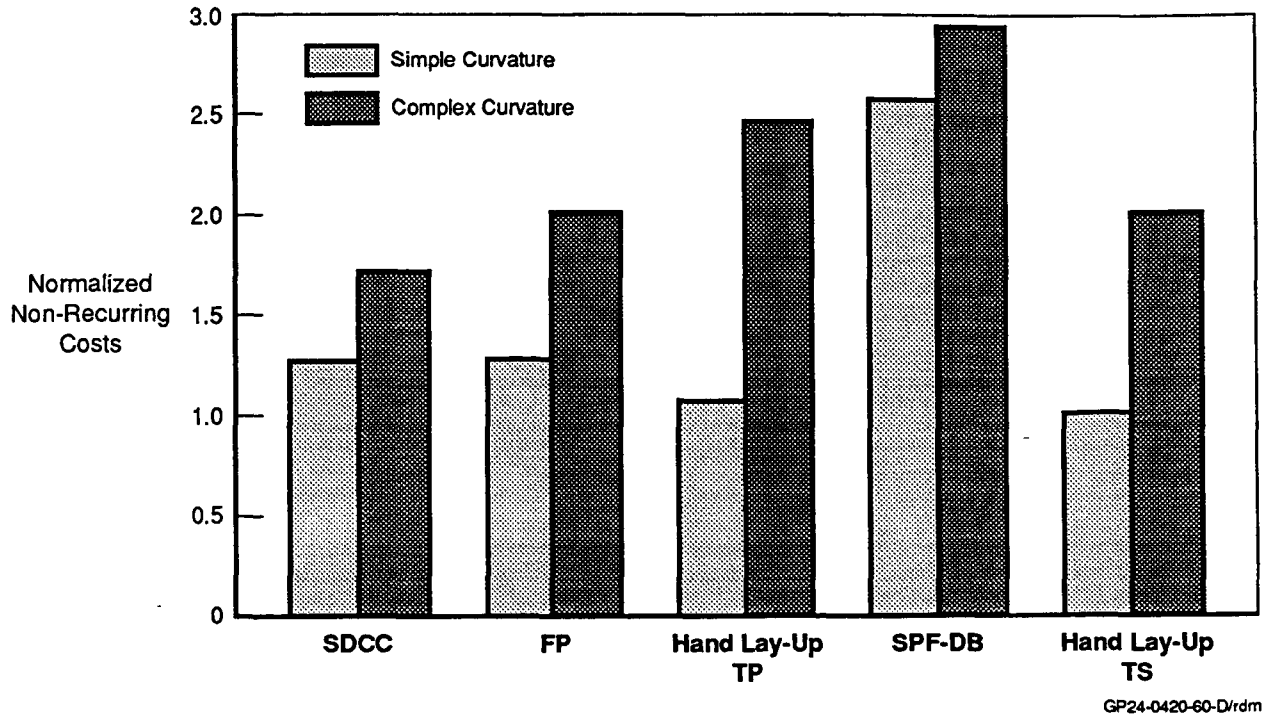

Figure 3.2.2-2. Non-Recurring Cost Comparisons Indicate Potential Cost Savings for Selected Manufacturing Approaches

3.3 Fabrication Development

3.3.1 Subcomponent Concepts – The fiber placement manufacturing process concept consisted of roll-forming of the hat stiffeners, inverting and placing them into an aluminum fiber placement tool, Figure 3.3.1-1. Aluminum mandrels are placed in the hat stiffeners to prevent skin deflection during the fiber placement process. Retainers are utilized to hold the stiffeners and mandrels in place during processing. The hat is positioned in the tool as shown in Figure 3.3.1-2. The hat flange is off-set slightly above the aluminum tool to allow for adhesive and the first ply. Also, a heat blanket is embedded into the aluminum tool that supports the preformed thermoplastic composites stiffeners to minimize heat dissipation away from the nip point. Following fiber placement of the skin, the panel is trimmed and retainers removed. The mandrels are then removed and the part prepared for nondestructive testing.

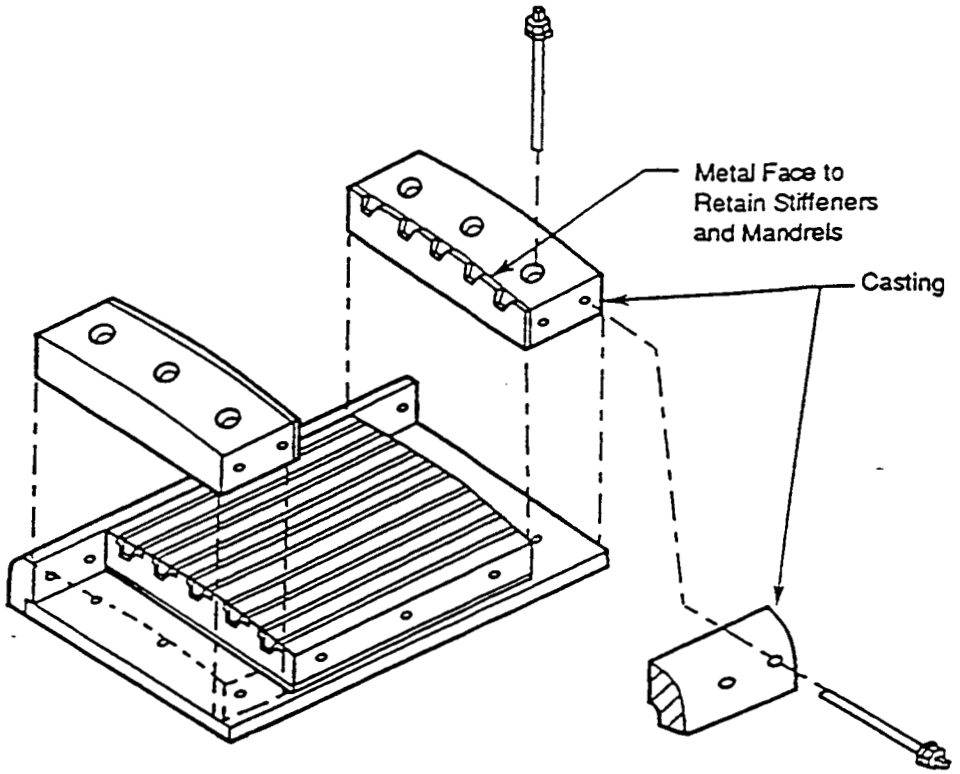

Figure 3.3.1-1. Fiber Placement Tooling Accommodates Embedded Stiffeners for "On-the-Fly" Coconsolidation

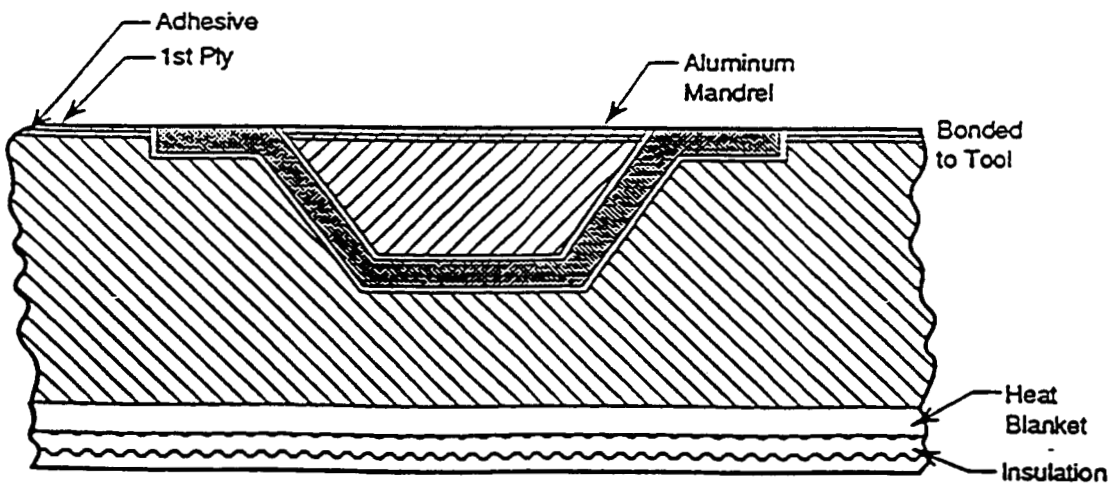

Figure 3.3.1-2. Hat Stiffener Embedded in Fiber Placement Tool

The SDCC concept is unique in that there is but one diaphragm, and the IML pan and OML skin are coconsolidated during the diaphragm forming process. The SDCC tooling concept is illustrated in Figure 3.3.1-3. A vacuum frame is utilized to hold the IML ply pack prior to heat-up and pressurization. Bridging is the greatest risk in diaphragm forming over hat mandrels. To reduce this risk, wide hat spacing is used to increase ply surface area between mandrels. The increased surface area increase the forces

exerted to form the ply pack and prevent bridging. In addition, the mandrels are fabricated with a slight radius, Figure 3.3.1-4. The gap between the mandrel, OML skin and IML pan are filled with a predetermined amount of unidirectional tow. This fillet area has the highest probability for bridging, however, with the unidirectional fillet, the pressure will be equally distributed to facilitate a quality consolidation.

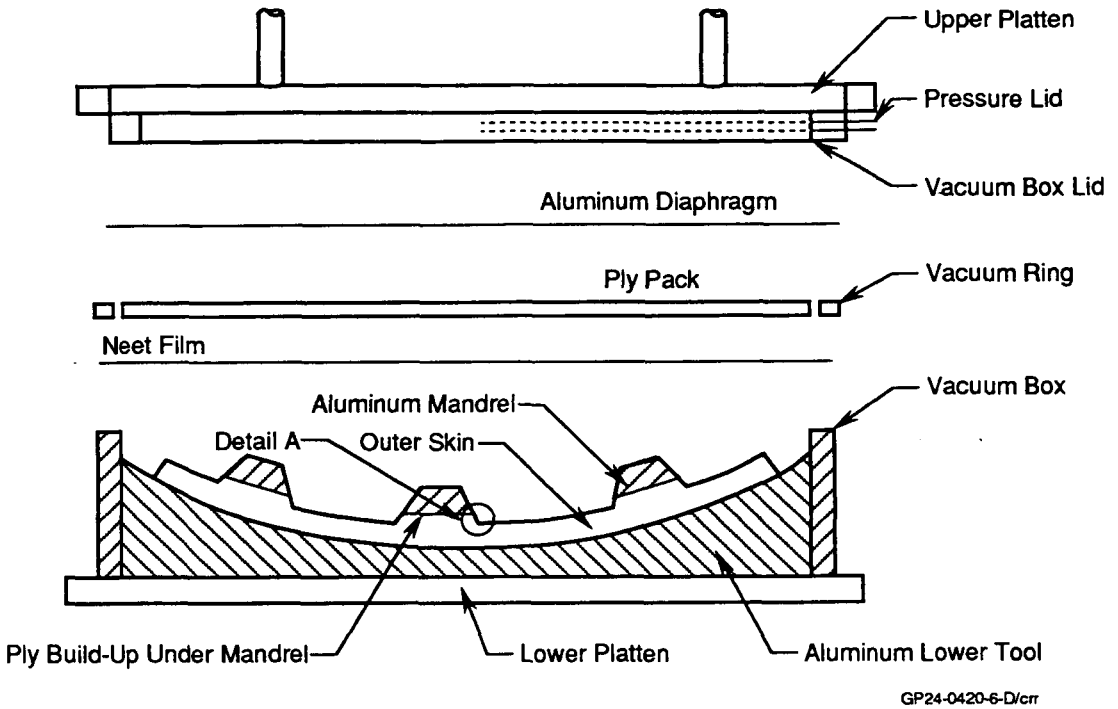

Figure 3.3.1-3. Single Diaphragm Coconsolidation (SDCC) Tooling Concept

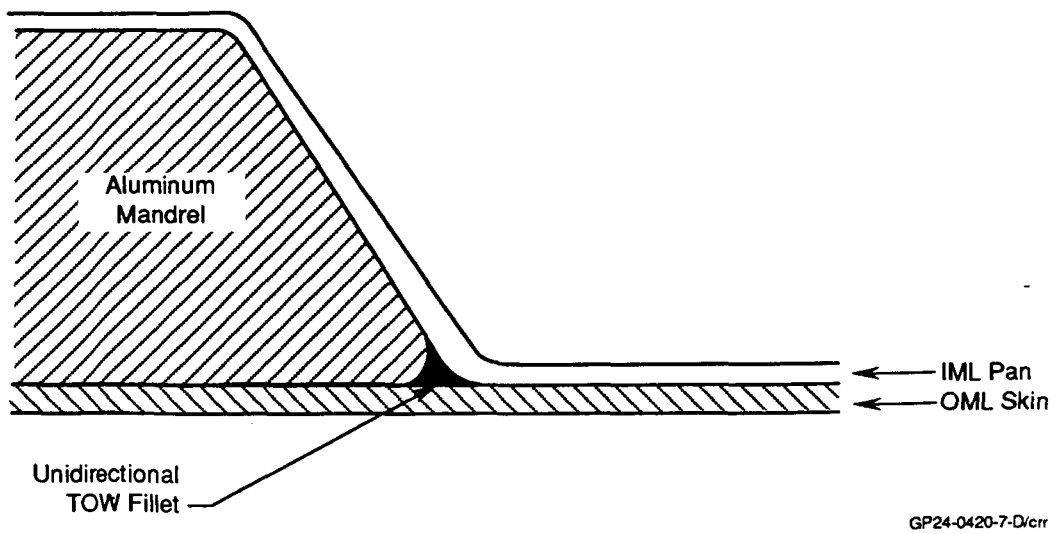

Figure 3.3.1-4. Unidirectional Tow Used in Fillet Area to Assure Part Quality

A vacuum ring and a neat film layer aid in ply pack location. The IML ply pack are contained between the aluminum diaphragm and a layer of neat film. A vacuum ring surrounds the IML ply pack and vacuum draws the aluminum diaphragm to the upper surface of the IML ply pack, and the neat film to the lower surface of the IML ply pack. The IML ply pack is then positioned above the tool prior to application of heat and pressure. The neat film is coconsolidated between the IML and OML ply packs during the press operation. This permits accurate location of the IML ply pack and aids in the prevention of wrinkles.

Concepts for the subcomponent tool included machined steel weldment, cast bulk ceramic, machined aluminum, and a metal arc sprayed tool. A metal arc sprayed tool which could accommodate integral heating, faster cycle times, and low tool cost for production-type environments showed high potential for this program.

3.3.2 SDCC Y-Frame Elements – An SDCC element verification tool, Figure 3.3.2-1, was developed which incorporated either two hat mandrels or a single triangular mandrel to simulate fabrication of subcomponent stiffener and frame design, respectively. The entire tool was located in a vacuum forming box to facilitate the SDCC manufacturing process.

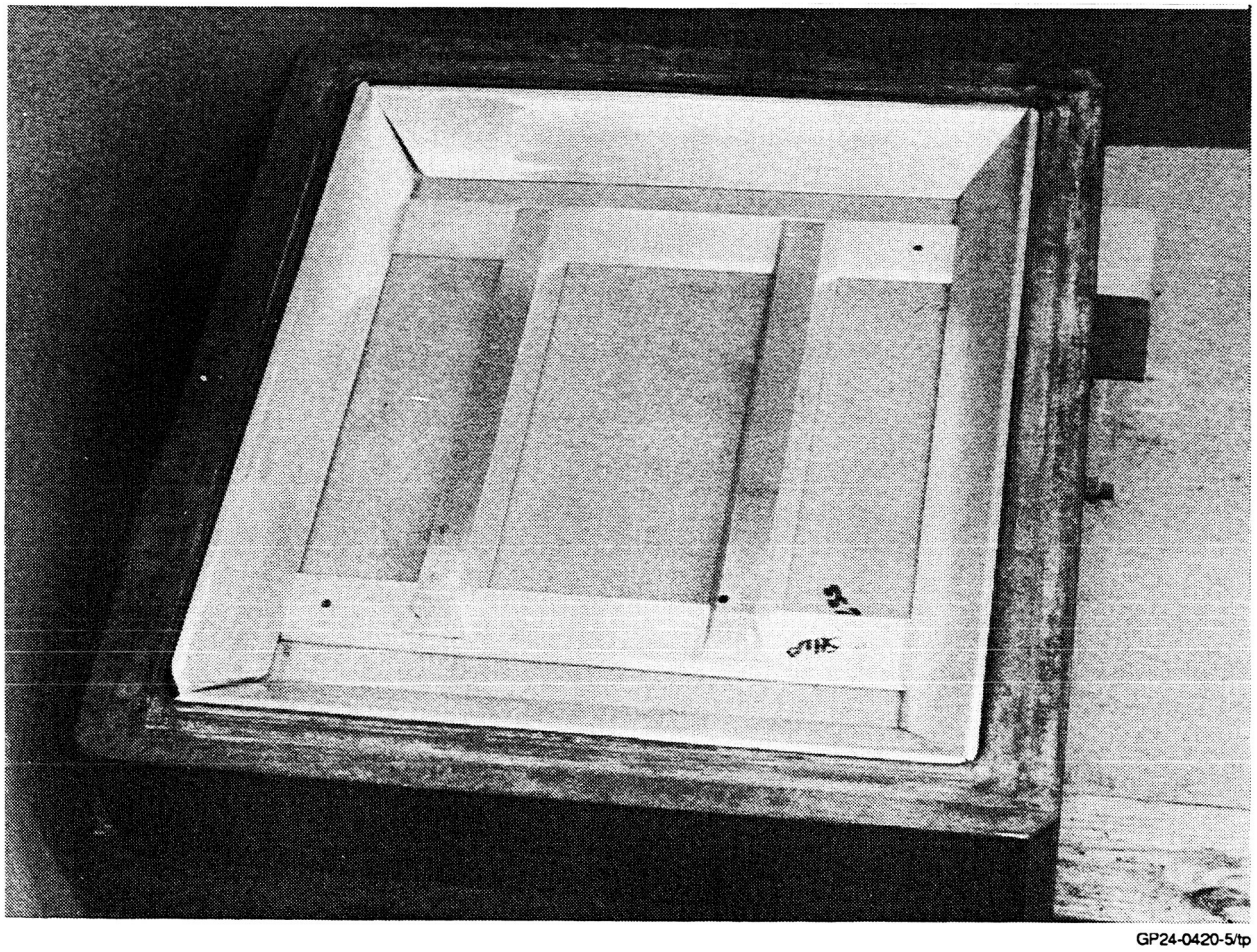

GP24-0420-5/tp

Figure 3.3.2-1. SDCC Element Verification Tool Incorporated Full Scale Design Features

The verification tool was first utilized as a parallel hat-section tool to verify subcomponent fabrication. The hat dimension, spacing, height, and width simulated preliminary subcomponent design. The hat stiffener mandrels, located by pins, float on the unconsolidated skin. The inner skin was then formed over the mandrels in a press operation. A pinning arrangement allows the mandrels to float during consolidation. These pins permit the consolidation force to be transferred through the mandrels to the part to insure a quality consolidation. The aluminum tools were readily extracted following forming.

During initial hat-section forming using a seven ply laminate representative of the subcomponent design, bridging of the ply stack occurred at the deepest point of draw of the base of the hat web. A limited amount of interplay slip was also noted during these trials. In addition, to minimize diaphragm rupture due to sharp corners, the tooling was modified by extending the mandrels to the ramps of the forming box, Figure 3.3.2-2.

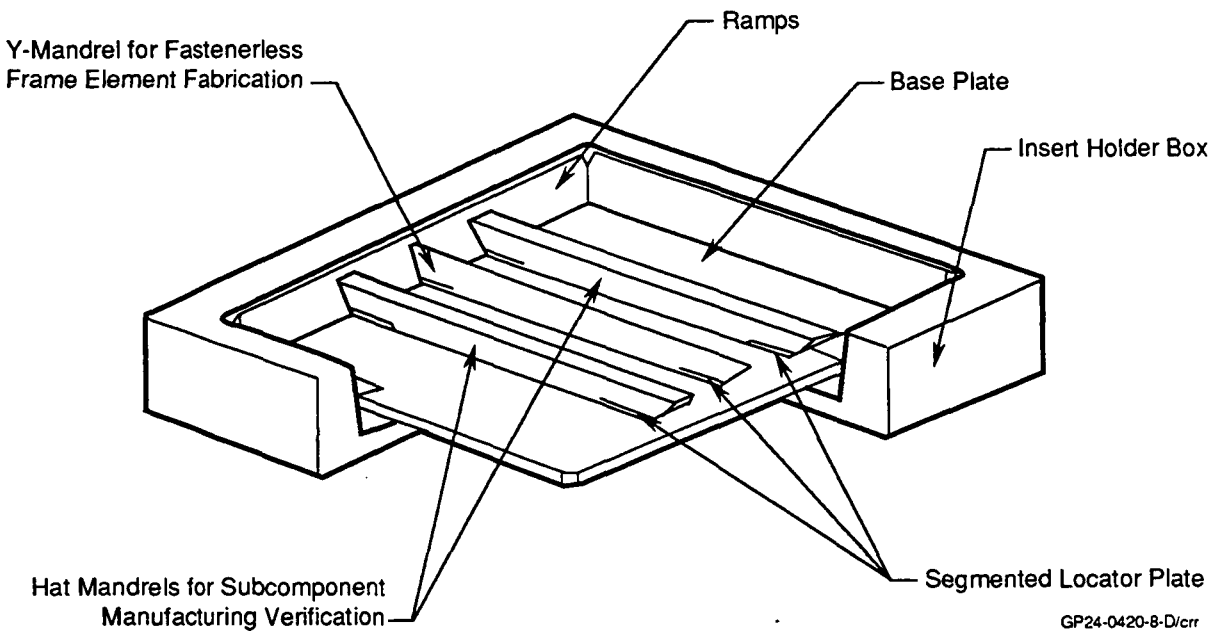

Figure 3.3.2-2. Modified SDCC Element Tool Extended Mandrels to Minimize Diaphragm Rupture

As a result of forming tests, the angle of the hat web-lower skin intersection was increased to smooth the transition from skin surface up to the cap of the hat. This geometric change was incorporated into the subcomponent design. Bridging tendencies of the ply stack were minimized by this configuration change. New hat mandrels were designed and fabricated.

Process parameters used on the first forming trials were reviewed and adjustments made. Application of full pressure was delayed until after the plies had reached melt temperature instead of just before melt. This allows the matrix to reach its minimum viscosity before forming is initiated. Previously, pressure was introduced prior to melt temperature to encourage interply slippage between the upper and lower ply packs. Due to the bridging observed on the room temperature forming trials, it was decided that forming

depth would be improved if the ply pack was at full melt temperature. Interply slip may still occur, due to the effects of the lubricant between matrix layers.

Due to program redirection, hat-section forming trials were discontinued and attention concentrated on forming of the Y-frame elements. Lessons learned from the hat-section trials were incorporated into this effort.

Forming trials on the single "Y" configuration used one diaphragm to consolidate the upper ply pack with the lower plies. Initially, full pressure (150 psi) was applied after the melt temperature of the ITX was reached, but it was maintained for only 5 minutes before the diaphragm ruptured. In spite of the short hold time the pressure was sufficient to fully consolidate the flat areas of the part and to form the material over the mandrel. The upper ply pack conformed to the mandrel surface, but diaphragm rupture caused the outer ply to lift and bridge across the mandrel/skin intersection. The other plies remained in the formed condition, nesting closely to the mandrel and showed an excellent definition at the interface between stiffener web and lower skin.

Forming was next done below melt temperature because of anticipated problems where the two ply packs met each other beyond the stiffener area. For the next trial full melt temperature was achieved before pressurizing. The upper ply pack was also widened so it extended out to the ramps in all directions. This change required notches to be cut along the edge of the ply pack so it wouldn't buckle and rupture the diaphragm. Kapton tape was used to cover the notches for additional protection.

Forming trials were performed with the noted changes and the diaphragm survived fairly well up through 150 psi. Since the plies were well melted by this time, relatively good consolidation was achieved between the upper and lower packs. Rupture occurred along the edge of the mandrel in a notch location that allowed the film to over elongate. A large percent of the plies remained formed to the mandrel surface along its base. Only one ply lifted and bridged away from the radius area of the formed plies, Figure 3.3.2-3. The inside of the stiffener shape revealed very good contact between the plies being formed and the base of the mandrel even with loss of the diaphragm. Photomicrographs of the area revealed the upper plies dragged the lower plies in toward the mandrel and formed wrinkles in the lower skin.

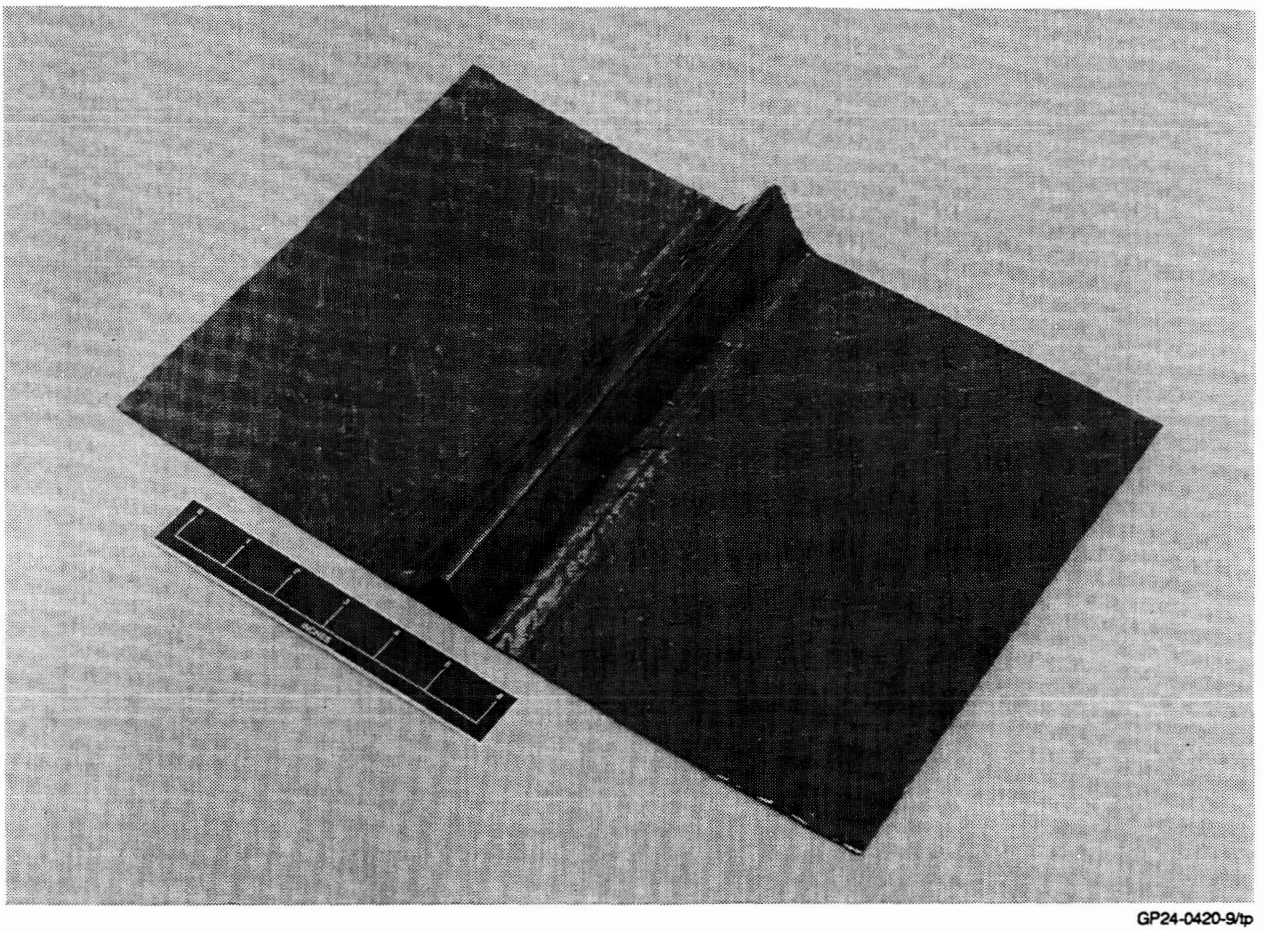

GP24-0420-9/tp

Figure 3.3.2-3. Initial Y-Frame Element Experienced Bridging in the Radius

In an attempt to alleviate dragging of the base ply pack, the upper ply of the base pack was extended to run under the ramp areas of the tool. This change would maintain pressure on the top ply to allow slippage of the two ply packs without wrinkling. Also, a fiber glass cloth, (picture frame), was placed around the ramp areas and over the mandrel to cover any areas that could potentially allow the diaphragm to rupture. An additional change to the process was to initiate application of the forming pressure at 600°F. The rational was to apply pressure below melt-temperature of the material, to allow ply slippage prior to a viscosity change. During this run the diaphragm ruptured in a gap between the ramp and forming box causing incomplete forming of the element. However, improved ply slippage was noted due to the reduced temperature.

Due to the frequency of rupture of the UPILEX diaphragms, an aluminum (SUPRAL) diaphragm was selected for further trials. The aluminum diaphragm offered greater elongation capabilities not only at processing temperatures, but also at temperatures below the melt temperature of the PEEK resin.

During the first run with an aluminum diaphragm, the pressure was applied at 550°F. Applying the pressure at this low temperature allowed for additional ply slippage prior a viscosity change of the resin. During this fabrication attempt, the top ply of the lower ply pack was extended beneath the forming ramps in an attempt to "lock" the ply in place, thus avoiding wrinkles. After applying pressure (120 psi) at 550°F, the temperature was increased to 750°F and held for 30 minutes.

The result was a stiffened panel with good surface quality but bridging in the radius. NDE results revealed a porosity free part in the flat areas. However, photomicrographs revealed the lower ply pack wrinkled. Since the upper ply of the lower ply pack wrinkled, and the ends were contained beneath the forming ramps, the ply obviously split between the fibers of this outer 45° ply.

Following review of the results of the run, two changes to the manufacturing process were identified to alleviate the wrinkling problem in the next run. First a .003" layer of neat resin was applied to the bondline to serve as lubricant. The film would allow the two contacting plies to slip past each other and form in the radius area. A photomicrograph of the radius area following processing utilizing the neat resin is presented in Figure 3.3.2-4. As can be seen, radius cracking and bridging is present along with wrinkling in the lower ply pack. 0° plies were then added at the interface to allow the inner and outer ply packs to more readily slip past one another. The results revealed similar problems as noted with the neat resin.

To overcome friction between the two surfaces, it was decided that the upper ply pack should be driven into the radius areas prior to reaching the glass transition temperature. This would allow the plies to slip past one another prior to a viscosity change. To accomplish this, the upper ply pack was preconsolidated and then coconsolidated to the lower ply pack in a second operation. With this approach the risk level is significantly reduced while maintaining a major processing cost reduction.

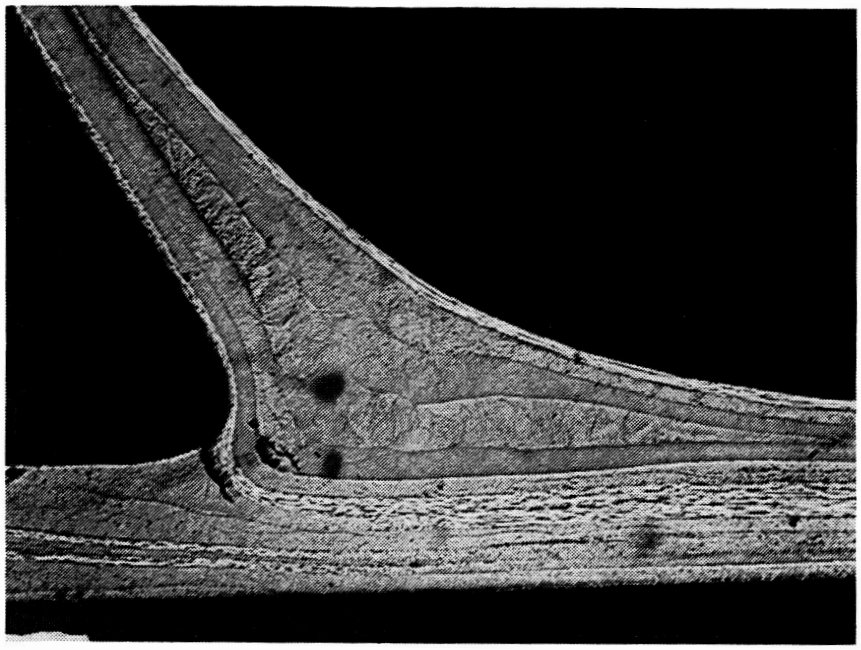

GP24-0420-10/crr

Figure 3.3.2-4. Ply Wrinkling Occurred in SDCC Y-Frame Corner during One-Step Forming

The 45° and 60° Y-stiffened element panels were fabricated successfully using the two-step process as shown in Figures 3.3.2-5 and 3.3.2-6. The upper ply pack was preconsolidated utilizing the diaphragm forming process. Following consolidation, the upper ply pack was coconsolidated to the lower ply pack. Although this is a change from the original SCDD concept, a cost savings is still realized by reducing the process to two steps from a traditional three-step process.

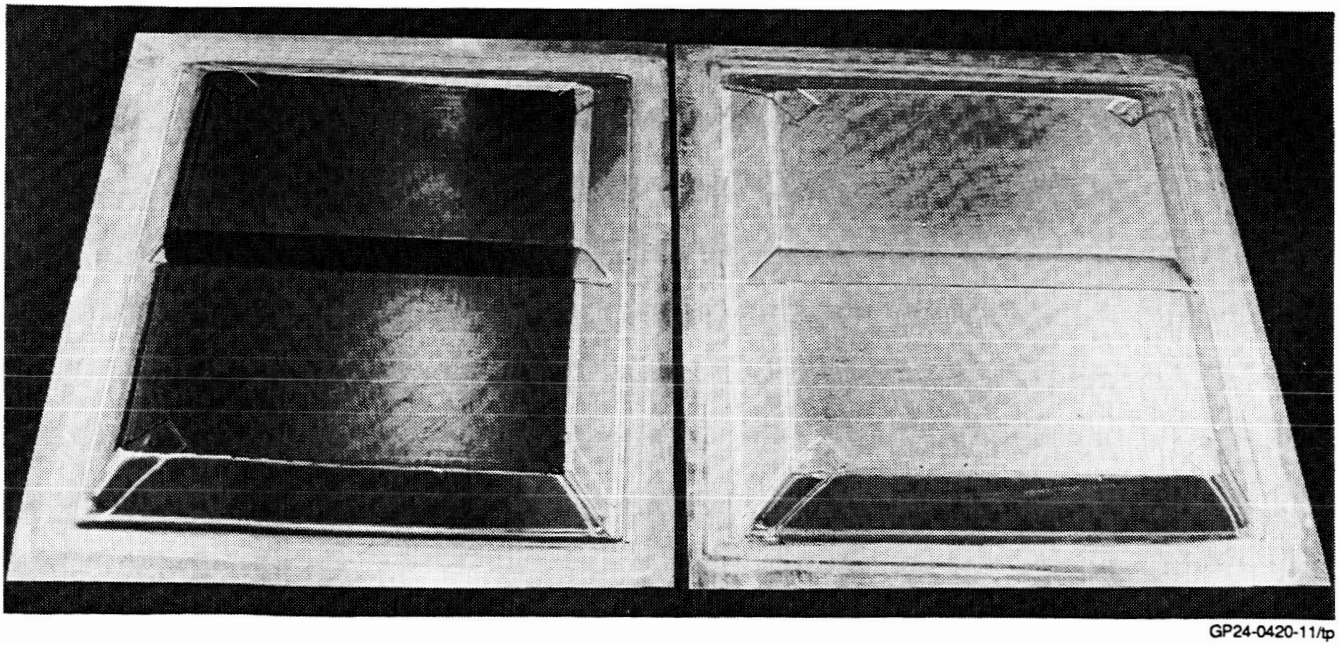

GP24-0420-11/tp

Figure 3.3.2-5. Aluminum Diaphragms and Two-Step Forming Provided Quality Y-Frame Elements

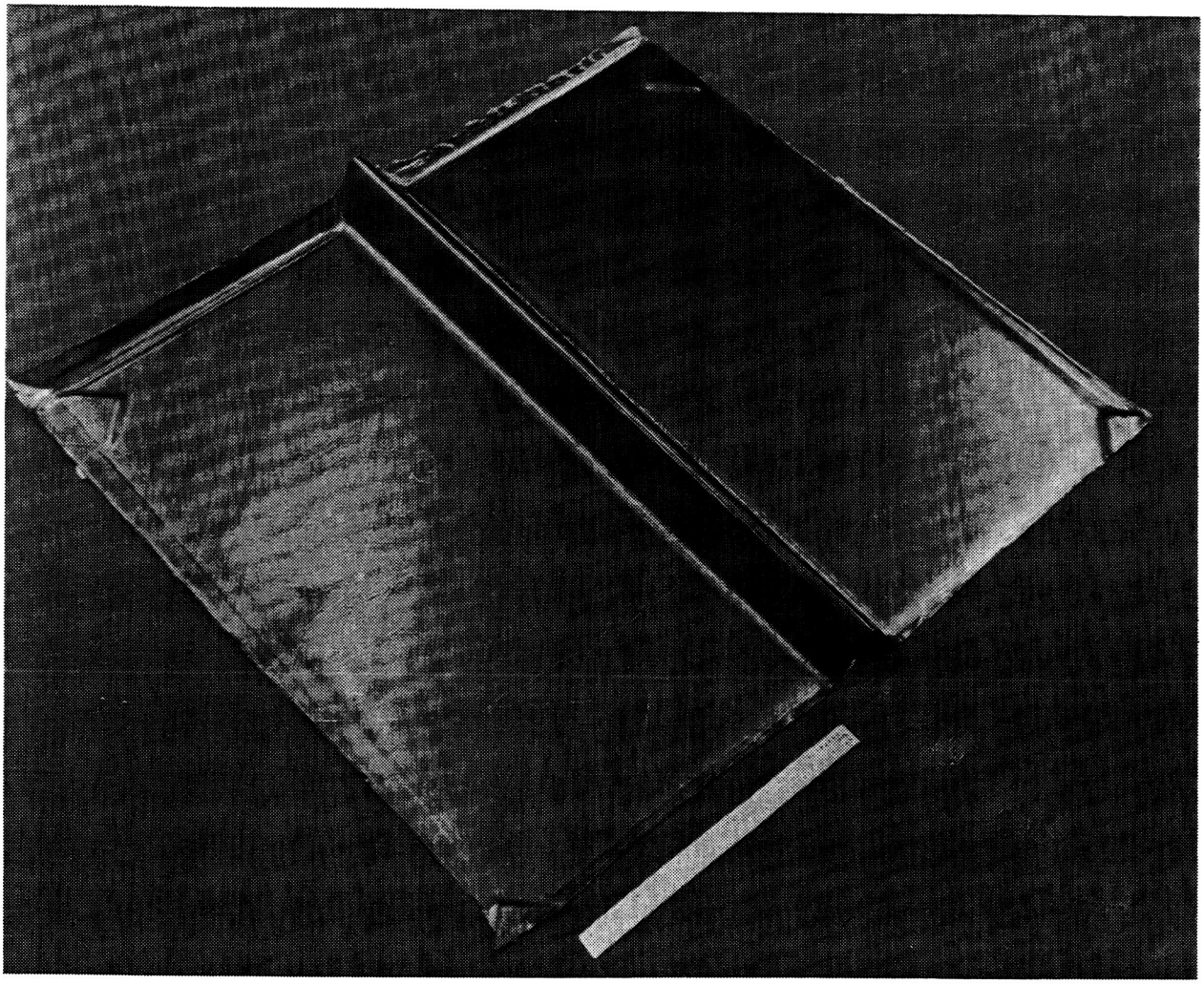

GP24-0420-12/tp

Figure 3.3.2-6. Typical Two-Step Diaphragm Formed 60° Y-Frame Elements

The 45° and 50° Y-stiffener panels were nondestructively evaluated. The C-scan results on the 60° panel showed a quality part free of voids. The 45° Y-stiffened panel however revealed slight porosity under the mandrel due to a piece of sheet metal slipping beneath the mandrel during consolidation. The sheet metal was modified and another 45° panel fabricated with excellent results. Test specimens were machined and subsequently tested (Section 4).

The dual-step SDCC process reflects a significant cost reduction compared to conventional diaphragm forming of integrally stiffened skin structure which involves a three-step approach; forming of the inner corrugated skin, forming of the outer skin, and subsequent coconsolidation. In addition, the three-step process involves the use of an additional diaphragm for outer skin forming.

Our original intent was to develop a single-step SDCC process. Our attempts were unsuccessful due primarily to dragging of outer moldline skin plies into corner radii of the corrugations during forming of the inner moldline skin. The dual-step process was then adopted to insure timely fabrication of the element test specimens.

3.3.3 Blade Frame Elements – Using two aluminum block details a blade panel was hand laminated by bending and edge tacking each of seven plies with a soldering iron, Figure 3.3.3-1. The fillet was filled with thin strips (.30" to .90") of ITX unidirectional tape using a sharp cone tip on the soldering iron, Figure 3.3.3-2. A flat skin was preconsolidated and a strip grit blasted across the center where the blade attached, Figure 3.3.3-3. The two angles with fillet in place were inverted onto this skin, Figure 3.3.3-4, and vacuumed bagged to a project plate. There was a released UPILEX film between the angle plies (web) and the aluminum details. Upon consolidation, at 750°F and 100 psi, the part did not show acceptable c-scan results. The web area had many depressions in it that appeared to be oriented along the second ply down from the surface, i.e., normal to the surface ply fiber direction.

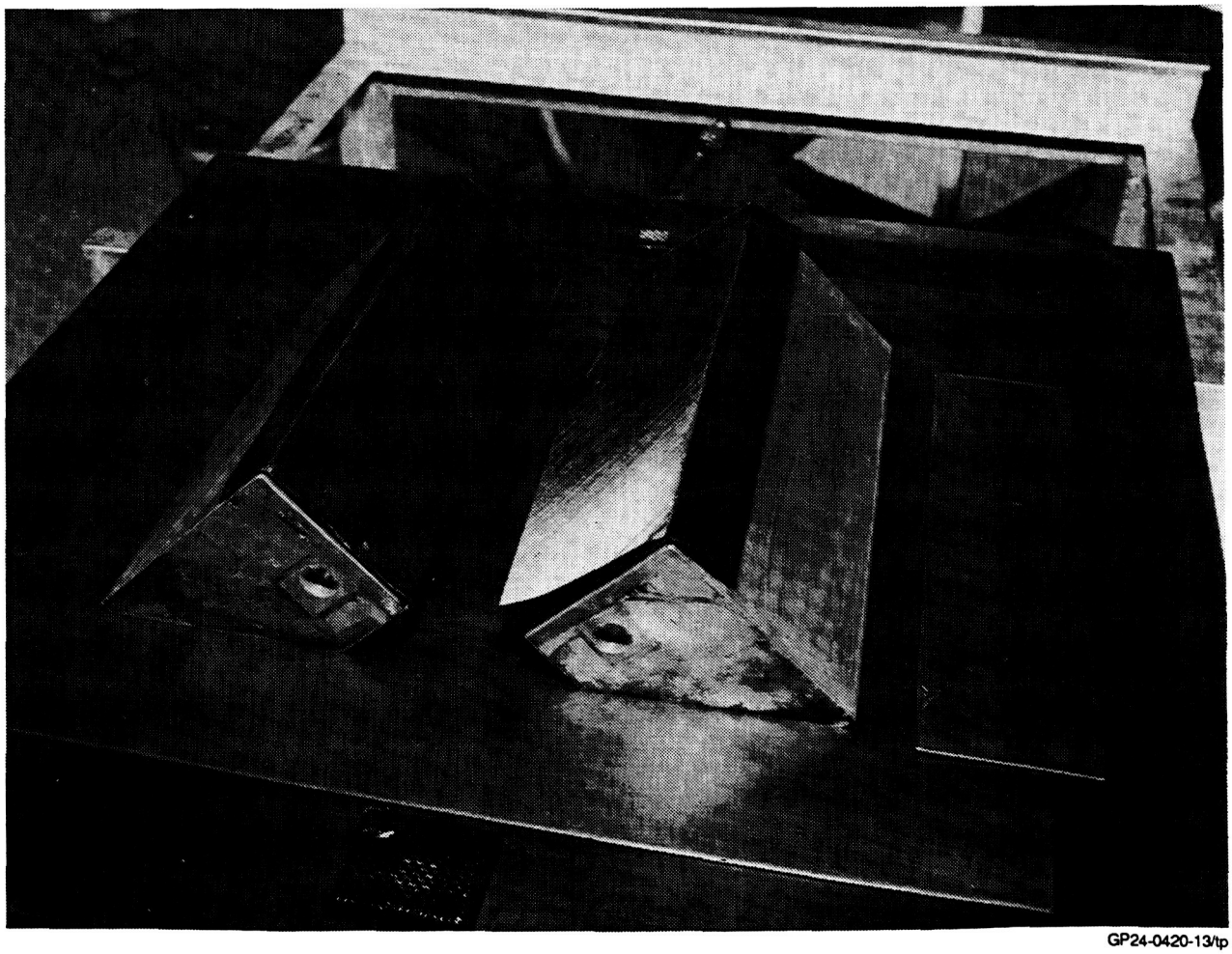

GP24-0420-13/tp

Figure 3.3.3-1. Blade L-Section Plies Were Formed on Tooling Blocks to Form Web

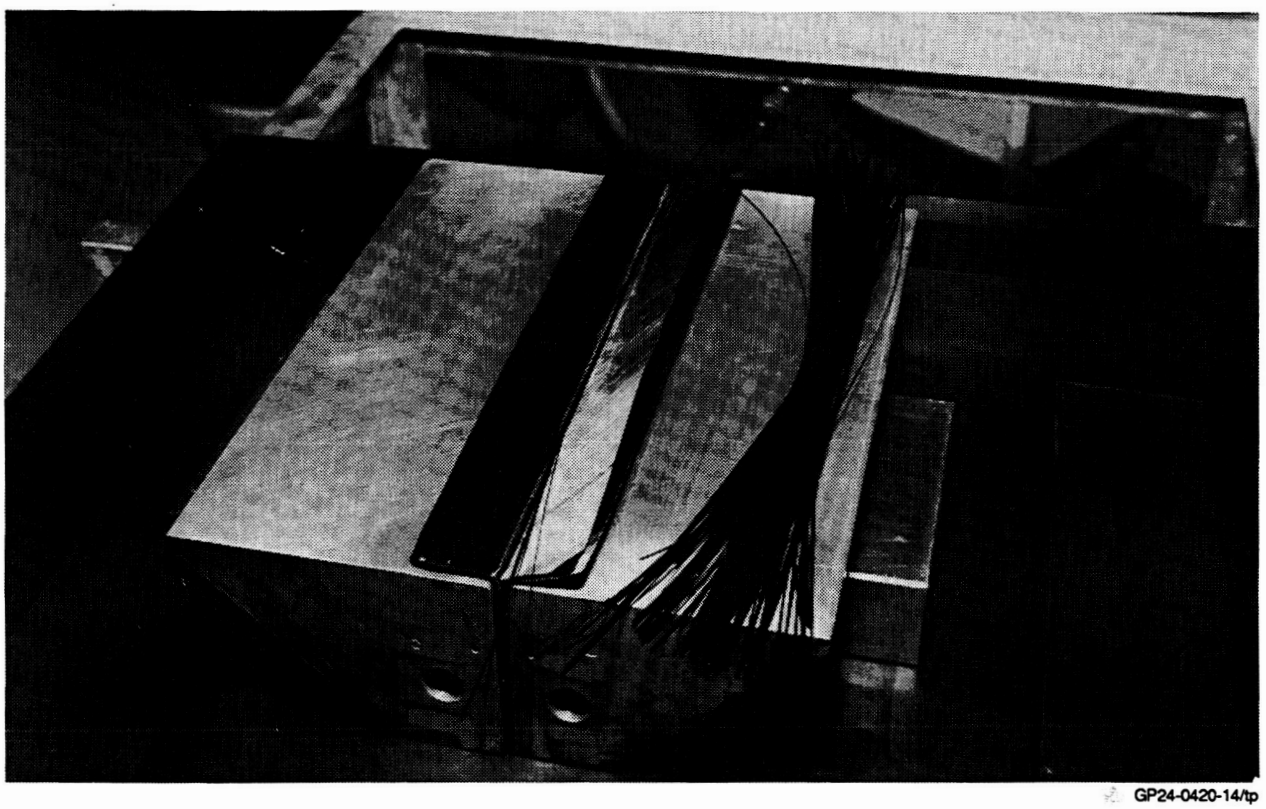

GP24-0420-14/tp

Figure 3.3.3-2. Unidirectional Tow Was Placed in Fillet for Material Continuity

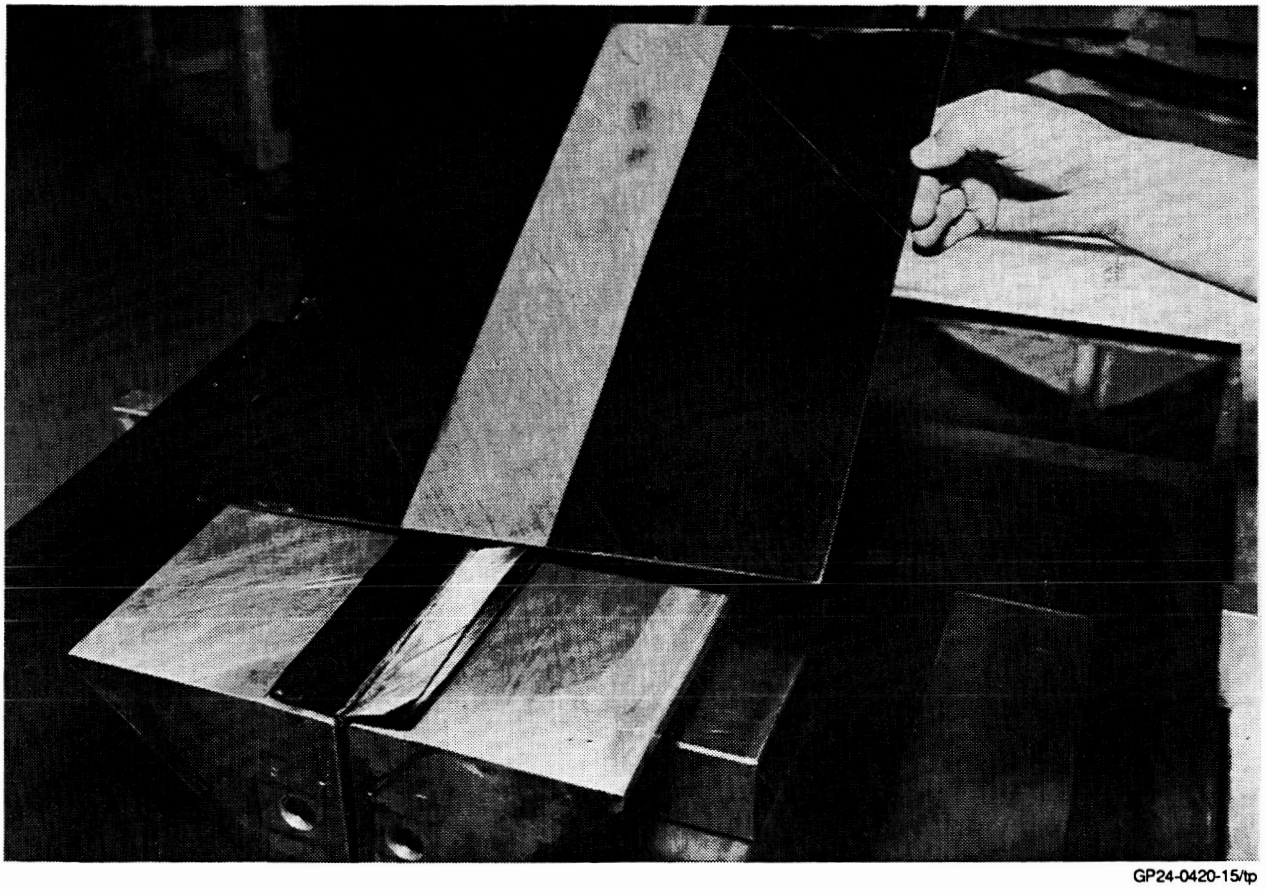

GP24-0420-15/tp

Figure 3.3.3-3. Base Plies Were Consolidated Separately and Grit Blasted Prior to Assembly

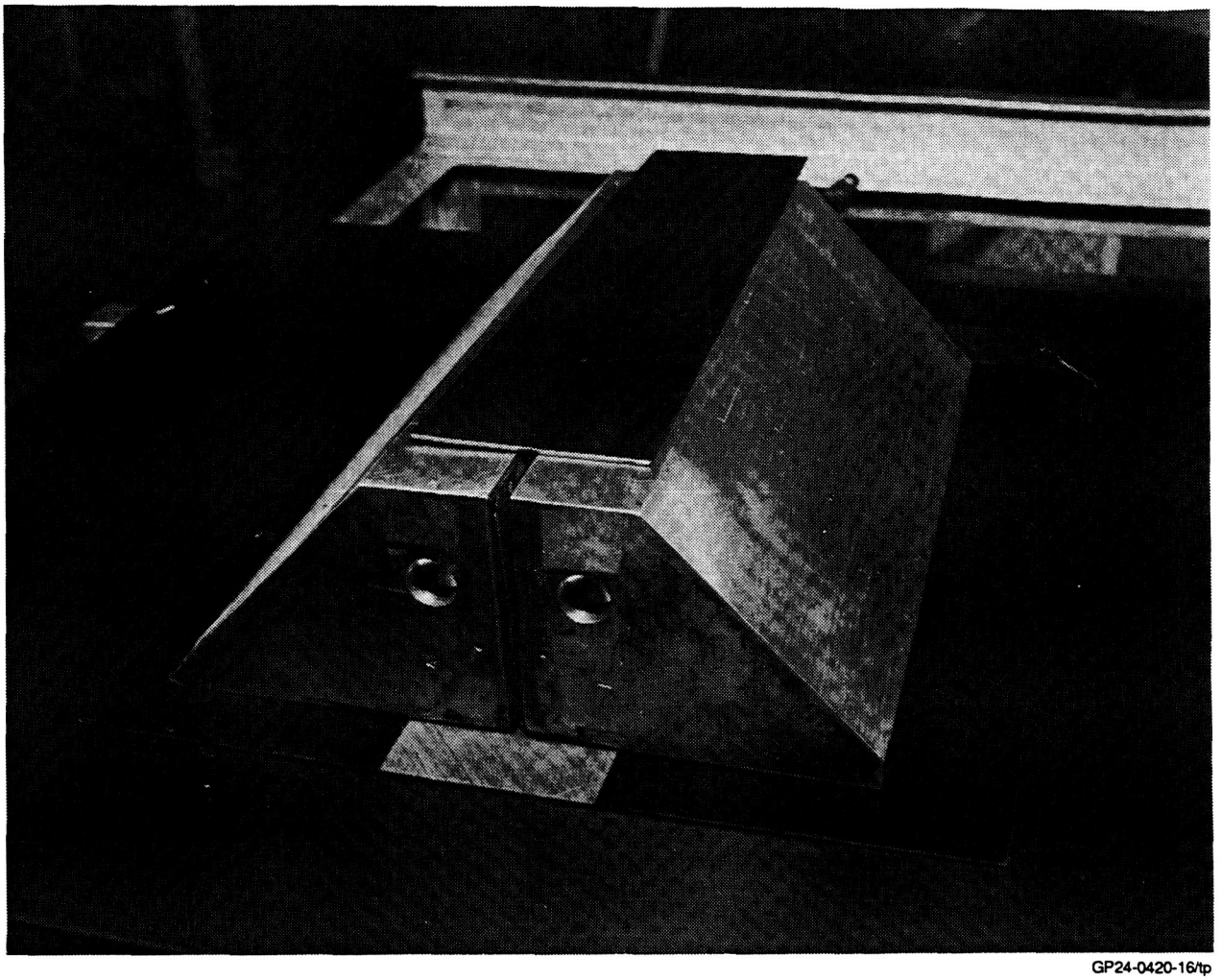

GP24-0420-16/tp

Figure 3.3.3-4. Assembly Prior to Autoclave Consolidation

Outgassing from the release coated UPILEX and the lack of earfolds in the vacuum bag at the base (which may have prevented sliding of the blocks) were identified as probable causes for the poor consolidation. Therefore, a second blade was fabricated with no UPILEX on the tool details and with extensive ear folds in the vacuum bag. Nondestructive inspection of the second blade revealed porosity in the radius areas. Although the part quality was improved over the first blade, it was not the level desired. One of the tool details had rotated during consolidation causing poor consolidation in the web and radius areas.

The consolidation tools were then modified to permit a positive control of the details. A trimetric view of the modification is shown in Figure 3.3.3-5. Keyways were milled into the ends of the web details and fit to guides in the end plates. This modification maintained the movement of the detail in the direction desired thus maintaining constant and equal pressure across the part surfaces. In addition, an upper slotted plate maintained minimum differential vertical displacement between the tooling blocks for the back-to-back L-sections which comprise the T-section.

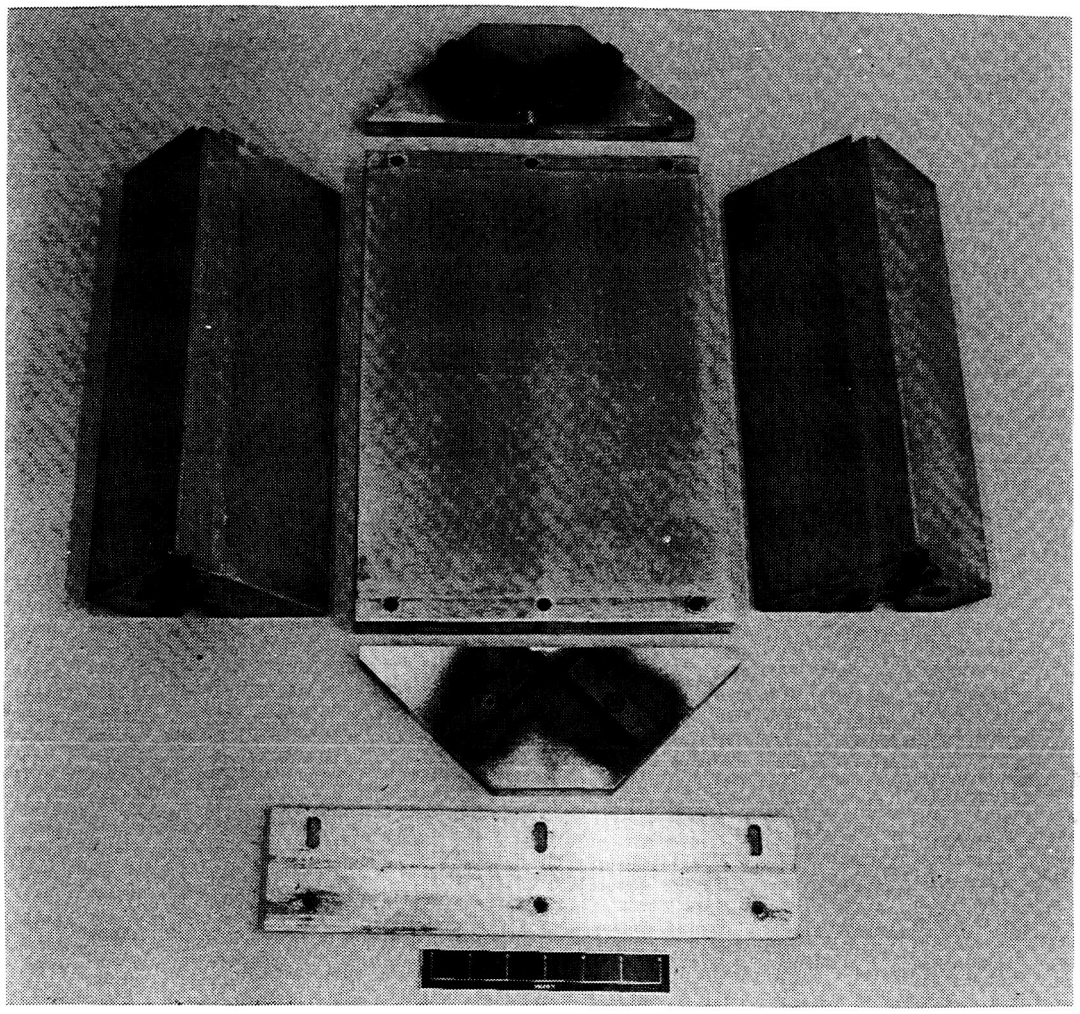

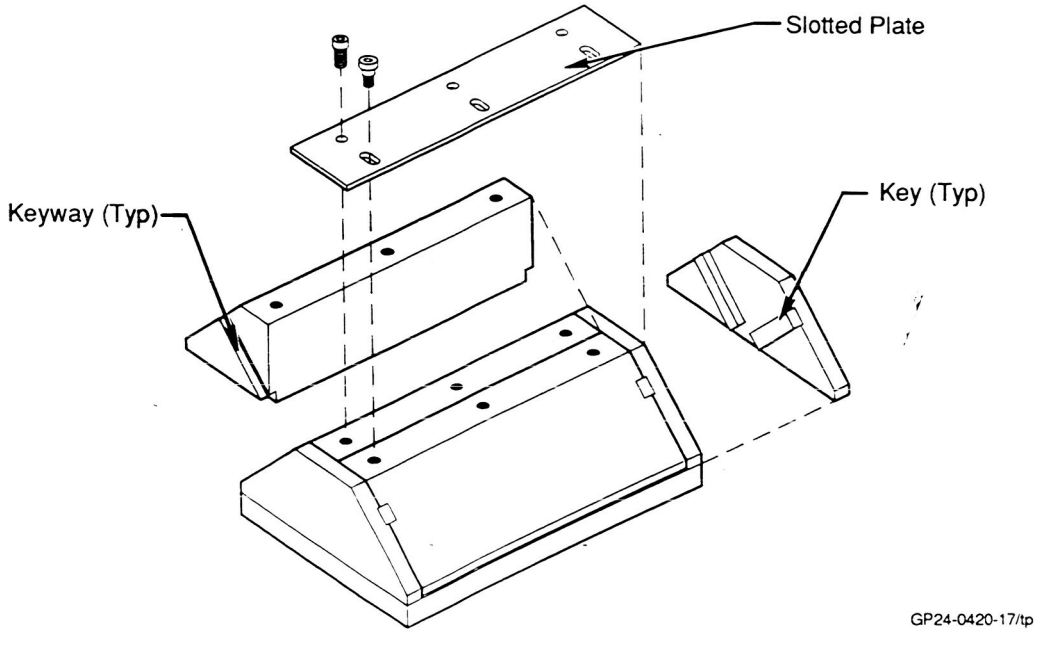

Figure 3.3.3-5. Modification to Blade Element Tooling Provided Necessary Pressure on Web and Radius

The modified tooling concept is a positive drive concept designed to maintain cap and web thickness while providing adequate pressure on the part. Conventional forming tools utilize mechanical stops to provide constant web and cap thickness. However, mechanical stops can contact the project plate prematurely reducing pressure on the part and ultimately causing porosity.

Using the same lay-up approach previously described and the positive drive tooling concept, a quality part was achieved on the first attempt, Figure 3.3.3-6. However, due to amount of fillet material used, a slight void was noted in a photomicrograph of the radius area. Following review of the photomicrograph, it was concluded that excessive 0° tow was being used in the fillet, and that the dwell time should be increased. During a second run, the two changes were incorporated in the consolidation process. The element was then C-scanned revealing a quality consolidation. Photomicrographs show total consolidation in the fillet area as well as the cap and web. A thickness check of the cap and web show only a .001" variation. This element panel was cut into specimens for pull-off testing, Figure 3.3.3-7

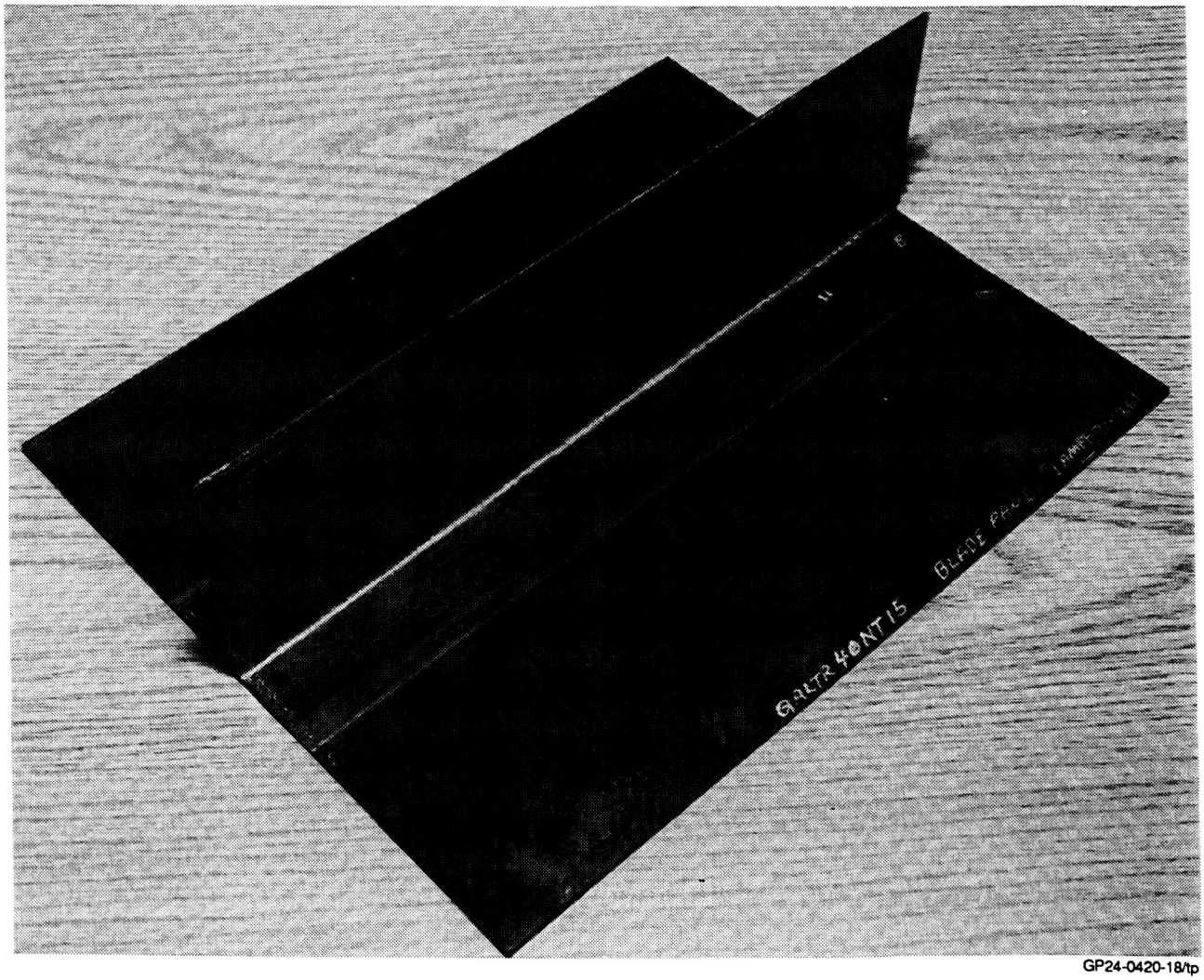

GP24-0420-18/tp

Figure 3.3.3-6. Typical Blade Frame Element

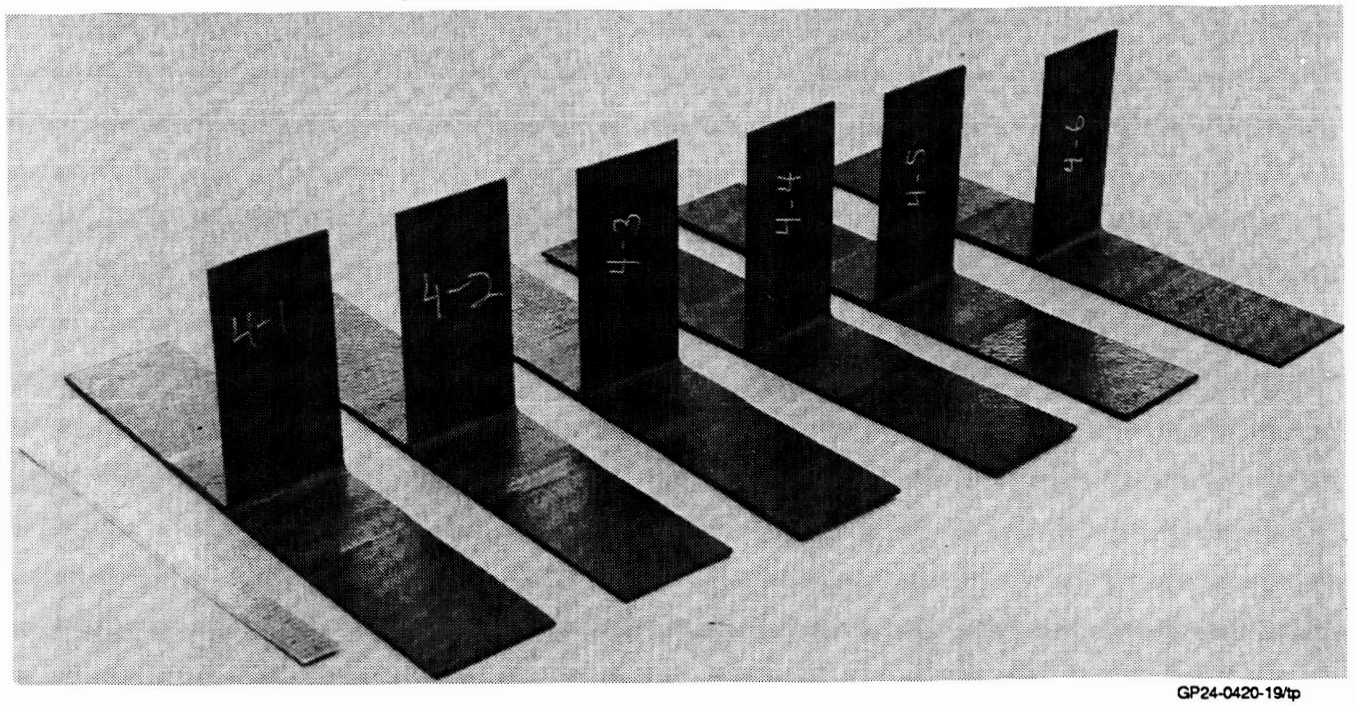

GP24-0420-19/tp

Figure 3.3.3-7. Blade Frame Element Panels Were Machined Into Pull-Off Specimens

A blade panel previously consolidated with the original tooling concept and exhibiting unacceptable levels of porosity was reconsolidated using the positive drive tooling. Both C-scan and photomicrographic inspections revealed a quality part. This blade element was also machined into element specimens in order to investigate the effects of reconsolidation.

3.3.4 Roll-Formed Stiffeners – Vanguard Composites Company (Anaheim, CA) was subcontracted to fabricate 45 feet of roll formed hat stiffeners. These stiffeners were to be originally used in subcomponent fabrication using the fiber placement process, but served as a manufacturing demonstration due to the redirection.

The thermoplastic hat stiffener consisted of 7 plies of IM7/ITX which incorporates a 4 ply drop-off in the flanges representative of the fiberplaced panel design. A single layer of 3 mil neat PEEK film is incorporated on the IML of the flanges for future bonding trials. C-scans of the first article hat stiffener showed a lack of consolidation in the flange ply drop-off area as well as in the stiffener walls in the area of the upper radius. The first article also had visible roller lines transverse to the stiffeners length and dry patches on the IML flanges where the neat resin film had thinned out.

A second article showed slightly better consolidation in the ply drop-off areas but still had poor consolidation in the stiffener walls. The roller marks were eliminated and the neat resin film application looked much better on the second article. It was discovered by Vanguard that the roller for consolidation of the stiffener walls has a 1/2° mismatch which was most likely the reason for the inadequate consolidation in this area. The problem was corrected and fabrication continued.

Forty-five feet of roll formed hat stiffeners were received from Vanguard Composites Company. A typical section is shown in Figure 3.3.4-1. NDT results from a random sample of the hat stiffeners show a lack of adequate consolidation in the tapered flange area. The constant thickness portion of the flanges showed significantly better consolidation. Based on these observations, it is felt that roll forming of constant cross-section, thermoplastic composite stiffeners with uniform flanges is a viable manufacturing process. However, tapered flanged stiffener concepts would require additional development.

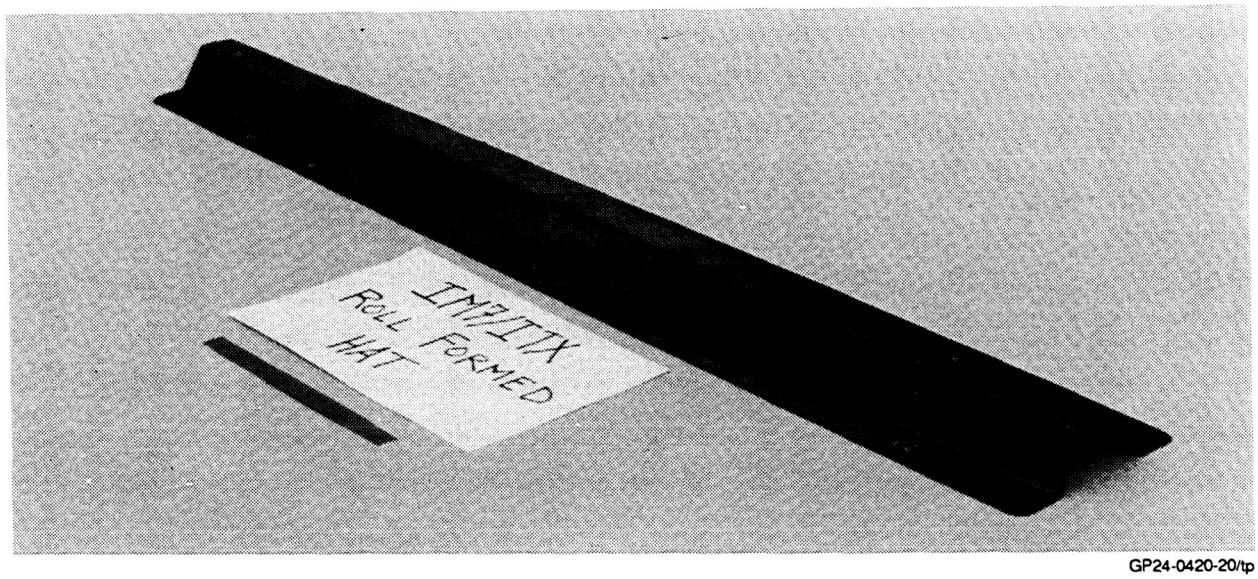

GP24-0420-20/tp

Figure 3.3.4-1. Roll-Formed Hat Sections Demonstrated Potential for Low Cost Manufacturing

3.3.5 Lug Elements – The lugs were fabricated using AS4/APC-2 unidirectional tape since it was readily available early in the program and the lugs were primarily being tested for analytical model verification. Tooling for the lug specimens consisted of simple project plates with steel plates positioned to allow for expansion during consolidation.

The lugs were fabricated from eighteen 30" x 16" sublaminate panels of four different 30 ply lay-ups. The sublaminates were consolidated in a hydraulic press. Six sublaminates were stacked to form the three different 180 ply stacking sequences which were coconsolidated in the autoclave. Excellent consolidation of the sublaminates was verified by photomicrograph inspection, as shown in Figure 3.3.5-1. Panels with the final lug lay-ups were C-scanned to ensure their quality.

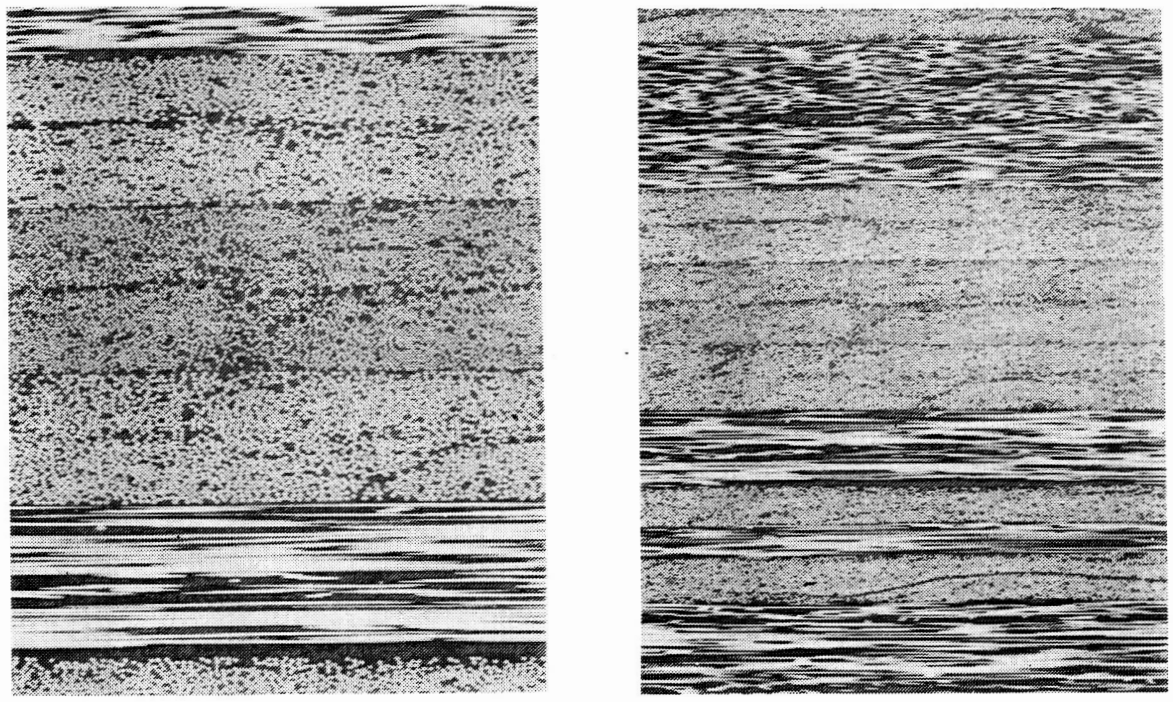

GP24-0420-21/tp

Figure 3.3.5-1. Excellent Consolidation in Thick Lugs Verified by Photomicrographic Inspection

Water jet cutting (WJC) was used to obtain four lugs from each of the panels, Figure 3.3.5-2. The finish associated with this cutting procedure was acceptable as the final external finish on the test articles. Initial lugs showed a minor defect on the external surface at the beginning of the radius. This was associated with the initiation of the WJC process and to avoid this stress riser the cutting pattern was altered to begin in the middle of the lug rather than at a radius.

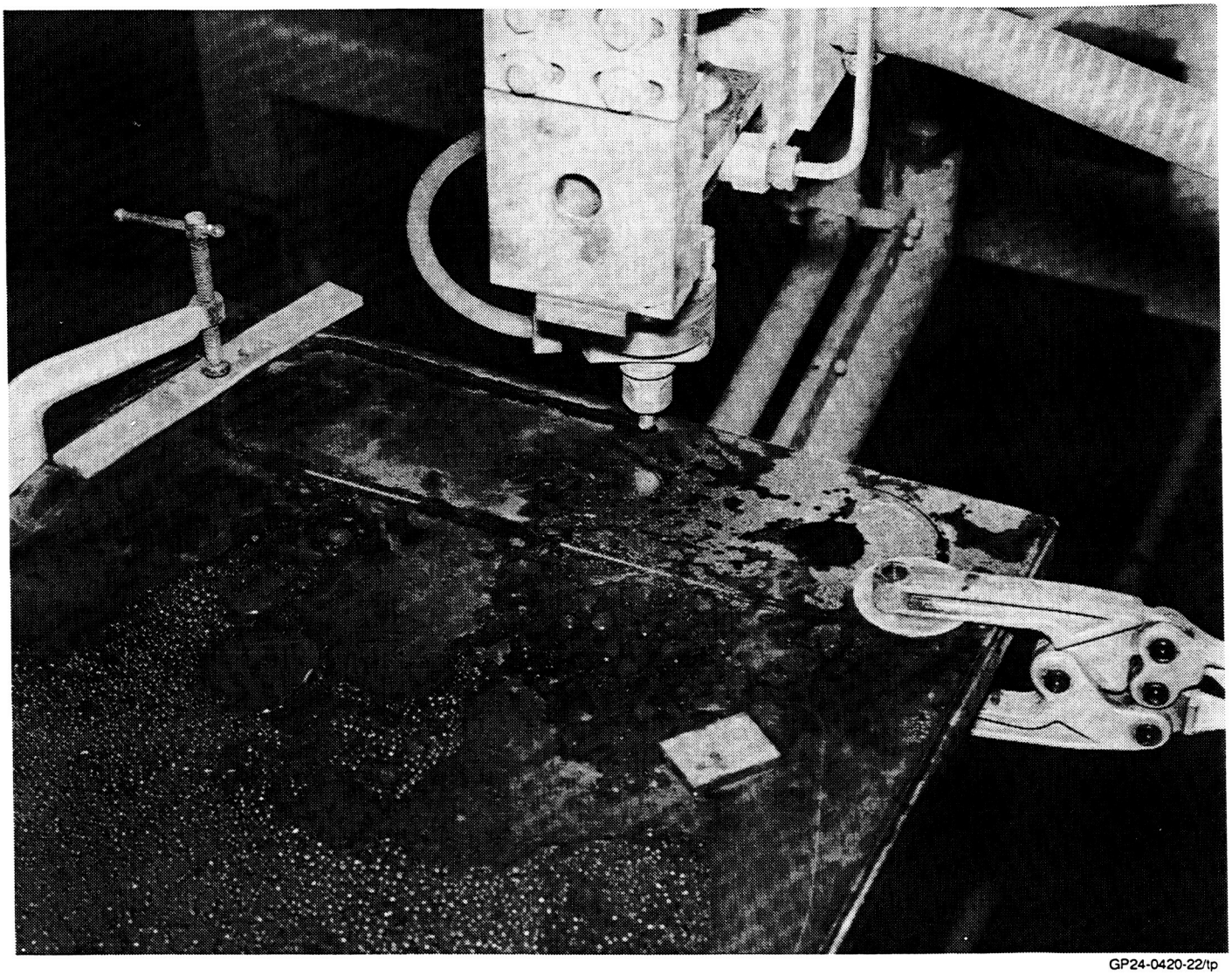

GP24-0420-22/tp

Figure 3.3.5-2. Thick Composite Lug Specimens Were Efficiently Machined Using Abrasive Water Jet Cutting

The WJC process was used to rough cut the pin holes which were then secondarily milled to the tolerances of ±.005 inch. C-scans were taken of the finished lug to ensure the cutting procedure had not induced any delamination, Figure 3.3.5-3. The final lug specimens as typified in Figure 3.3.5-4, were found to be void-free.

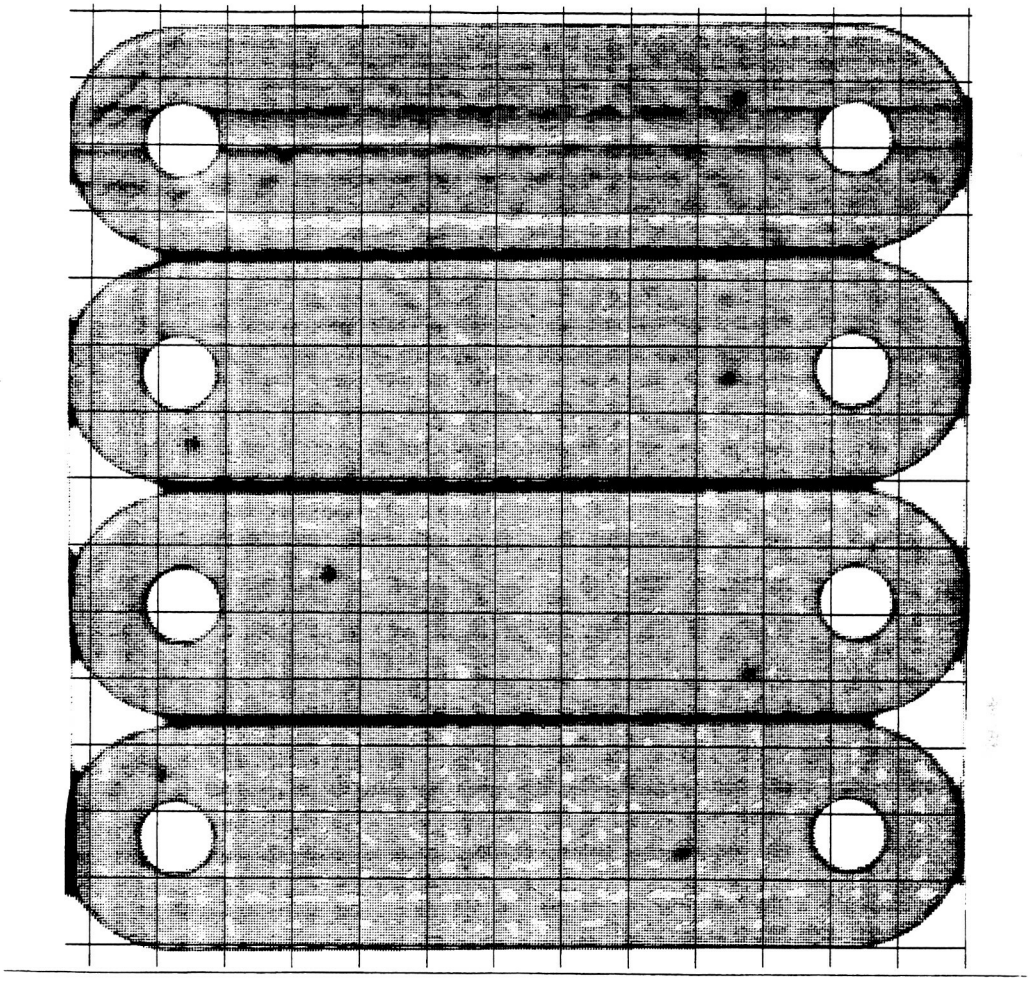

GP24-0420-23/tp

Figure 3.3.5-3. Final Machined Thick Composite Lugs Were Void-Free

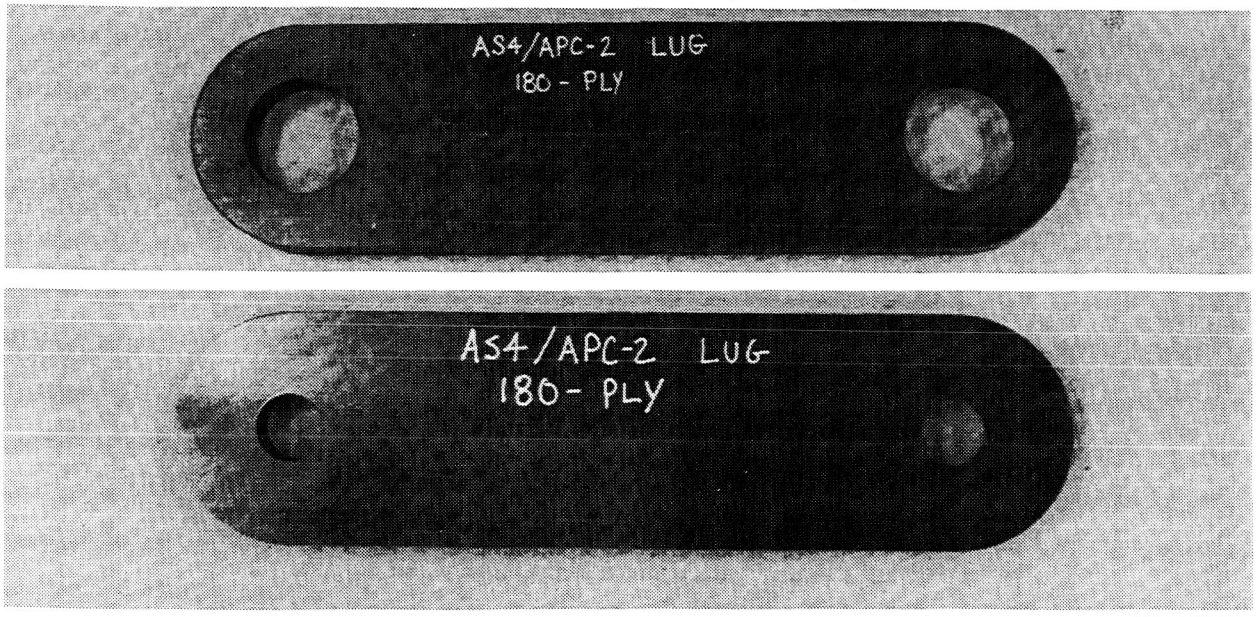

GP24-0420-24/tp

Figure 3.3.5-4. Typical Lug Specimens Prior to Structural Testing

Overview of Fabrication Development

Lessons learned during element fabrication are summarized as follows:

- A smooth transition between stiffener mandrel termination and vacuum pressure box ramps can reduce diaphragm rupture.
- The use of aluminum diaphragms during SDCC verification trials prevented diaphragm rupture due to increased durability and elongation properties compared to available polymeric diaphragms.
- Tooling movement control through utilizing selected keyways ensured cap and web thicknesses and supplied adequate pressure in the fillet area for blade fabrication.
- Quality, thick panels (for lug elements) can be successfully fabricated from thermoplastic composites by consolidating a series of sublaminates.
- Abrasive waterjet cutting can be used to efficiently machine thick composite panels.
- Initial investigation indicate that roll forming of thermoplastic composite stiffeners may be a potential low-cost manufacturing technique.

4. FUSELAGE ELEMENT TESTS

In support of the D/MI and building block approaches, structural element testing was planned to provide the necessary insight in order to eliminate any potential design flaws from being overlooked in a full-scale effort.

Element testing focused on demonstrating the efficiency of the design concepts being proposed for subcomponent scale-up and eventual full-scale development. In addition, structural analysis methodologies were to be fully verified for accuracy and used in future design of the ASTOVL structure. Lug and frame pull-off testing were conducted to provide the link between the element and subcomponent design phases in the building block approach.

4.1 Lug Elements

Lug testing was conducted to verify the design and analysis procedure developed in Section 2.3.1. A total of twenty-three thermoplastic (AS4/APC-2) lugs were manufactured (Section 3.3.4) and subjected to static axial tension test. Results of the nondestructive evaluation (NDE) indicated that all final specimens were of good quality.

Room temperature testing was performed with a load rate of 500 lb/sec, and all lugs were tested in as received moisture condition. The testing setup is shown in Figure 4.1-1. In order to keep the gap between the lug and loading clevis surface at 0.1", which was used in the analytical models, special bushings were fabricated. A different gap size might cause unexpected failure loads due to different pin bending effects.

The lugs with 1.75" diameter holes (W/D = 2.0) exhibited a catastrophic fiber failure at the net section, whereas the lugs with 1.0" diameter holes (W/D = 3.5) showed permanent yielding around the hole prior to shear/bearing failure. The initial bearing failure load was determined by observing the behavior of axial strain data from rosettes located at 0.5" away from the edge of the 1.0" hole and 0.25" away from the 1.75" hole at the center line of specimens (Figure 4.1-2). Load versus strain data indicates that axial strain decreases with associated material failure ahead of the pin the 1.0" hole lugs, Figure 4.1-3. Typical failed specimens are shown in Figure 4.1-4 and 4.1-5 for the 1.0" hole and 1.75" hole specimens, respectively.

Analytical predictions were in close agreement with actual lug performance, Figure 4.1-6. Test results for the six lug configurations are summarized in Figure 4.1-6 along with analytical predictions. Sensitivity study indicated that 0° ply strain convergence was achieved using more than four elements through-the-thickness. Therefore, for numerical accuracy with minimum run-time, four elements through-the-thickness were used for strength prediction of lugs. A comparison of bearing strain distributions at 40 kips predicted by models consisting of one, two or four elements, through-the-thickness is shown in Figure 4.1-7. The FATLAM and STAFLM predicted failure loads were within 8% of average test results.

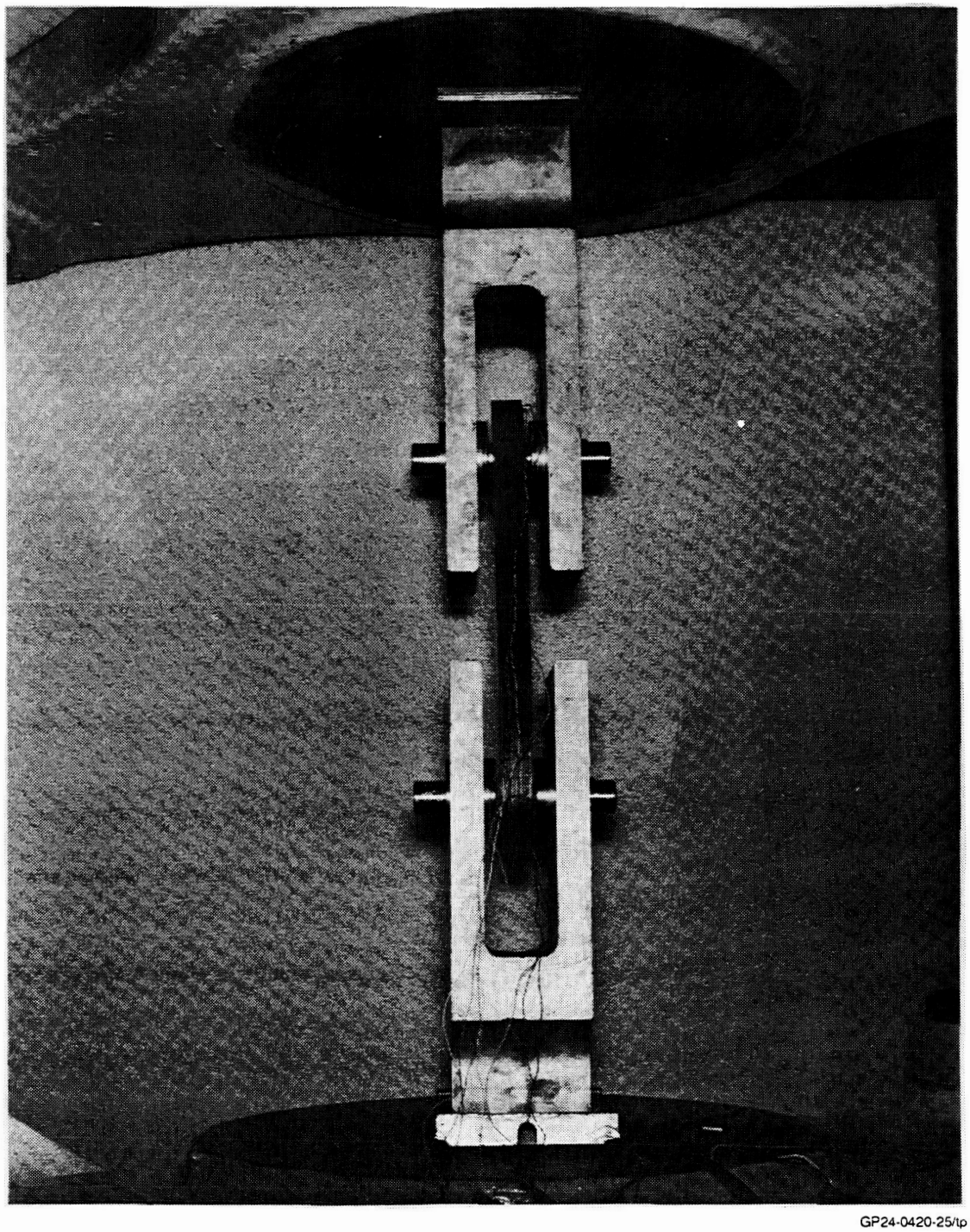

GP24-0420-25/tp

Figure 4.1-1. Lug Element Testing Apparatus and Set-Up

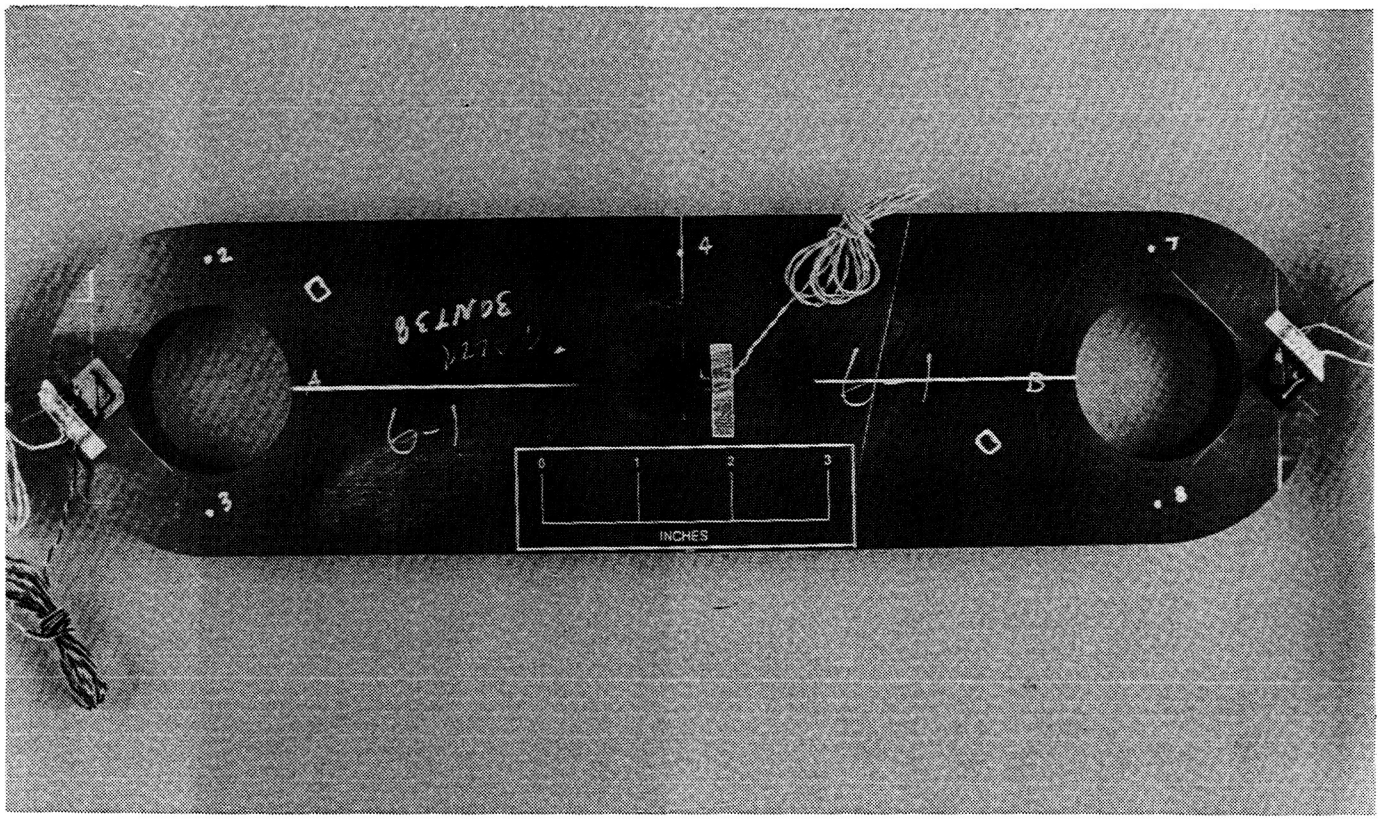

GP24-0420-26/tp

Figure 4.1-2. Strain Gage Locations for Lug Specimens

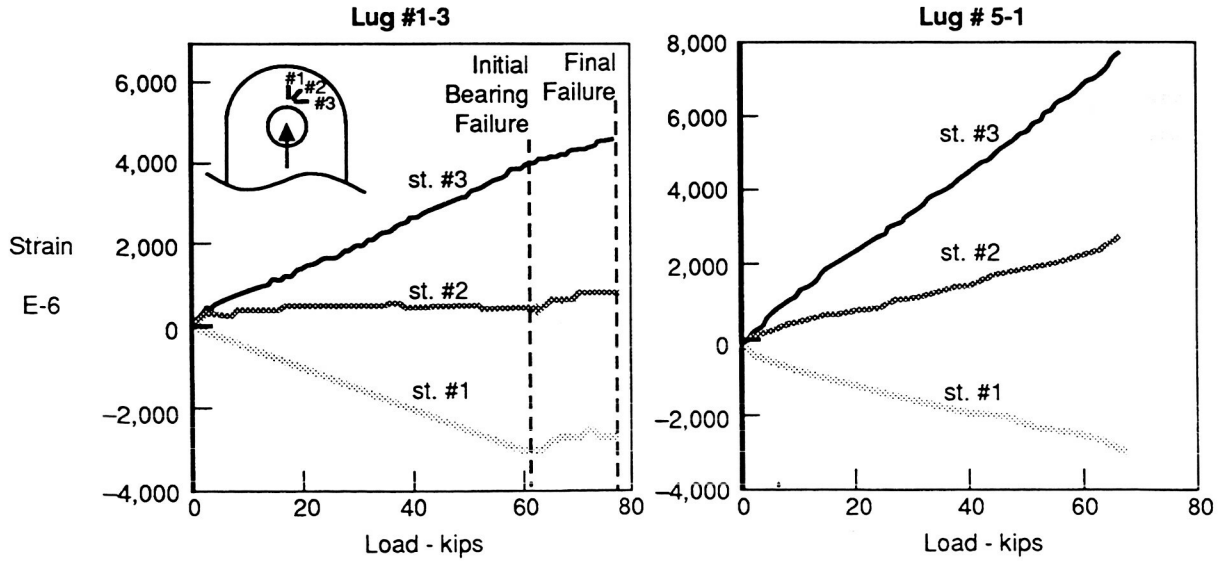

GP24-0420-39-D/crr

Figure 4.1-3. Typical Load vs Strain Test Data

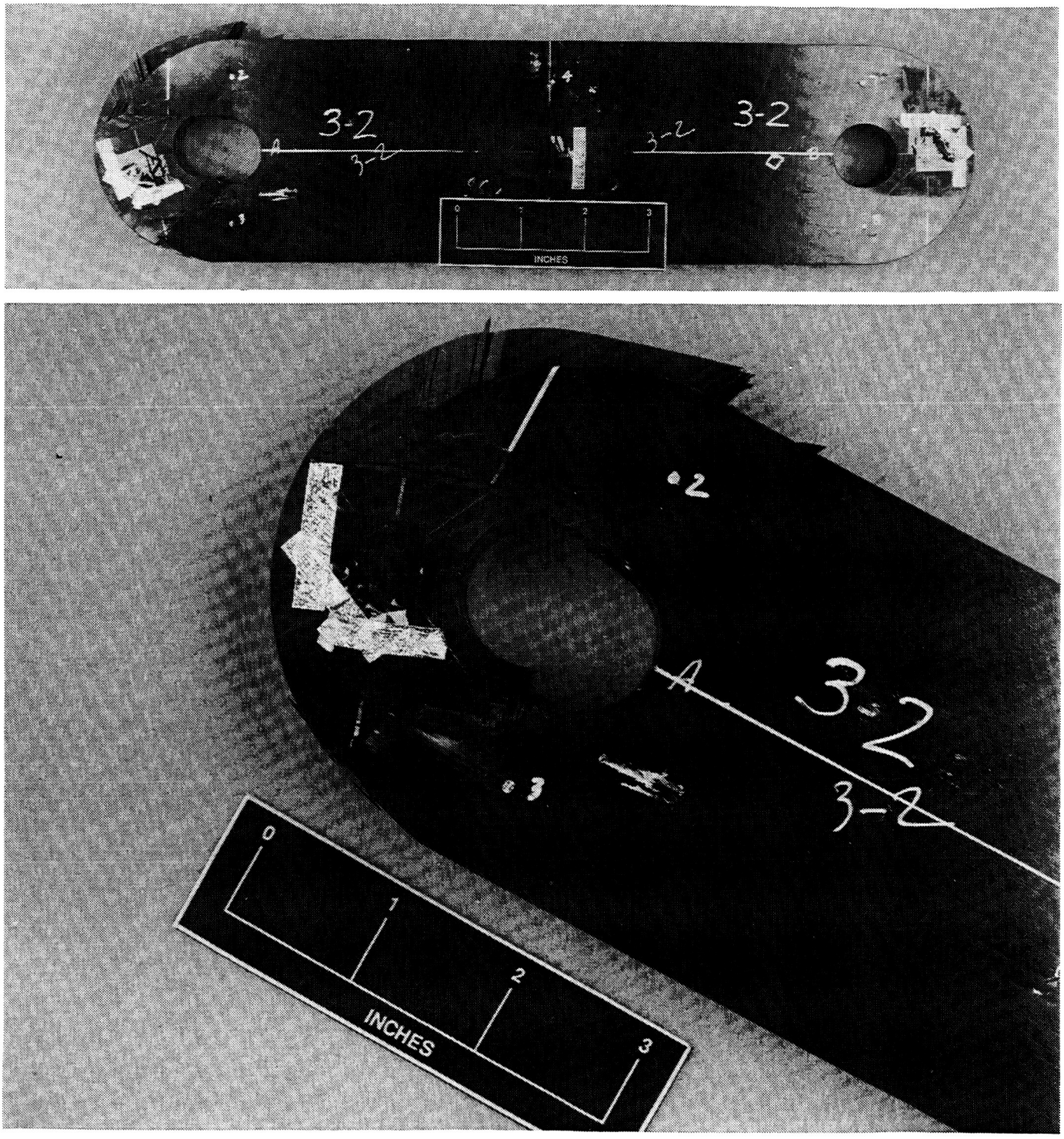

Figure 4.1-4. Typical Shear-Out Failure for 1.0" Diameter Lugs

ORIGINAL PAGE
BLACK AND WHITE PHOTOGRAPH

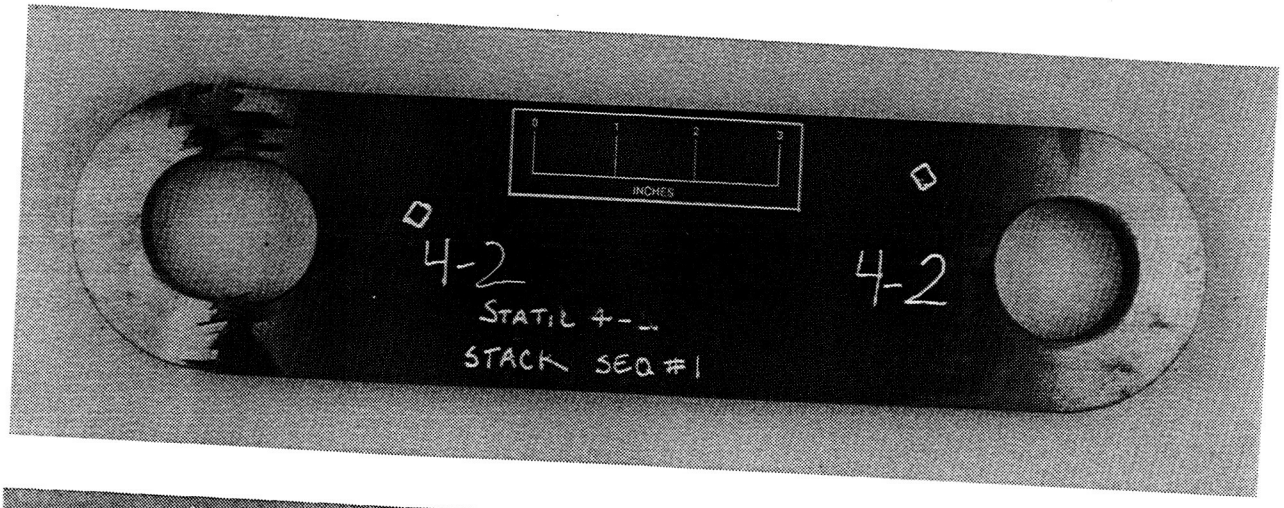

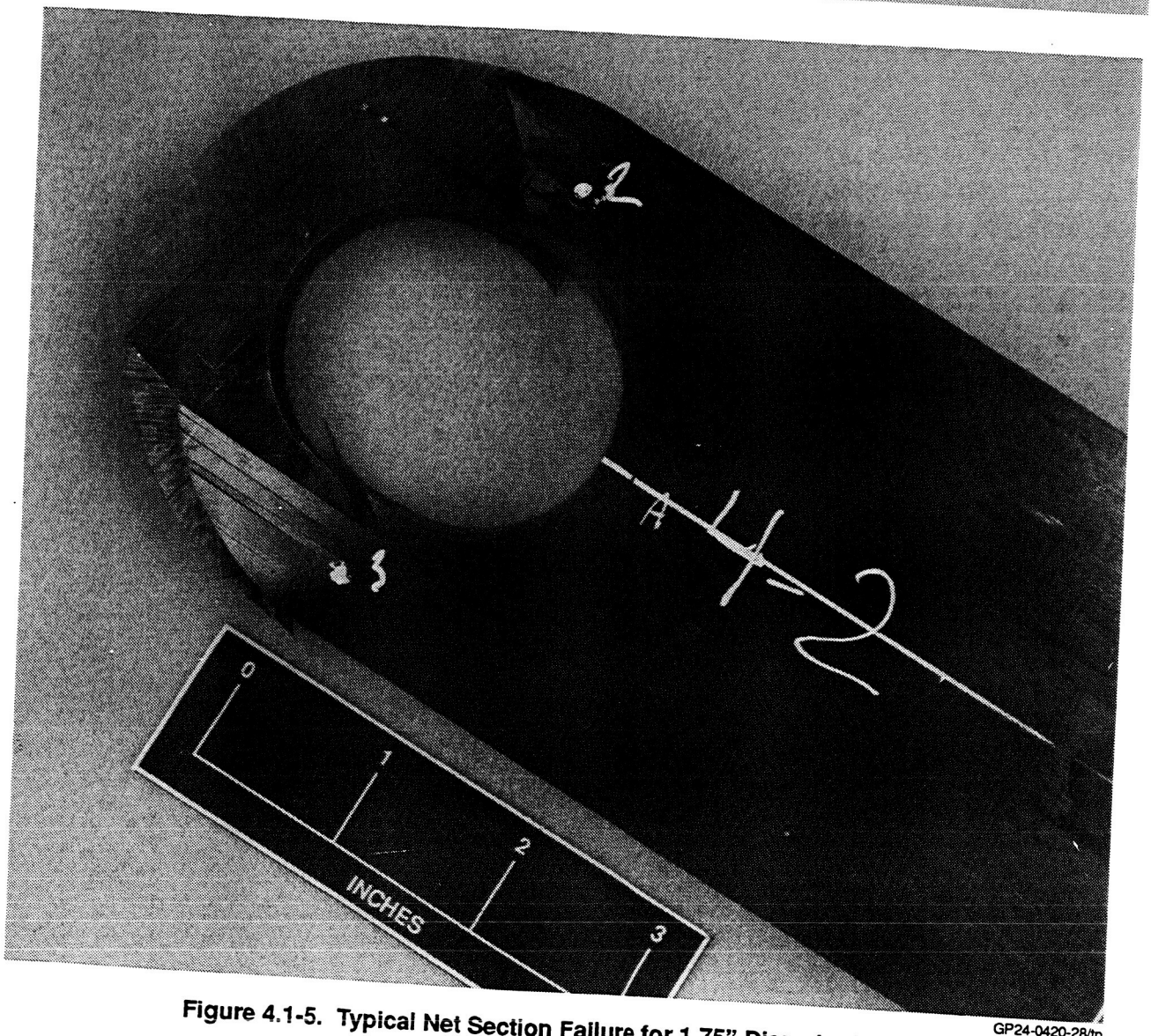

Figure 4.1-5. Typical Net Section Failure for 1.75" Diameter Lugs

GP24-0420-28/tp

Lug Specimen	Quantity Each	Hole Dia. (in)	Pred. Failure Load (kips)	Average Test Results (kips)	Standard Deviation
#1	4	1.0	64.2	60.1 (76.7)*	4.3 (2.2)
#2	3	1.0	65.9	62.3 (74.3)*	6.9 (3.0)
#3	4	1.0	57.3	62.2 (74.7)*	7.0 (2.0)
#4	4	1.75	66.9	69.3**	3.1
#5	4	1.75	66.5	68.7**	2.9
#6	4	1.75	61.5	66.8**	1.8

* Initial Bearing Failure Load (Final Failure Load)

** Failure Load

Figure 4.1-6. Prediction vs Test Results

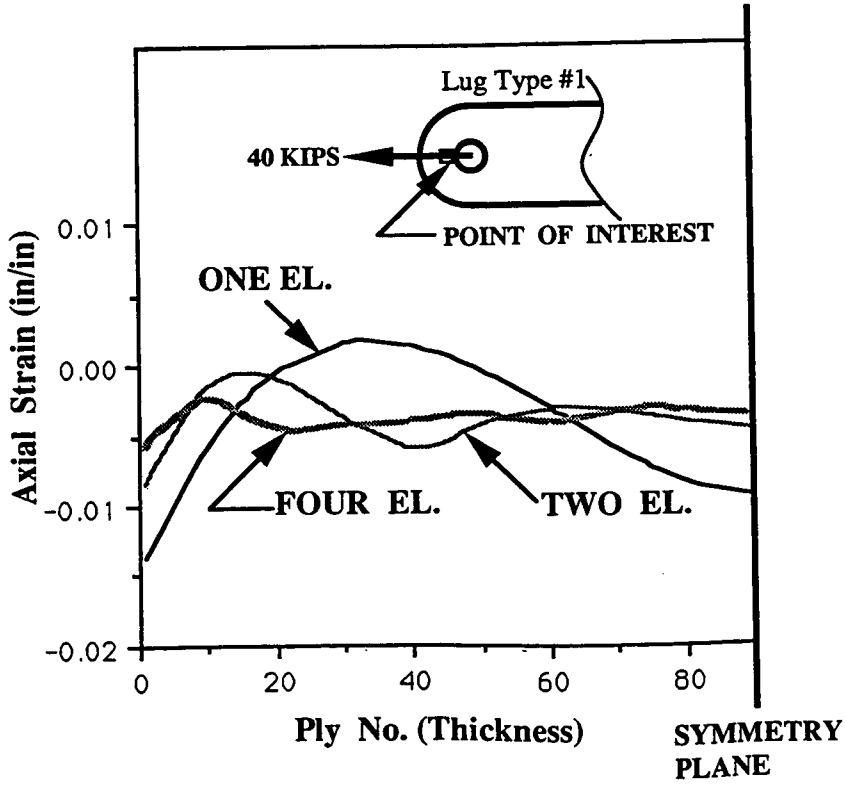

Figure 4.1-7. Sensitivity Study on Lug Finite Element Analysis

The strength of each lug was predicted assuming that any fiber failure resulted in failure of the lug. Using the modified Hashin failure criteria, predicted failure modes were not in agreement with observed failure modes (Figure 4.1-8). However, parallel in-house activities indicate that other failure theories (i.e., maximum strain) may yield better correlation. These theories could be easily programmed into the developed code.

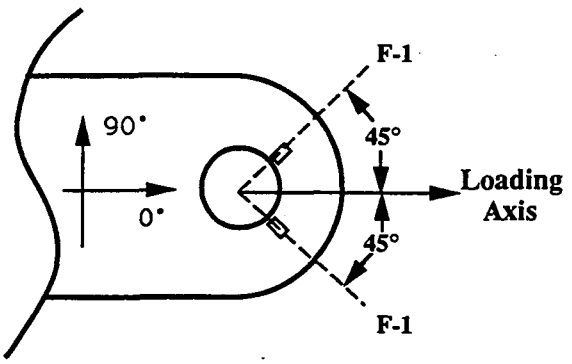

Lug Type	FAILURE MODE	
	FEM	Actual
1.0" Hole Lug	F-1 : Comp. Fiber Failure on +45,-45 Layer	Bearing + Shear-out Failure
1.75" Hole Lug	F-1 : Comp. Fiber Failure on +45,-45 Layer	Shear-out + Net Section Failure

Figure 4.1-8. Failure Mode Prediction

4.2 Frame Element Tests

Frame element testing was conducted on the fastenerless frame/skin attachment designs which were selected for subcomponent and full-scale development. In addition, testing was conducted on an induction welded frame concept in order to initially assess the feasibility of this joining method for later use under the full-scale development.

Nondestructive Evaluation (NDE) revealed some minor porosity and defects in the 45° Y-specimen panel. An additional panel was fabricated to provide specimens. With the exception of induction welded Y-frame specimens, all coconsolidated specimens were determined to be of good quality. Examination of the corner radii was difficult for all specimens. Based upon available C-scan data and examination of the specimens after final trimming all specimens were accepted.

A dimensional check was conducted to further verify the accuracy of fabrication of all specimens and to establish a database for later failure correlation. The results of the dimensional checks showed minor variations (less than 10% deviation from nominal) in thicknesses and specimen widths (Appendix 2). The width dimension was utilized to normalize all reported load data to pounds per unit width.

All specimen configurations were subjected to two (2) testing conditions as shown in Figure 4.2-1. Room temperature dry (RTD) testing was conducted on specimens which underwent an initial weighing followed by exposure to 250°F until weight loss stabilized. Elevated temperature wet (ETW) test specimens experienced the same 250°F drying exposure followed by moisture conditioning at 160°F and 95% RH. Based on a time history of the moisture conditioning, Figure 4.2-2, an average equilibrium moisture content for the 1M7/ITX frame element was found to be 0.34% by weight.

Frame Configuration	Fabrication Process	Number of Specimens at Test Environment	
		RTD*	ETW**
Blade	Co-Consolidated	3	3
45° Y-Frame	Co-Consolidated	3	3
60° Y-Frame	Co-Consolidated	3	3
60° Y-Frame	Induction Welded	3	3

* RTD = Room Temperature / Dry Condiiton
** ETW = Elevated Temperature (250°F) / 0.34% wt. Moisture Content

Figure 4.2-1. Fastenerless Frame Pull-Off Testing Matrix

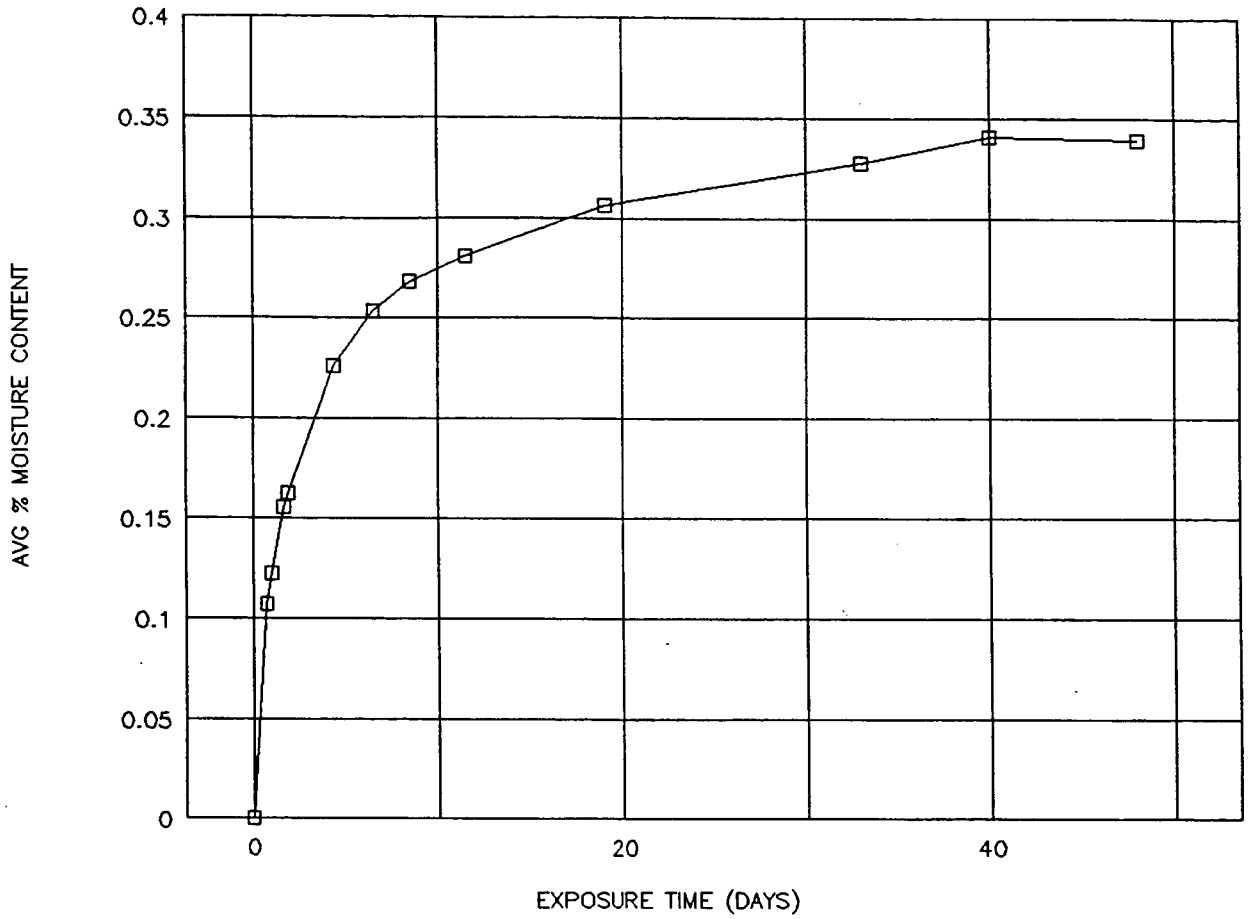

Figure 4.2-2. Moisture Conditioning History for 160°F and 95%RH

The test setup for room temperature specimens is shown in Figure 4.2-3 for both the baseline blade and Y-frame specimens. Load introduction for the blade specimens was accomplished through direct gripping of the upstanding flange. A loading mandrel and clevis were utilized for the Y-frames. Initial testing showed substantial deflections due to the 5" span used between end clamps. In order to eliminate excessive deflections the test procedure was modified to provide a 3" span. The identical setup was used for the elevated temperature testing, with the test apparatus enclosed within a temperature control chamber. A thermocouple was utilized to ensure accurate control of the temperature to the required 250°F. A hold time of 5 minutes was utilized to ensure temperature uniformity for the part while reducing the risk of desorption associated with longer hold times.

Testing was carried out utilizing a displacement control rate of 0.1 in/min. Load versus deflection plots were obtained for each test condition. In addition to on-line recording of the load history, continuous visual inspection of the specimens was carried out during testing in order to establish initial failure modes and a correlation to the loading data. Videotaping of the initial room temperature tests provided a means of reviewing the test procedures (including load and displacement histories monitored on digital readouts). In addition, specimen edges were painted white prior to testing in order to provide contrast and enhance visual identification of failure initiation and location.

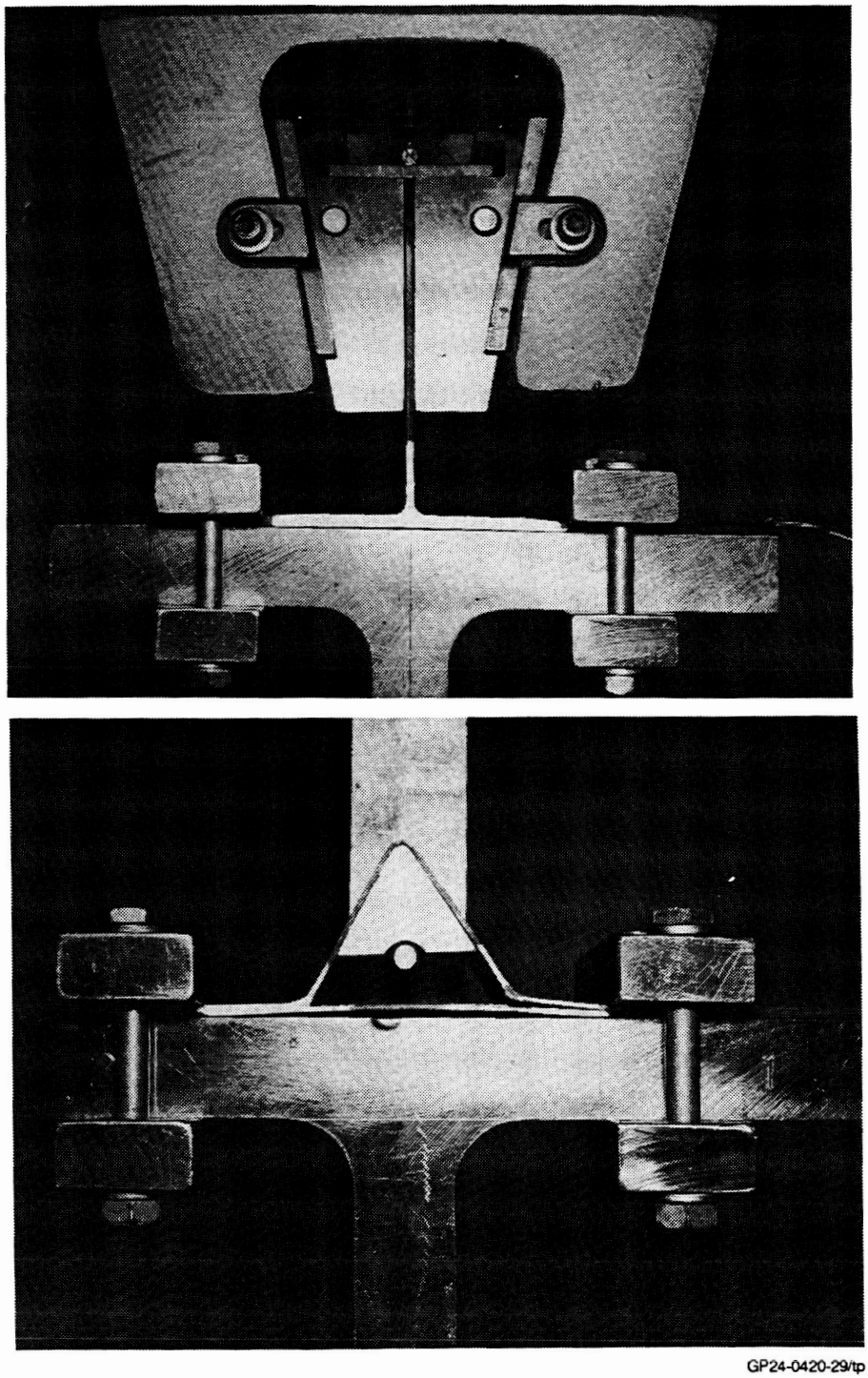

GP24-0420-29/tp

Figure 4.2-3. Frame Pull-Off Testing Equipment

Results from individual test runs are tabulated in Appendix 1. A summary of test results is presented in Figures 4.2-4 and 4.2-5. The following sections provide a detailed discussion of each of the specimen groups that were examined under element testing. A final overview and discussion of results follows these sections.

Frame Configuration	Initial Failure			Final Failure		
	Load (lbs/in)	Deflection (in)	Failure Mode	Load (lbs/in)	Deflection (in)	Failure Mode
Blade	328	0.124	ILT Failure* at Corner	315	0.178	Interface Failure**
45° Y-Frame	554	0.148	Skin Surface Failure at Clamp	655	0.216	ILT + Interface Failure
60° Y-Frame	504	0.161	Skin Surface Failure at Clamp	574	0.247	ILT + Interface Failure

* Interlaminar Tension Failure at Frame Corner
** Interface Failure between Base Skin and Flange

Figure 4.2-4. Test Data Summary for Room Temperature Pull-Off Testing

Frame Configuration	Initial Failure			Final Failure		
	Load (lbs/in)	Deflection (in)	Failure Mode	Load (lbs/in)	Deflection (in)	Failure Mode
Blade	372	0.155	Comp. Failure in Lower Skin	417	0.255	Interface Failure*
45° Y-Frame	530	0.145	Skin Surface Failure at Clamp	746	0.270	Interface Failure
60° Y-Frame	—	—	—	615	0.192	Interface Failure

* Interface Failure between Base Skin and Flange

Figure 4.2-5. Test Data Summary for Elevated Temperature Pull-Off Testing

RTD Blades

Blade specimen testing was utilized as a baseline for comparison to the fastenerless frame attachment designs. Failure modes were anticipated to occur as the result of flatwise tension loading of the interface directly beneath the upstanding leg of the blade.

Test results for the RTD blade elements are summarized in Figure 4.2-4. Average failure corresponded to a 328 lb/in load and a 0.124" displacement. The test data exhibited a fair amount of variation with a standard deviation of 43 lb/in and 0.018", respectively. These values have associated coefficients of deviation of approximately 12% for both measurements.

A typical load history is shown in Figure 4.2-6 with an indication of the failure locations and initial stiffness of the specimens. Each of the RTD blade specimens exhibited a distinctive initial failure which was associated with a radius crack within the angle ply pack. This initial failure was visually observable and correlated exactly with the initial load drop-off. Propagation of the initial crack continued through the remainder of the loading sequence. The second failure was observed to correspond to the loss of the bond between the skin and frame laminates as the radius crack progressed to the interface. The final portion of the load/displacement curve indicates the continued loss of the interface as a result of the crack propagation. The second failure load associated with the blade elements was always of lower magnitude than the crack initiation load. Cracks associated with initial and final failure are readily observable for a typical failed specimen shown in Figure 4.2-7.

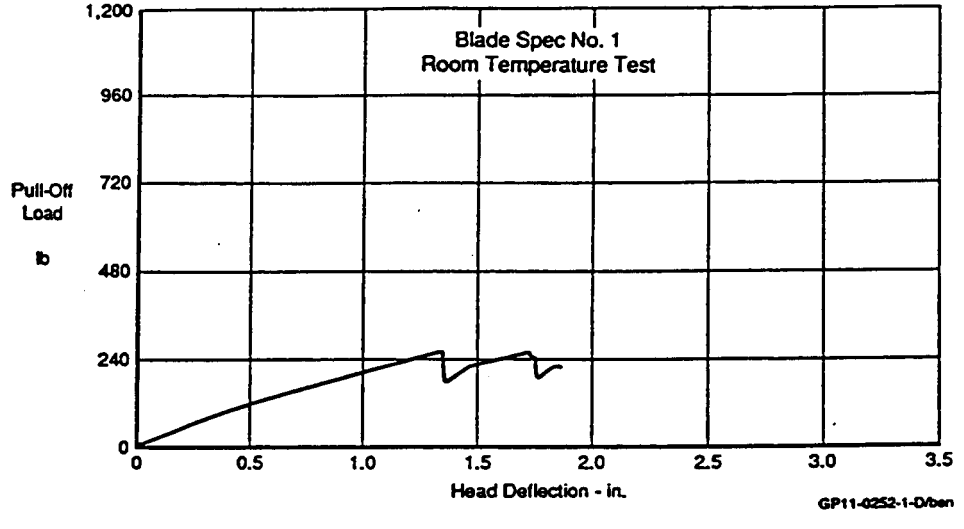

Figure 4.2-6. Room Temperature Blade Typical Load History

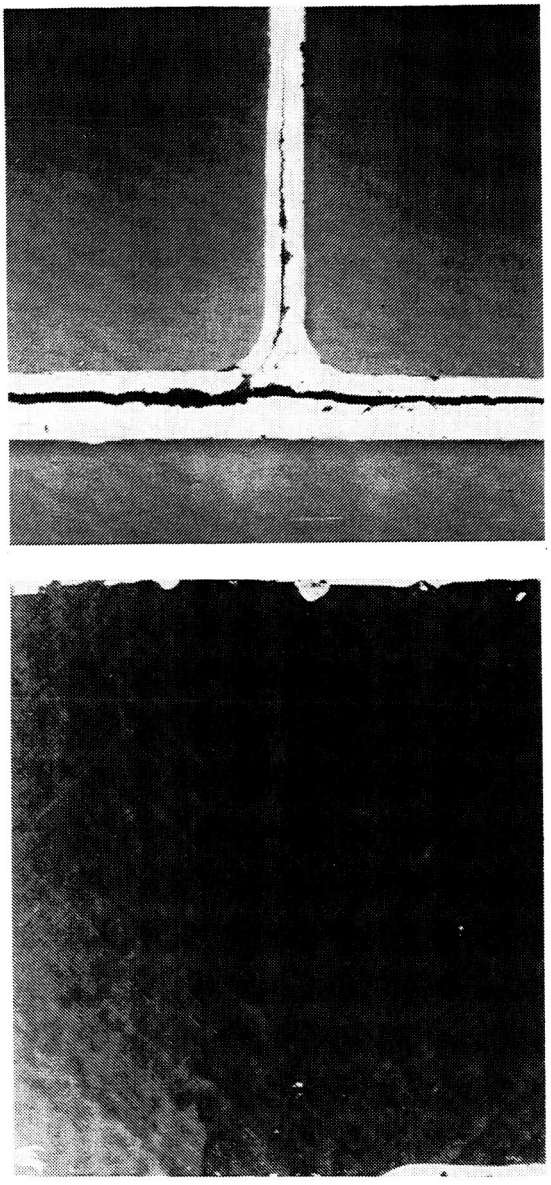

GP24-0420-31/crr

Figure 4.2-7. Typical Failure for Room Temperature Blade Specimens

RTD 60° Y-Frames

Average initial failure for 60° Y-frame elements corresponded to a 504 lb/in load and a 0.161" displacement. Final failure averages were calculated to be 574 lb/in and 0.247". Low scatter in both initial and final loads as well as initial displacement measurements indicated excellent repeatability. Coefficients of deviation were less than 8% for all of these parameters. Final failure displacements however, varied by as much as 0.1" (50% of the average).

A typical load versus deflection plot for the Y-frame design is shown in Figure 4.2-8. Under initial loading the thin skin associated with the Y-section deflected substantially. The eventual interference between the lower skin section and the loading mandrel resulted in an enhanced section stiffness. This

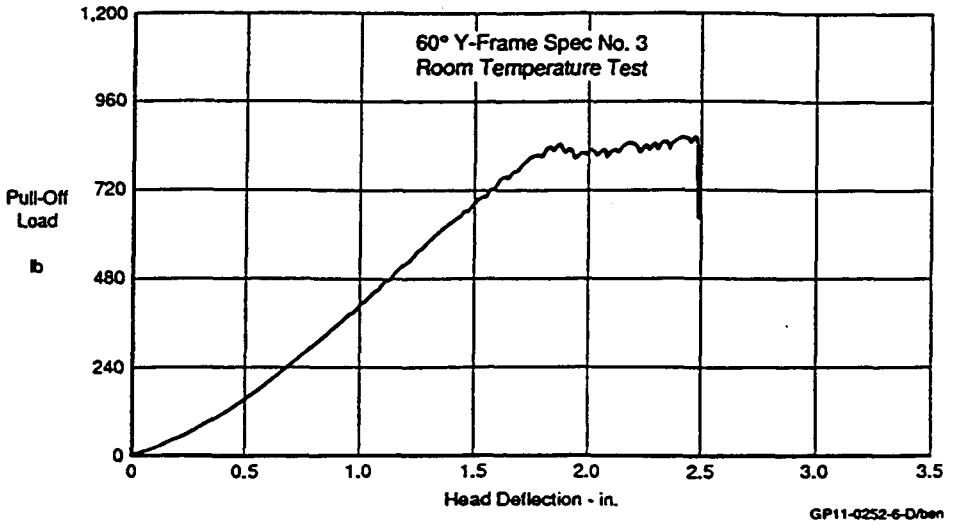

Figure 4.2-8. Room Temperature 60°-Y Typical Load History

observation shows the necessity of increased skin thicknesses for future developments on Y-frame concepts. It is anticipated that such a local padup would have yielded bending resistance on the order of those due to the interference. Initial failures in the Y-frames were associated with compression failure of the skin laminates at the clamped boundary condition.

Increases in the final failure load for Y-frame element over the blade configuration are a result of decreased interlaminar tension stresses through redistribution of the pull-off load into combined interlaminar tension (ILT) and interlaminar shear (ILS). In addition, ILT stress within the upstanding flange laminates is reduced due to the increased radius associated with this geometry. Observation of the final failure for the 60° element, Figure 4.2-9, showed crack initiation occurred as a result of interlaminar tension within the IML skin and resulted in catastrophic failure of the section.

RTD 45° Y-Frames

For the RTD 45° frame elements average initial failure corresponded to a 554 lb/in load and a 0.148" displacement. Final failure averages were calculated to be 655 lb/in and 0.216". As with the 60° elements, initial and final load measurements were very repeatable. Coefficients of deviation were less than 10%. All displacement measurements showed significant deviations with coefficients of approximately 20%.

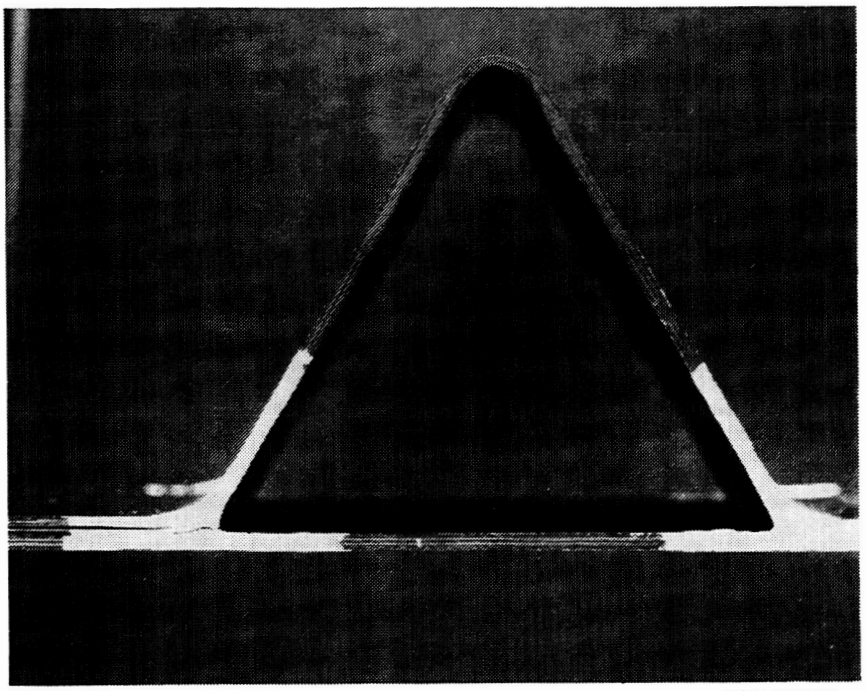

GP24-0420-30/crr

Figure 4.2-9. Typical Failure for Room Temperature 60°-Y Specimens

A typical load versus deflection plot for the 45° frame geometry is given in Figure 4.2-10. Nearly identical specimen response as observed for the 60° element can be seen. This similarity includes initial non-linearity, minor variations due to slip, initial failure due to skin compression and associated reduction in modulus, and substantially higher ultimate pull-off strength. However, the 45° elements all showed continued load carrying capacity following the secondary ILT failure. This additional loading is more pronounced than any observed in the 60° elements and is associated with geometry and load redistribution effects. The larger open angle of the IML skin and further increase in corner radius decreases the ILT stresses within the IML laminate. In addition, loading continues to be redistributed into predominantly ILS stresses, as in the 60° frame. Failure observation for the 45° element showed crack initiation occurred as a result of ILT within the IML skin as previously witnessed in the 60° specimens. However, final failure eventually resulted from propagation of this crack to the interface and continuation of this delamination primarily through a shear mechanism. This crack growth proceeded at a slower rate than observed for either of the previous designs.

ETW Blades

Elevated temperature testing of blade elements results are summarized in Figure 4.2-5. As previously outlined, testing occurred on moisture conditioned specimens subjected to 250°F. Averages for test data load and displacement data were calculated for initial failure to be 372 lb/in and 0.155", respectively. Final failures were 417 lb/in and 0.255", respectively. All of the data appeared to be consistent between replicates with deviations consistently below 10%.

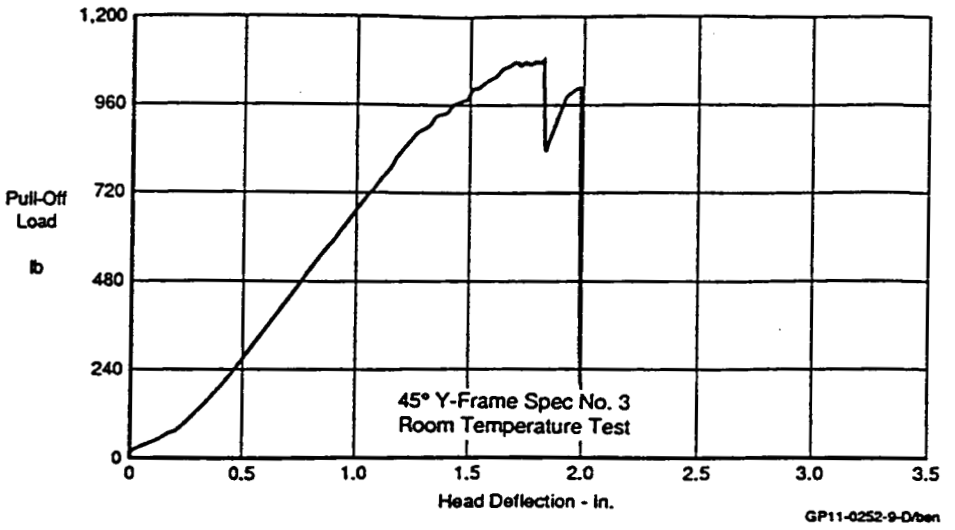

Figure 4.2-10. Room Temperature 45°-Y Typical Load History

Failure of the blade specimens became a more complicated phenomena for the elevated temperature wet condition as can be seen in Figure 4.2-11. A higher degree of non-linearity in the initial load/displacement curve was recorded. Initial failures occurred as the result of compression in the lower skin. Both of these results are attributed to the softening of the material associated with the ETW condition. Very shortly after initial failure, a secondary failure in the interface was observed. Crack initiation occurred at the identical location as for the RT tests, Figure 4.2-12. Following this secondary failure, the frame attachments continued to carry load beyond the initial failure loads. Crack propagation was observed to progress far more slowly due to the plastitization of the matrix material. Eventual loss of all strength was associated with the loss of a significant portion of the flange to skin interface (approximately 50%).

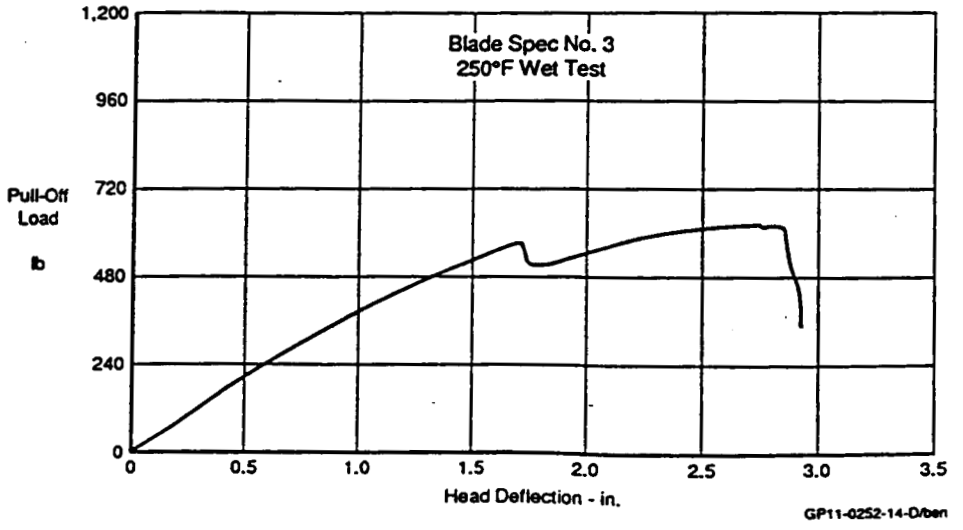

Figure 4.2-11. Load vs Displacement History for Elevated Temperature Blade Specimen

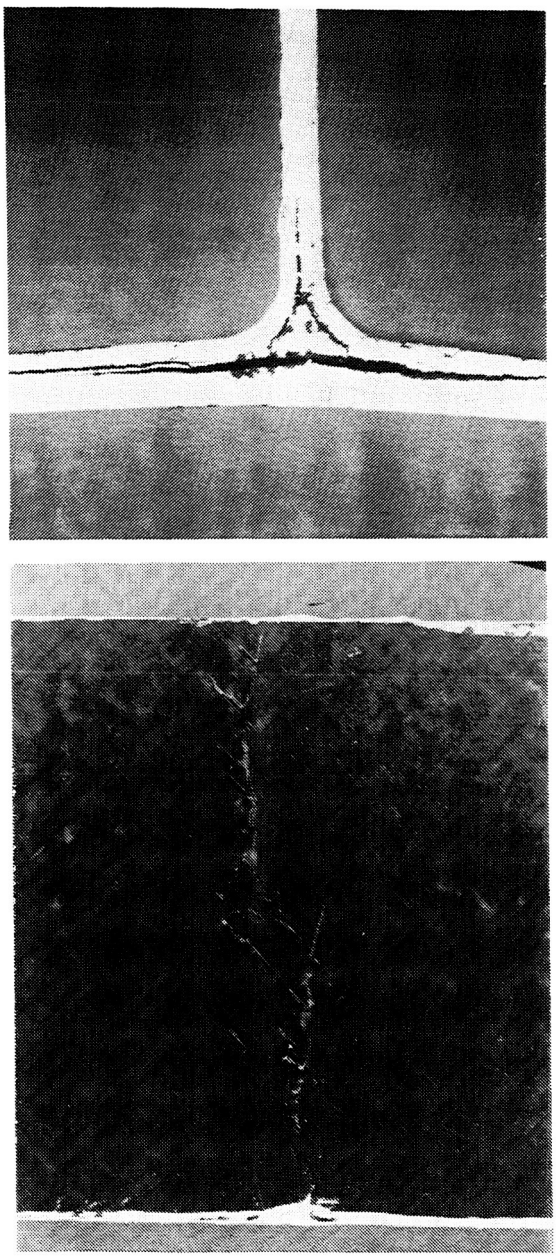

GP24-0420-32/crr

Figure 4.2-12. Typical Blade Failure for Elevated Temperature Testing

Failure loads for all of the blade specimens were considerably higher than in the RTD tests. Similar results for lap shear specimens have been reported in previous work conducted at MCAIR. The mechanism for this increase in ETW strength is identical for both test situations. Elevated temperature response for the interface material shows a decrease in both stiffness and strength. However, an associated increase in ultimate strain is associated with the material due to its plastic response. The lap shear data has shown that the associated energy that the material is capable of absorbing prior to failure is significantly increased due to the large plastic deformations that become possible for the ETW material. The effect of the plasticity is to lower the peak stresses at the ends of interfaces while increasing the stresses across the remainder of the interface. This results in an increase in the total load carrying capacity of the interface. The plasticity also accounts for the non-linearity observed during the initial portion of the load/displacement plot.

ETW 60° Y-Frames

Testing of the ETW 60°F frame elements resulted in an average failure load of 615 lb/in corresponding to a 0.192" final failure deflection. Unlike room temperature specimens, multiple failures were not observed during elevated temperature testing. Test scatter was low for both load and deflection.

The 60° frame elements exhibited the same degree of non-linearity that was observed for the blade specimens. Skin compression failures occurred at the clamp location but to a much lesser extent than previously encountered for RT testing. No indication of skin compression failures beneath the frame attachment point were evident during the test or in the load/deflection history, Figure 4.2-13. A typical failed specimen is shown in Figure 4.2-14. Failure at the IML to OML interface occurred with immediate propagation of this failure to the clamp locations. No failures were witnessed within the IML skin due to interlaminar tension as observed in the RTD testing.

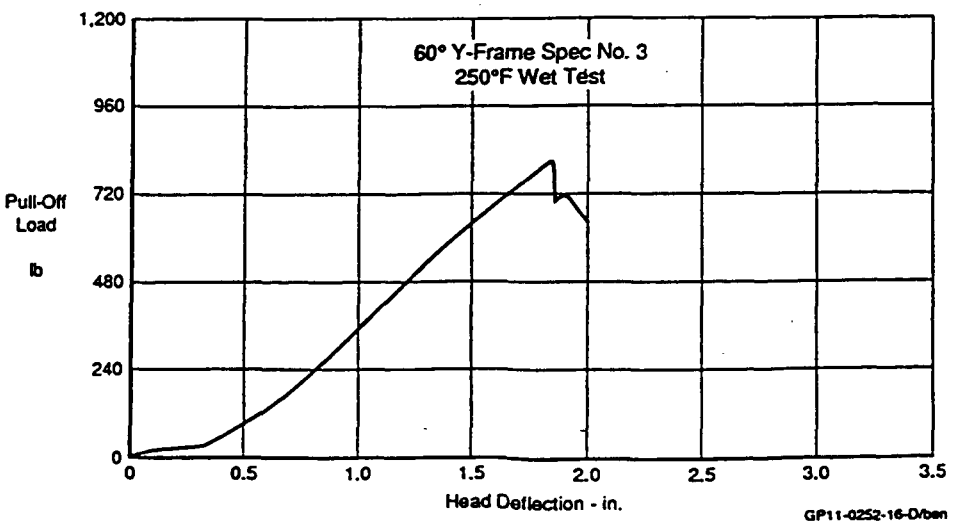

Figure 4.2-13. Load vs Displacement History for Elevated Temperature 60°-Y Specimen

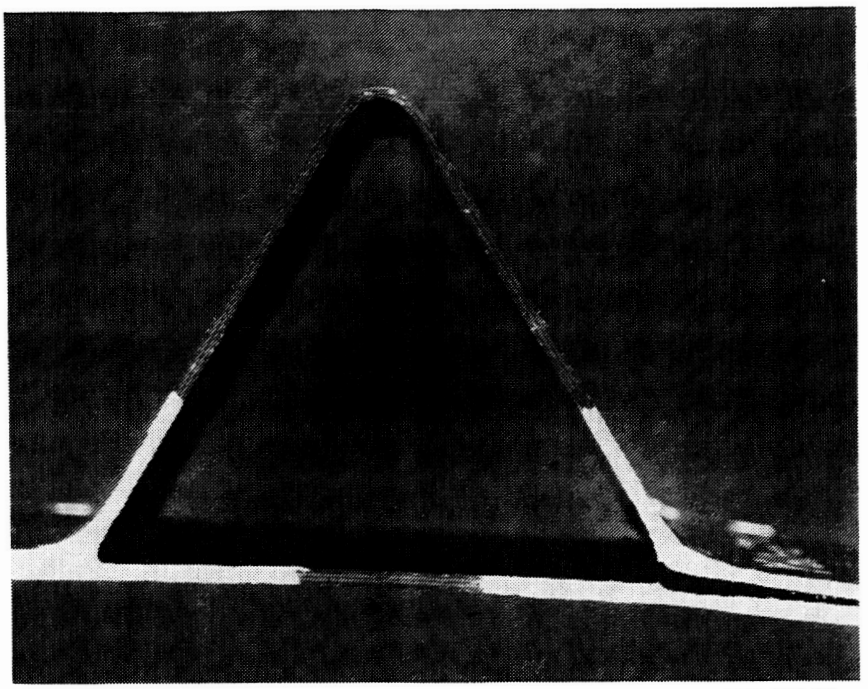

GP24-0420-33/crr

Figure 4.2-14. Typical 60°-Y Failure for Elevated Temperature Testing

The increase in ultimate loading over the baseline blade configuration was also observed for these specimens and again indicates the advantage of redistributing load into ILS and ILT through the Y-frame design.

ETW 45° Y-Frames

Additional increases in pull-off strength were realized in the 45° frame element tests for 250°F. Specimens averaged an ultimate strength of 746 lb/in with less than a 5% coefficient of deviation; associated displacement average was 0.27" with a slightly higher measure of variation. It should be noted that these averages were based upon two specimen runs. The third element sustained a displacement of greater than 0.35" without any inter-radii or interface failures before the test was stopped.

Failure of the 45° frame specimens was more severe than had been witnessed in the 60° frame specimens and is attributed to the increased deflection observed in these specimens. A typical load/deflection plot for a failed specimen is shown in Figure 4.2-15. This plot does not indicate the high degree of non-linearity previously encountered. The change in slope which is evident at approximately 70% of ultimate load is a reflection of the compression failure which occurred at the clamped boundary. Final failure again occurred with the total failure of the interface due to primarily shear loading, Figure 4.2-16. The full failure of the interface is another indication that the plasticity of the matrix material is allowing the entire interface to carry more load than in the room temperature cases. This increased plastic loading prohibits the interface from resisting any cracks which initiate.

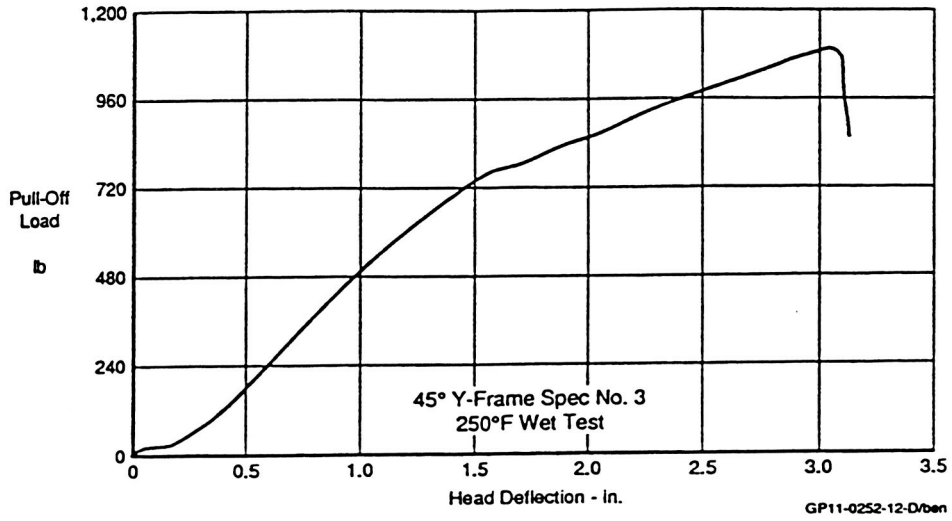

Figure 4.2-15. Load vs Displacement History for Elevated Temperature 45°-Y Specimen

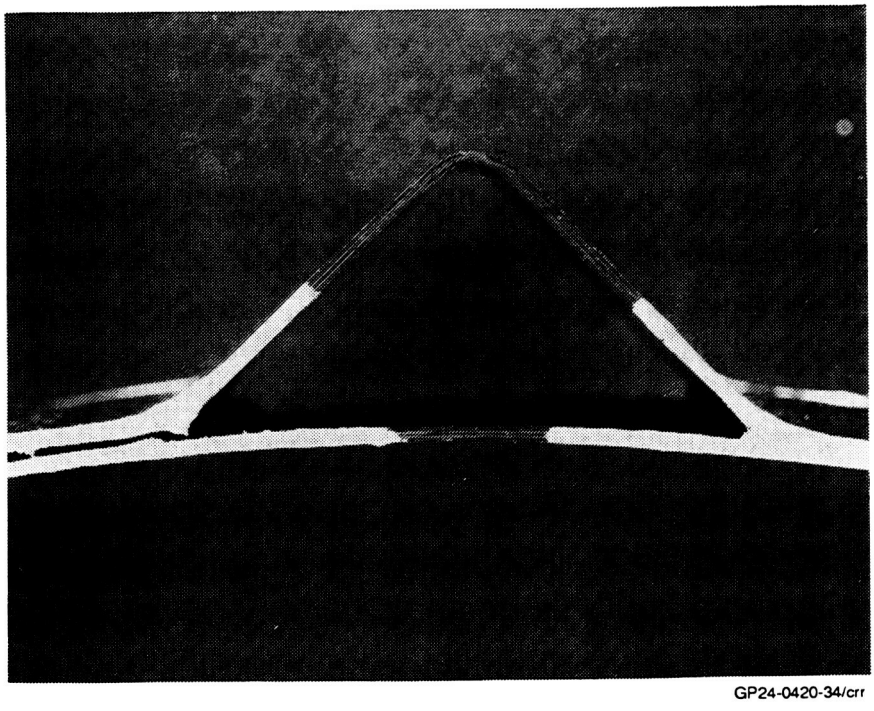

Figure 4.2-16. Typical 45°-Y Failure for Elevated Temperature Testing

Induction Welded 60° Frames

In support of efforts for fastenerless designs, testing was conducted on frame elements formed by induction welding. These elements are of identical geometry and laminate design as the 60° frame elements previously described. Testing provided a means of assessing the relative strengths that can be obtained through the induction welding process.

C-scan results from the induction welded panel showed severe porosity throughout the flange. In addition, the skin laminate exhibited severe deformations beneath the Y-section. This curvature is the result of thermal stresses which resulted from local heating generated by the welding process. The problem of laminate deformation was worsened by the lack of an internal mandrel to maintain geometry during welding. Despite the poor quality of the specimens testing was conducted in order to obtain some initial data which might be later correlated to parameters used during the induction welding process. Due to the program redirection, further investigation of this technique was not carried out.

A summary of the test results were given in Figure 4.2-18. Induction welded elements showed no definitive trends in either initial or final failure. Observation of the tests showed a nearly immediate separation of one flange interface for two of the tests. These specimens continued to carry load primarily through the IML skin with substantial bending of the corner radius occurring. Final failure occurred with the complete separation of the IML and OML skins, Figure 4.2-17, but was not consistent with respect to either load or deflection. All ultimate strengths for the room temperature specimens were approximately 35% of the ultimate loads associated with the coconsolidated elements. It is difficult however, to associate this strength with the interface strength of the welding process. The value more likely represents the ability of the individual IML skin to resist the out-of-plane load. Elevated temperature test data proved to be equally ambiguous as can be seen in the tabulated results, Figure 4.2-18.

Overview of Element Tests

Testing of the fastenerless frame attachments provided the necessary experience with these designs to allow for risk reduction in future scale up to subcomponent and full-scale articles. Of primary importance has been the demonstration of significant increases in the pull-off strength of frame attachments that can be achieved through Y-section designs. Through the examination of two geometries an initial understanding of the effects of geometry on load redistribution and strength improvements has been gained. Gains on the order of 50% were achieved for designs involving a 60° frame element as compared to the baseline blade. An additional improvement of 10% was obtained when the interior angle of the Y-section was reduced to 45°. These improvements are based upon initial failure loads for all of these sections and are summarized in Figure 4.2-19. Increases in section deflections were also evident in the test data. This fact points out the importance of including a local pad-up beneath the Y-section for future design developments.

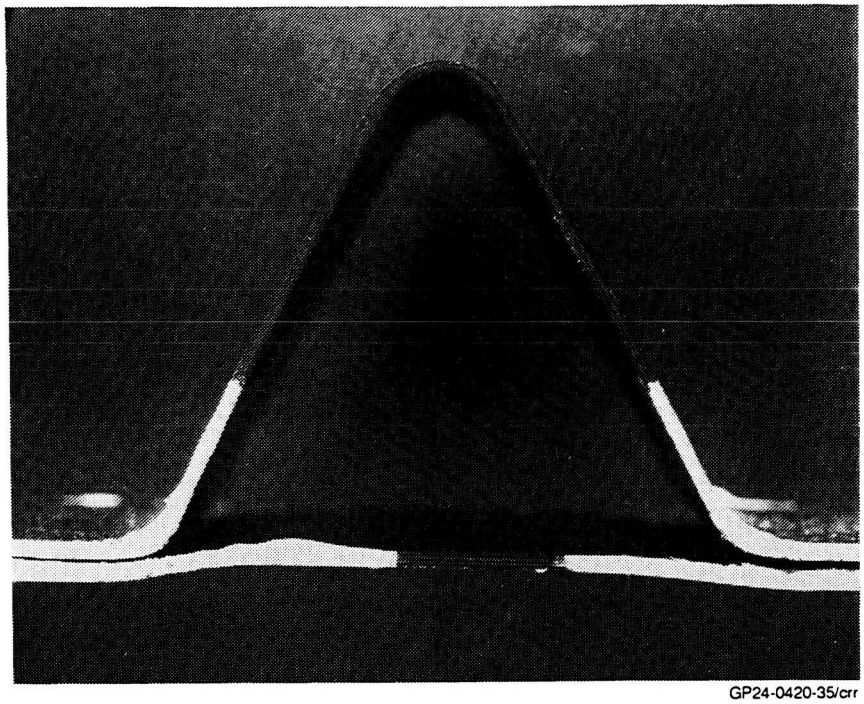

GP24-0420-35/crr

Figure 4.2-17. Typical Failure Associated With Induction Welded Specimens

Induction Welded Specimen	Initial Failure		Final Failure	
	Load (lbs/in.)	Deflection (in.)	Load (lbs/in.)	Deflection (in.)
Room Temp No. 1	65	0.039	224	0.212
Room Temp No. 2	22	0.186	225	0.209
Room Temp No. 3	90	0.044	100	0.080
Elevated Temp No. 1	–	–	127	0.110
Elevated Temp No. 2	–	–	131	0.053
Elevated Temp No. 3	–	–	68	0.040

GP24-0420-64-D/mld

Figure 4.2-18. Test Data Summary of Induction Welded 60° Y-Frame Specimens

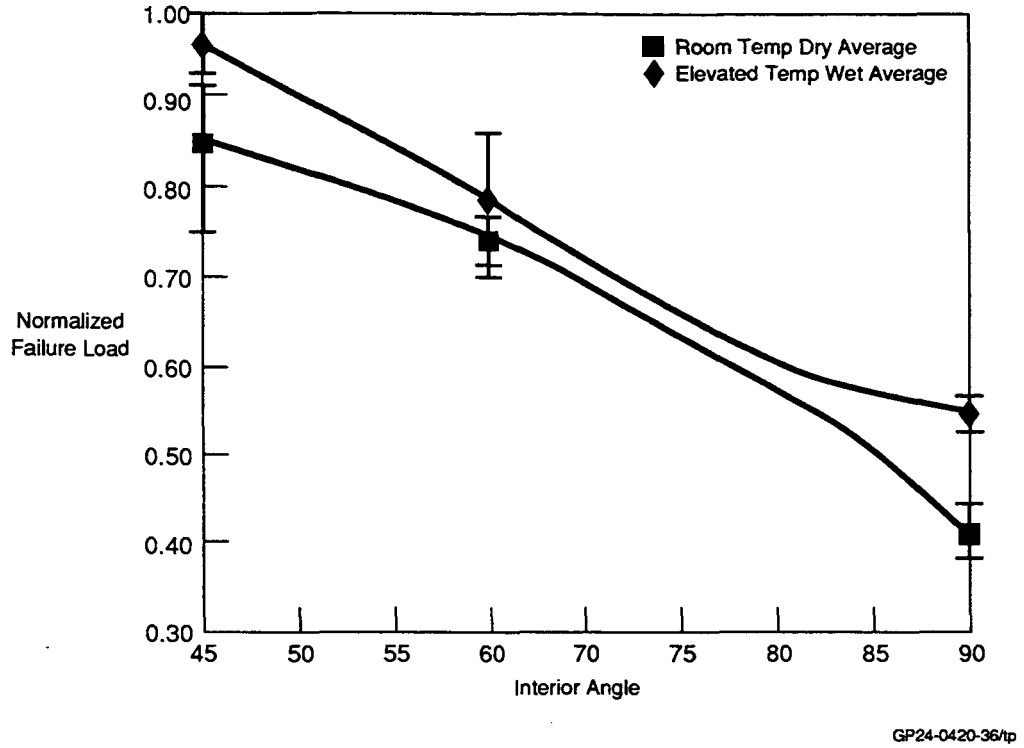

Figure 4.2-19. Performance Improvements Associated With Y-Frame Designs

Elevated temperature testing demonstrated the improvements in performance associated with a thermoplastic material subjected to interlaminar shear and tension. These increases are justified when considering the potential for plastic deformation of the matrix material in the interface. Some concern over this type of response will undoubtedly remain until an understanding of the possible fatigue response is investigated.

An adequate optimization of the induction welding process was not achieved due to redirection of the program. As a result, the testing that was performed under this task should not be considered representative of the final strengths that this method may be able to achieve. However, the results obviously point out the need for improvements not only to the process but to the concept for application as well. In future work tooling must be provided which will maintain part geometry during critical heat-up and cool-down periods. The lack of such tooling proved to be detrimental to part quality for the specimens tested.

With regard to testing, it is evident that future attempts must identify a means of load introduction which will not produce an interference between the load mechanism and the lower skin section. It is also recommended that skin thicknesses be increased to prohibit bending failures at the grip locations. These changes to the base laminate should include the addition of the previously mentioned pad-up region beneath the Y-section. A means of eliminating slipping beneath the clamping device should be found. As an alternative, the use of simple (or rollered) supports might be examined. This problem might also be advantageously influence by the increased skin thickness already proposed. Finally, it should be mentioned that the use of video-taping in conjunction with the use of white-out on the specimen edges proved to be invaluable in correlating test results with observed failure modes.

THIS PAGE INTENTIONALLY LEFT BLANK

5. CONCLUSIONS AND RECOMMENDATIONS

Thermoplastic composite development pursued in this program, while directed toward fighter aircraft structure, are equally applicable to commercial vehicle structure. These developments focused on critical composite issues associated with primary fuselage structure, fastenerless moldline, upper fuel cell cover structure, and thick lugs representative of those on carry-through bulkheads. Activities by a D/MI team were carried out in the areas of structural mechanics, manufacturing concepts development, and structural validation.

In the structural mechanics area, progress was made in the utilization and understanding of the dissipated strain energy (DSE) technique as a design/analysis tool. Further implementation of this approach for structural simulation requires the completion of the cross-ply-to-lamina and lamina-to-laminate translators at NRL. In addition, it is suggested that future structural simulations be carried out in a building block approach (i.e., coupons, notched coupons, unstiffened panels, stiffened panels, etc.) to validate the DSE technique.

An analytical code, utilizing a previously developed subparametric laminated solid element, was developed to predict through-the-thickness stress fields associated with thick composite lugs. While strength predictions were in good agreement with test results, observed failure modes were generally not in agreement with those predicted. However, it was noted that predicted secondary failure locations and failure mode were in agreement with those observed. This leads to the conclusion that predicted failure mode is sensitive to the selected failure theory. The developed code has the capability to accommodate additional failure theories. This activity could be pursued after the analysis package is installed in NASA's COMET library.

Selection of the upper fuel cell cover allowed for conceptual development of two promising cost-effective, innovative manufacturing approaches; fiber placement, and single diaphragm/coconsolidation (SDCC), which have potential applications for a majority of the remaining components of the generic fuselage section. Based on these approaches, elemental specimens were designed, fabricated, and structurally tested to validate manufacturing concepts.

Elemental manufacturing verification trials produced valuable lessons learned. In the SDCC Y-frame activities simple tooling modifications such as blended stiffener mandrel and pressure box ramp intersections coupled with aluminum diaphragms eliminated diaphragm ruptures. Polymeric diaphragms are still desirable from a cost point of view, but as yet do not have the necessary elongation properties needed for complex forming.

A one-step SDCC process was a program goal, however ply dragging/wrinkling problems necessitated going to a two-step process which yielded production quality parts. While the two-step process provides

cost savings over conventional three-step diaphragm forming, the one-step technique should still received industry attention since additional cost savings could be realized.

The development of a positive drive tooling concept for the blade frame elements came about as a need to correct inadequate intersection consolidation pressure inherent in the original tooling. The addition of selected keyways to the tooling allowed for segmented tooling details to be directed (positively driven) during pressure application resulting in a first-time quality part. In addition, a previously rejected blade element was reconsolidated to production quality in the modified tooling demonstrating the potential cost savings associated with the ability to reconsolidate thermoplastic composites.

Roll-forming may be a viable technique for producing long, relatively constant cross-section stiffeners. While sections produced in this effort did not reach production quality consolidation, overall cross-section geometrical tolerances, straightness in length, and repeatability were quite good. Investigations in this program revealed that while there is still some development necessary, this approach should receive additional industry attention.

Thick laminates (1.0 inch) were manufactured to production quality by consolidating a series of sublaminates. An additional benefit of this effort was the demonstration of abrasive water jet cutting as an effective means of machining thick composites. Edge surface finish was found to be very acceptable for high tolerance areas requiring only modest surface reaming or finishing for low tolerance areas.

Significant pull-off strength increases were demonstrated in the Y-frame concepts compared to conventional blade design. Testing of the fastenerless frame concepts has provided the necessary experience with these designs to allow for risk reduction in future scale-up to subcomponent and full-scale structure.

REFERENCES

1) Mast, P., Beaubien, L., Mulville, D., Sutton, S., and Wolock, I., ASME Paper No. 80-WA/APM-9, "Fracture Criteria of Fibrous Laminated Composites Under In-Plane Multidirectional Loading."

2) Wilkins, D. J., "Anistropic Curved Panel Analysis," Report FZM-5567, Air Force Contract No. F33615-69-C-1494, May 1973.

3) Lundstrom, E. A., NWC TP 6770 "Structural Response of Flat Panels to Hydraulic Ram Pressure Loading," December 1987.

4) Lundstrom, E. A., JTCG/AS-74-T-018, Fluid Dynamic Analysis of Hydraulic Ram IV, (User's Manual for Pressure Wave Generation Model), October 1976.

5) Goering, J., "Initial Impact Damage of Composites," Material Science Corporation Report MSC TFR 1801/1207, March 1987.

6) Hashin, Z., "Failure Criteria for Unidirectional Fiber Composites," Journal of Applied Mechanics, Vol. 47, 1980, p. 329-334.

7) Wanthal, S., MCAIR Tech Note AMS-TN-91-2, "The Determination of Stresses in Cocured and Adhesively Bonded Skin-Stiffener Interfaces," March 1991.

8) Hoffman, P. L. R. and Gibler, J. A., "Design for Manufacturing, Producibility Issues for Thermoplastic Composites," presented at SAMPE Spring Meeting, Anaheim, CA, April 4, 1990.

THIS PAGE INTENTIONALLY LEFT BLANK

```
**************************************************************************
****                                                                  ****
****                          F A T L A M                             ****
****                                                                  ****
****        FAILURE ANALYSIS OF THICK LAMINATED COMPOSITES            ****
****                                                                  ****
****                 DEVELOPED BY J.GOERING   5/89                    ****
****                                                                  ****
****                          REVISION 2.0                            ****
****                                                                  ****
**************************************************************************
```

DATA INPUT FORMAT (FILE01.DAT):

**** CONTROL INPUT ****

TITLE	78 CHARACTER ALPHANUMERIC TITLE.
NCHECK,NATYPE,NORDER,IMPRNT	THE DATA CHECK FLAG, ANALYSIS TYPE FLAG, NUMERICAL INTEGRATION ORDER, AND THE EXPANDED MATERIAL PROPERTY PRINTOUT FLAG. IF NATYPE = 0, NORDER AND IMPRINT ARE IGNORED. NCHECK = 0 (DEFAULT), DATA CHECK ONLY. = 1, ANALYSIS NATYPE = 0, BACK SUBSTITUTION. = 1, 3-D GENERATION. 2 < NORDER < 4 IMPRNT = 0 (DEFAULT), PRINT MATRICES. = 1, DO NOT PRINT MATRICES.
NAME1	BACK SUBSTITUTION DATA STORAGE FILE NAME. (40 CHARACTER MAXIMUM)
NAME2	LAMINA DEFINITION STORAGE FILE NAME. (40 CHARACTER MAXIMUM)
NAME3	ELEMENT DEFINITION STORAGE FILE NAME. (40 CHARACTER MAXIMUM)
NAME4	CONSTRAINT DEFINITION STORAGE FILE NAME. (40 CHARACTER MAXIMUM)
NAME5	IF NATYPE > 0, CONSTRAINED, CONDENSED SUBSTRUCTURE MASS AND STIFFNESS MATRIX STORAGE FILE NAME. IF NATYPE = 0, DISPLACEMENT VECTOR STORAGE FILE NAME. (40 CHARACTER MAXIMUM)

NAME6 — POST PROCESSING DATA STORAGE FILE NAME. (40 CHARACTERS MAXIMUM)

**** BACK SUBSTITUTION INPUT ****

NSUBS — THE INDEX NUMBER OF THE SUBSTRUCTURE TO BE ANALYZED. IF NATYPE > 0, THE WILL SKIP THIS INPUT AND JUMP TO THE LAMINATE DEFINITION INPUT.

IDPRNT,(NPRINT(I),I=1,7) — THE EXPANDED DISPLACEMENT VECTOR PRINT-OUT FLAG AND THE STRESS AND STRAIN PRINT-OUT FLAGS. WHEN A FLAG IS SET TO 0 (DEFAULT), THE ASSOCIATED DAT SET WILL BE PRINTED, IF SET TO 1, THE DATA WILL NOT BE PRINTED.

- IDPRNT - DISPLACEMENT VECTOR.
- NPRINT(1) - GLOBAL STRESSES.
- NPRINT(2) - GLOBAL STRAINS.
- NPRINT(3) - LOCAL STRESSES.
- NPRINT(4) - LOCAL STRAINS.
- NPRINT(5) - PLY PRINTOUT.
- NPRINT(6) - INTERFACE PRINTOUT.
- NPRINT(7) - SURFACE PRINTOUT.

**** LAMINATE DEFINITION ****

NMAT — THE NUMBER OF MATERIALS. THE PROGRAM WILL LOOK FOR NMAT SETS OF MATERIAL PROPERTY INPUT FOLLOWING THIS ENTRY.

*** MATERIAL DEFINITION ***

LABEL — 40 CHARACTER ALPHANUMERIC MATERIAL LABEL.

LTYPE — THE LAMINA TYPE FLAG. THE NEXT LINE OF INPUT DEPENDS UPON THE VALUE OF LTYPE.

- LTYPE = 1, ISOTROPIC LAYER
- = 2, TRANSVERSELY ISOTROPIC TAPE
- = 3, BALANCED CLOTH (E1=E2)

** PROPERTIES FOR LTYPE = 1 LAMINA **

E,NU,T — ELASTIC CONSTANTS FOR ISOTROPIC LAYERS.

** PROPERTIES FOR LTYPE = 2 LAMINA **

E1,E2,NU12,NU23,G12,T — ELASTIC CONSTANTS FOR TRANSVERSELY ISOTROPIC LAYERS (TAPE).

** PROPERTIES FOR LTYPE = 3 LAMINA **

E1,E3,NU12,NU23,G12,G23,T	ELASTIC CONSTANTS FOR BLANACED CLOTH LAYERS.
** STRENGTHS **	
S1T,S1C,S2T,S2C,S12,S23	STRENGTHS FOR THIS MATERIAL. S1T AND S1C ARE THE AXIAL TENSILE AND COMPRESSIVE STRENGTHS, S2T AND S2C ARE THE TRANSVERSE TENSILE AND COMPRESSIVE STRENGTHS, AND S12 AND S23 ARE THE AXIAL AND TRANSVERSE SHEAR STRENGTHS.
*** LAMINATE PARAMETERS ***	
NPLY,IFMAT	THE NUMBER OF PLIES IN THE LAMINATE, AND THE INDEX NUMBER OF THE MATERIAL TO BE USED FOR CALCULATING INTERFACE STRESSES AND STRAINS. THE PROGRAM WILL LOOK FOR NPLY LAMINA DEFINITIONS FOLLOWING THIS ENTRY.
** LAMINA DEFINITIONS **	
MAT,THETA	THE MATERIAL INDEX NUMBER AND ORIENTATION OF THE PLY. THETA MUST BE INPUT IN DEGREES, AND IS MEASURED FROM THE GLOBAL X AXIS TO THE PLY 1 AXIS.
**** SUBSTRUCTURE DEFINITION ****	
NLAYER	THE NUMBER OF LAYERS OF ELEMENTS THROUGH THE THICKNESS OF THE LAMINATE. THE PROGRAM WILL LOOK FOR NLAYER LAYER DEFINITIONS FOLLOWING THIS ENTRY.
IPLYB,IPLYT	INDEX NUMBERS FOR THE BOTTOM AND TOP PLIES IN THIS LAYER. LAYERS MUST BE DEFINED STARTING WITH THE BOTTOM MOST PLY (PLY 1), AND INPUT IN ORDER OF INCREASING PLY INDICIES. IPLYB(N) = IPLYT(N-1)+1.
NC	THE NUMBER OF COLUMNS OF NODES TO BE DEFINED. THE PROGRAM WILL LOOK FOR NC COLUMN DEFINITIONS FOLLOWING THIS ENTRY.
NCOL,X,Y,BETA	THE X AND Y POSITION OF COLUMN NCOL, AND THE ROTATION OF THE NODAL COORDINATE SYSTEM RELATIVE TO THE GLOBAL AXES. BETA IS INPUT IN DEGREES.
NS	THE NUMBER OF ELEMENT STACKS TO BE DEFINED. THE PROGRAM WILL LOOK FOR NS STACK DEFINITIONS FOLLOWING THIS ENTRY.
NCOL(I),I=1,NNS	THE NODE COLUMNS DEFINING THIS STACK.
**** CONSTRAINTS ****	

NZDF	THE NUMBER OF DISPLACEMENTS SET TO ZERO. THE PROGRAM WILL LOOK FOR NZDF LINES OF INPUT WITH ONE CONSTRAINT PER LINE.
NCOL,LABELP,ILAYER,DIR	THE COLUMN WHICH IS CONSTRAINED, THE THROUGH-THE-THICKNESS POSITION AT WHICH THE SPECIFICATION APPLIES, THE INDEX NUMBER OF THE LAYER INTERFACE AT WHICH THE SPECIFICATION APPLIES, AND THE DIRECTION IN WHICH IT IS CONSTRAINED. VALID LABELS FOR THE THROUGH-THE-THICKNESS POSITIONS ARE: LABELP = 'B' - BOTTOM SURFACE = 'T' - TOP SURFACE = 'L' - LAYER INTERFACE ILAYER = 'A' - ALL POSITIONS NOTE THAT THE PARAMETER ILAYER IS ONLY USED WHEN THE PARAMETER LABELP = 'L'. THE DIRECTION IS SPECIFIED BY THE LABEL 'Unm', WHERE n IS BETWEEN 1 AND 3, AND m IS BETWEEN 0 AND 3. 'Un0' IS THE TRANSLATION IN THE n DIRECTION, AND 'Unm' IS THE DERIVATIVE OF Un WITH RESPECT TO COORDINATE m, WHEN m IS NOT ZERO. OPTIONAL DIRECTION LABELS ARE 'Snm', WHICH SPECIFIES SYMMETRY ABOUT THE nm PLANE, AND 'FIX' WHICH SPECIFIES THAT THE NODE WILL BE CLAMPED (ALL DISPLACEMENT COMPONENTS SET TO ZERO).
NCS	THE NUMBER OF COUPLED SETS. THE PROGRAM WILL LOOK FOR NCS GROUPS OF COUPLED SET DATA.
NIS,DIR	THE NUMBER OF POINTS IN THE SET, AND THE DIRECTION IN WHICH THEY ARE COUPLED. THE PROGRAM WILL LOOK FOR NIS POSITION SPECIFICATIONS FOLOWING THIS ENTRY.
NCOL,LABELP,ILAYER	COUPLED DOF POSITION SPECIFICATIONS. THE FIRST SPECIFICATION WILL BE RETAINED AS AN ACTIVE DOF.
NCE	THE NUMBER OF CONSTRAINT EQUATIONS. THE PROGRAM WILL LOOK FOR NCE GROUPS OF CONSTRAINT EQUATION DATA.
NTE	THE NUMBER OF TERMS IN THE EQUATION. THE PROGRAM WILL LOOK FOR NTE LINES OF INPUT WITH ONE TERM PER LINE.
NCOL,LABELP,ILAYER,DIR,VALUE	CONSTRAINT EQUATION TERMS. THE FIRST TERM WILL BE DEACTIVATED.

**** MASTER DEGREES OF FREEDOM ****

NMDF	THE NUMBER OF MASTER DEGREES OF FREEDOM. THE PROGRAM WILL LOOK FOR NMDF LINES OF INPUT WITH ONE MASTER SPECIFICATION PER LINE.
NCOL,LABELP,ILAYER,DIR	MASTER DEGREE OF FREEDOM POSITION SPECIFICATION. THESE PARAMETERS HAVE THE SAME MEANING AS SIMILAR PARAMETERS USED TO DEFINE CONSTRAINED DOF'S. DIR MAY BE ANY VALID DIRECTION (Unm), OR 'ALL'. WHEN 'ALL' IS SPECIFIED, ALL DEGREES OF FREEDOM AT THE SPECIFIED NODE ARE RETAINED AS MASTERS.

```
**************************************************************************
****                                                                  ****
****                          S T A F L M                             ****
****                                                                  ****
****                STATIC ANALYSIS OF FATLAM MODELS                  ****
****                                                                  ****
****                  DEVELOPED BY J.GOERING  8/89                    ****
****                                                                  ****
****                          REVISION 1.0                            ****
****                                                                  ****
**************************************************************************
```

INPUT DATA FORMAT (FILE01):

*** CONTROL INPUT ***

TITLE	80 CHARACTER ALPHANUMERIC TITLE.
NDOF,IRFP,NITR	THE NUMBER OF DEGREES OF FREEDOM PER NODE, THE REACTION FORCE PRINTOUT FLAG, AND THE MAXIMUM NUMBER OF ITERATIONS. 0 < NDOF < 7 IF IRFP = 0 (DEFAULT) REACTION FORCES WILL BE CALCULATED AND PRINTED, IF IRFP = 1 THEY WILL NOT.
NAME1	40 CHARACTER ALPHANUMERIC FILE NAME. THE DISPLACEMENT VECTORS WILL BE WRITTEN TO NAME1.
NE	THE NUMBER OF SUBSTRUCTURES TO BE INPUT. THE PROGRAM WILL LOOK FOR NE SUBSTRUCTURE DEFINITIONS IN THE FOLLOWING FORM.

*** SUBSTRUCTURE DEFINITION FORMAT ***

NAME2	40 CHARACTER ALPHANUMERIC FILE NAME. THE PROGRAM WILL LOOK FOR THE STIFFNESS MATRIX OF THIS SUBSTRUCTURE ON NAME2.
NNE	THE NUMBER OF NODES IN THIS SUB-STRUCTURE. THE PROGRAM WILL LOOK FOR NNE NODE NUMBERS FOLLOWING THIS ENTRY, ARRANGED IN GROUPS OF TEN PER LINE.
NODES(I),I=1,NNE	THE NODES DEFINING THIS SUBSTRUCTURE, ARRANGED IN GROUPS OF TEN PER LINE.

*** CONSTRAINTS ***

NSD		NUMBER OF SPECIFIED DISPLACEMENTS. THE PROGRAM WILL LOOK FOR NSD LINES OF INPUT FOLLOWING THIS ENTRY, WITH ONE DISPLACEMENT SPECIFICATION PER LINE.
NODE,DIRECTION,VALUE		SPECIFIED DISPLACEMENT DEFINITION. VALID DIRECTIONS ARE Ui, FOR i = 1 TO NDOF.
NCS		NUMBER OF COUPLED SETS. THE PROGRAM WILL LOOK FOR NCS GROUPS OF COUPLED SET INPUT, FOLLOWING THIS ENTRY.
NIS,DIRECTION	:	NUMBER OF NODES IN THE SET, AND THE DIRECTION IN WHICH THEY ARE COUPLED. THE PROGRAM WILL LOOK FOR NIS NODE NUMBERS FOLLOWING THIS ENTRY, ARRANGED IN GROUPS OF 10 PER LINE.
	: NCS GROUPS	
NODES(J)	:	NODES IN THE COUPLED SET, J=1 TO NIS. THE FIRST NODE IN THE SET REMAINS ACTIVE.
NCE		NUMBER OF CONSTRAINT EQUATIONS. THE PROGRAM WILL LOOK FOR NCE GROUPS OF CONSTRAINT EQUATION INPUT, FOLLOWING THIS ENTRY.
NTE	:	NUMBER OF TERMS IN THE EQUATION. THE PROGRAM WILL LOOK FOR NTE LINES OF INPUT FOLLOWING THIS ENTRY, WITH ONE TERM OF THE CONSTRAINT EQUATION PER LINE.
	: NCE GROUPS	
NODE(J),DIR(J),VAL(J)	:	DEFINITION OF TERM J, J=1 TO NTE. THE FIRST TERM IN THE SET IS DE-ACTIVATED.

*** GAP/CONTACT ELEMENTS ***

NGC	THE NUMBER OF GAP/CONTACT ELEMENTS USED IN THE MODEL. THE PROGRAM WILL NGC ELEMENT DEFINITIONS FOLLOWING THIS ENTRY, WITH ONE DEFINITION PER LINE.
N1,DIR1,N2,DIR2,CK,IOPEN,TRSHLD	GAP/CONTACT ELEMENT DEFINITION.

*** LOADS ***

NSF	THE NUMBER OF SPECIFIED FORCES. THE PROGRAM WILL LOOK FOR NSF LINES OF INPUT FOLLOWING THIS ENTRY, WITH ONE FORCE SPECIFICATION PER LINE.

NODE,DIRECTION,VALUE	POINT FORCE SPECIFICATION.

*** STIFFNESS MATRIX FORMAT ***

THE STIFFNESS MATRIX FOR A SUBSTRUCTURE MUST BE WRITTEN IN BINARY AND MUST BE IN DOUBLE PRECISION WORDS. THE FORMAT OF THIS FILE IS:

NDF	THE NUMBER OF DEGREES OF FREEDOM IN THE SUBSTRUCTURE.
K(1,I),I=1,NDF	FIRST ROW OF THE STIFFNESS MATRIX.
K(2,I),I=2,NDF	SECOND ROW OF THE STIFFNESS MATRIX.
K(3,I),I=3,NDF	THIRD ROW OF THE STIFFNESS MATRIX.
.	
.	
.	
K(NDF,NDF)	LAST ROW OF THE STIFFNESS MATRIX.

NOTE THAT ONLY THE UPPER TRIANGLE OF THE STIFFNESS MATRIX IS STORED.

APPENDIX 1-C Example Input Data for FATLAM (Lug)

```
EXAMPLE : LUG FATLAM (STIFFNESS GEN.) INPUT FILE

1" Thick Composite Lug Analysis. W/D=2.0 Lug Substructure - TITLE
1,1,3,1,0       - NCHECK, NATYPE, NORDER, IMPRNT, IANAL
BACKSUB.DAT     - BACK SUBSTITUTION DATA STORAGE FILE
LAMIDEF.DAT     - LAMINA DEFINITION DATA STORAGE FILE
ELEMDEF.DAT     - ELEMENT DEFINITION DATA STORAGE FILE
STIFDEF.DAT     - STIFFNESS MATRIX DATA STORAGE FILE
POSTPRO.DAT     - POST PROCESSING DATA STORAGE FILE
2               - THE NUMBER OF MATERIALS
AS4/APC-2       - THE FIRST MATERIAL LABEL
2               - THE LAMINA TYPE FLAG : Transversely Isotropic Tape
18.5D6,1.37D6,.35,.46,.75D6,.0052        - ELASTIC CONSTANTS FOR LAMINA
240.D3,185.D3,9.9D3,31.D3,27.1D3,11.1D3  - LAMINA STRENGTHS
APC-2 FILM      - INTERFACE MATERIAL : Resin Rich (APC-2) Interface
1               - THE SECOND MATERIAL FLAG : Isotropic Material
.5D6,.3,.001    - ELASTIC CONSTANTS FOR ISOTROPIC MATERIAL
10.D3,10.D3,10.D3,10.D3,5.D3,5.D3        - ISOTROPIC MATERIAL STRENGTHS
90,2        - THE NUMBER OF PLIES IN THE LUG, THE MATERIAL NUMBER FOR INTERFACE
1,90.       - THE MATERIAL NUMBER, ORIENTATION OF THE PLY
1,90.
1,-45.
1,-45.
1,0.
1,0.
1,45.
1,45.
1,90.
1,90.
1,-45.
1,90.
1,45.
1,90.
1,90.
1,90.
1,90.
1,45.
1,90.
1,-45.
1,90.
1,90.
1,45.
1,45.
1,0.
1,0.
1,-45.
1,-45.
1,90.
1,90.
1,90.
1,90.
1,-45.
1,-45.
1,0.
1,0.
1,45.
1,45.
```

```
1,90.
1,90.
1,-45.
1,90.
1,45.
1,90.
1,90.
1,90.
1,90.
1,45.
1,90.
1,-45.
1,90.
1,90.
1,45.
1,45.
1,0.
1,0.
1,-45.
1,-45.
1,90.
1,90.
1,90.
1,90.
1,-45.
1,-45.
1,0.
1,0.
1,45.
1,45.
1,90.
1,90.
1,-45.
1,90.
1,45.
1,90.
1,90.
1,90.
1,90.
1,45.
1,90.
1,-45.
1,90.
1,90.
1,45.
1,45.
1,0.
1,0.
1,-45.
1,-45.
1,90.
1,90.
 4        - THE NUMBER OF ELEMENTS THROUGH THE SYMMETRIC HALF OF LUG
 1,22     - THE BOTTOM AND TOP PLIES IN THE FIRST ELEMENT
 23,44    - THE BOTTOM AND TOP PLIES IN THE SECOND ELEMENT
 45,67    - THE BOTTOM AND TOP PLIES IN THE THIRD ELEMENT
 68,90    - THE BOTTOM AND TOP PLIES IN THE FOURTH ELEMENT
```

```
62        - THE TOTAL NUMBER OF NODES
   1,  0.0000000D+00,  5.8750000D+00,  9.0000000D+01,  - NODE DESCRIPTION
   2,  2.2646670D-01,  5.8451851D+00,  7.5000000D+01,
   3,  4.3750002D-01,  5.7577722D+00,  6.0000000D+01,
   4,  6.1871845D-01,  5.6187184D+00,  4.5000000D+01,
   5,  7.5777224D-01,  5.4375000D+00,  3.0000000D+01,
   6,  8.4518510D-01,  5.2264667D+00,  1.5000000D+01,
   7,  8.7500000D-01,  5.0000000D+00,  0.0000000D+00,
   8,  4.6794897D-08,  6.0000000D+00,  0.0000000D+00,
   9,  2.5881908D-01,  5.9659258D+00,  0.0000000D+00,
  10,  5.0000003D-01,  5.8660254D+00,  0.0000000D+00,
  11,  7.0710680D-01,  5.7071068D+00,  0.0000000D+00,
  12,  8.6602541D-01,  5.5000000D+00,  0.0000000D+00,
  13,  9.6592583D-01,  5.2588190D+00,  0.0000000D+00,
  14,  1.0000000D+00,  5.0000000D+00,  0.0000000D+00,
  15,  5.8493621D-08,  6.2500000D+00,  0.0000000D+00,
  16,  3.2352385D-01,  6.2074073D+00,  0.0000000D+00,
  17,  6.2500003D-01,  6.0825317D+00,  0.0000000D+00,
  18,  8.8388350D-01,  5.8838835D+00,  0.0000000D+00,
  19,  1.0825318D+00,  5.6250000D+00,  0.0000000D+00,
  20,  1.2074073D+00,  5.3235238D+00,  0.0000000D+00,
  21,  1.2500000D+00,  5.0000000D+00,  0.0000000D+00,
  22,  7.0192345D-08,  6.5000000D+00,  0.0000000D+00,
  23,  3.8822862D-01,  6.4488887D+00,  0.0000000D+00,
  24,  7.5000004D-01,  6.2990381D+00,  0.0000000D+00,
  25,  1.0606602D+00,  6.0606601D+00,  0.0000000D+00,
  26,  1.2990381D+00,  5.7500000D+00,  0.0000000D+00,
  27,  1.4488887D+00,  5.3882286D+00,  0.0000000D+00,
  28,  1.5000000D+00,  5.0000000D+00,  0.0000000D+00,
  29,  8.1891069D-08,  6.7500000D+00,  0.0000000D+00,
  30,  4.5293339D-01,  6.6903702D+00,  0.0000000D+00,
  31,  8.7500005D-01,  6.5155444D+00,  0.0000000D+00,
  32,  1.2374369D+00,  6.2374368D+00,  0.0000000D+00,
  33,  1.5155445D+00,  5.8750000D+00,  0.0000000D+00,
  34,  1.6903702D+00,  5.4529333D+00,  0.0000000D+00,
  35,  1.7500000D+00,  5.0000000D+00,  0.0000000D+00,
  36,  4.0945535D-08,  4.1250000D+00, -9.0000000D+01,
  37,  4.3750002D-01,  4.2422278D+00, -6.0000000D+01,
  38,  7.5777224D-01,  4.5625000D+00, -3.0000000D+01,
  39,  4.6794897D-08,  4.0000000D+00,  0.0000000D+00,
  40,  5.0000003D-01,  4.1339746D+00,  0.0000000D+00,
  41,  8.6602541D-01,  4.5000000D+00,  0.0000000D+00,
  42,  1.2500000D+00,  4.5000000D+00,  0.0000000D+00,
  43,  1.5000000D+00,  4.5000000D+00,  0.0000000D+00,
  44,  1.7500000D+00,  4.5000000D+00,  0.0000000D+00,
  45,  0.0000000D+00,  3.5000000D+00,  0.0000000D+00,
  46,  5.0000000D-01,  3.5000000D+00,  0.0000000D+00,
  47,  8.6600000D-01,  3.5000000D+00,  0.0000000D+00,
  48,  1.2500000D+00,  3.5000000D+00,  0.0000000D+00,
  49,  1.5000000D+00,  3.5000000D+00,  0.0000000D+00,
  50,  1.7500000D+00,  3.5000000D+00,  0.0000000D+00,
  51,  0.0000000D+00,  2.0000000D+00,  0.0000000D+00,
  52,  5.0000000D-01,  2.0000000D+00,  0.0000000D+00,
  53,  8.6600000D-01,  2.0000000D+00,  0.0000000D+00,
  54,  1.2500000D+00,  2.0000000D+00,  0.0000000D+00,
  55,  1.5000000D+00,  2.0000000D+00,  0.0000000D+00,
  56,  1.7500000D+00,  2.0000000D+00,  0.0000000D+00,
```

```
57,  0.0000000D+00,  0.0000000D+00,  0.0000000D+00,
58,  5.0000000D-01,  0.0000000D+00,  0.0000000D+00,
59,  8.6600000D-01,  0.0000000D+00,  0.0000000D+00,
60,  1.2500000D+00,  0.0000000D+00,  0.0000000D+00,
61,  1.5000000D+00,  0.0000000D+00,  0.0000000D+00,
62,  1.7500000D+00,  0.0000000D+00,  0.0000000D+00,
45      - THE TOTAL NUMBER OF ELEMENTS
    1,     2,     9,     8,  - THE NODE COLUMNS DEFINING THIS ELEMENT
    8,     9,    16,    15,
   15,    16,    23,    22,
   22,    23,    30,    29,
    2,     3,    10,     9,
    9,    10,    17,    16,
   16,    17,    24,    23,
   23,    24,    31,    30,
    3,     4,    11,    10,
   10,    11,    18,    17,
   17,    18,    25,    24,
   24,    25,    32,    31,
    4,     5,    12,    11,
   11,    12,    19,    18,
   18,    19,    26,    25,
   25,    26,    33,    32,
    5,     6,    13,    12,
   12,    13,    20,    19,
   19,    20,    27,    26,
   26,    27,    34,    33,
    6,     7,    14,    13,
   13,    14,    21,    20,
   20,    21,    28,    27,
   27,    28,    35,    34,
   36,    39,    40,    37,
   37,    40,    41,    38,
   38,    41,    14,     7,
   41,    42,    21,    14,
   42,    43,    28,    21,
   43,    44,    35,    28,
   45,    46,    40,    39,
   46,    47,    41,    40,
   47,    48,    42,    41,
   48,    49,    43,    42,
   49,    50,    44,    43,
   51,    52,    46,    45,
   52,    53,    47,    46,
   53,    54,    48,    47,
   54,    55,    49,    48,
   55,    56,    50,    49,
   57,    58,    52,    51,
   58,    59,    53,    52,
   59,    60,    54,    53,
   60,    61,    55,    54,
   61,    62,    56,    55,
17      - THE NUMBER OF DISPLACEMENTS SET TO ZERO
0,T,,S12 - THE CONSTRAINED COLUMN,THROUGH-THE-THICKNESS POSITION,CONSTRAINED
1,A,,S31                                                          DIRECTION
8,A,,S23
15,A,,S23
```

```
22,A,,S23       ** Through-The-Thickness Position Label Definition **
29,A,,S23
36,A,,S31              'T' : Top Surface Only
39,A,,S23              'A' : All Positions Through-The-Thickness
45,A,,S23
51,A,,S23       ** Optional Direction Level Definition **
57,A,,S23
57,A,,S31              'S12' : Symmetry about 1-2 plane
58,A,,S31              'S31' : Symmetry about 3-1 plane
59,A,,S31              'S23' : Symmetry about 2-3 plane
60,A,,S31
61,A,,S31
62,A,,S31
10          - THE TOTAL NUMBER OF MASTER DEGREE OF FREEDOMS
1,A,,U10    - THE COLUMN, THROUGH-THE-THICKNESS LABEL, MDF DIRECTION
2,A,,U10
3,A,,U10
4,A,,U10
5,A,,U10
6,A,,U10
7,A,,U10
38,A,,U10
37,A,,U10
36,A,,U10
```

```
EXAMPLE : PIN FATLAM (STIFFNESS GEN.) INPUT FILE

1.75" DIAMETER STEEL PIN MODES WITH .1" GAP
1,1,3,1,0
BKPIN.DAT
LAPIN.DAT
ELPIN.DAT
STPIN.DAT
POPIN.DAT
5                       - THE TOTAL NUMBER OF MATERIALS
.1000" THICK STEEL      - MATERIAL DESCRIPTION
1                       - MATERIAL FLAG : Isotropic Material
30.D6,.3,.1000
1.D6,1.D6,1.D6,1.D6,1.D6,1.D6
.1144" THICK STEEL
1
30.D6,.3,.1144
1.D6,1.D6,1.D6,1.D6,1.D6,1.D6
.1144" THICK STEEL
1
30.D6,.3,.1144
1.D6,1.D6,1.D6,1.D6,1.D6,1.D6
.1196" THICK STEEL
1
30.D6,.3,.1196
1.D6,1.D6,1.D6,1.D6,1.D6,1.D6
.1196" THICK STEEL
1
30.D6,.3,.1196
1.D6,1.D6,1.D6,1.D6,1.D6,1.D6
5,1  - THE NUMBER OF LAYERS IN THE PIN, THE MATERIAL NUMBER FOR INTERFACE
1,0  - THE MATERIAL NUMBER, ORIENTATION OF THE PLY
2,0
3,0
4,0
5,0
5    - THE NUMBER OF ELEMENTS THROUGH THE SYMMETRIC HALF OF PIN
1,1  - THE BOTTOM AND TOP PLIES IN THE FIRST ELEMENT
2,2  - THE BOTTOM AND TOP PLIES IN THE SECOND ELEMENT
3,3  - THE BOTTOM AND TOP PLIES IN THE THIRD ELEMENT
4,4  - THE BOTTOM AND TOP PLIES IN THE FOURTH ELEMENT
5,5  - THE BOTTOM AND TOP PLIES IN THE FIFTH ELEMENT
21   - THE TOTAL NUMBER OF NODES
   1,  0.0000000D+00,  5.0000000D+00,  0.0000000D+00,  - NODE DESCRIPTION -
   2,  2.3397448D-08,  5.5000000D+00,  0.0000000D+00,
   3,  1.2940954D-01,  5.4829629D+00,  0.0000000D+00,
   4,  2.5000001D-01,  5.4330127D+00,  0.0000000D+00,
   5,  3.5355340D-01,  5.3535534D+00,  0.0000000D+00,
   6,  4.3301271D-01,  5.2500000D+00,  0.0000000D+00,
   7,  4.8296291D-01,  5.1294095D+00,  0.0000000D+00,
   8,  5.0000000D-01,  5.0000000D+00,  0.0000000D+00,
   9,  4.3301271D-01,  4.7500000D+00,  0.0000000D+00,
  10,  2.5000001D-01,  4.5669873D+00,  0.0000000D+00,
  11,  2.3397448D-08,  4.5000000D+00,  0.0000000D+00,
  12,  4.0945535D-08,  5.8750000D+00,  9.0000000D+01,
  13,  2.2646670D-01,  5.8451851D+00,  7.5000000D+01,
  14,  4.3750002D-01,  5.7577722D+00,  6.0000000D+01,
```

```
   15,  6.1871845D-01,  5.6187184D+00,  4.5000000D+01,
   16,  7.5777224D-01,  5.4375000D+00,  3.0000000D+01,
   17,  8.4518510D-01,  5.2264667D+00,  1.5000000D+01,
   18,  8.7500000D-01,  5.0000000D+00,  0.0000000D+01,
   19,  7.5777224D-01,  4.5625000D+00, -3.0000000D+01,
   20,  4.3750002D-01,  4.2422278D+00, -6.0000000D+01,
   21,  4.0945535D-08,  4.1250000D+00, -9.0000000D+01,
18   - THE TOTAL NUMBER OF ELEMENTS
      1,     3,     2,     1,  - THE NODE COLUMNS DEFINING THIS ELEMENT
      1,     4,     3,     1,
      1,     5,     4,     1,
      1,     6,     5,     1,
      1,     7,     6,     1,
      1,     8,     7,     1,
      1,     9,     8,     1,
      1,    10,     9,     1,
      1,    11,    10,     1,
      2,     3,    13,    12,
      3,     4,    14,    13,
      4,     5,    15,    14,
      5,     6,    16,    15,
      6,     7,    17,    16,
      7,     8,    18,    17,
      8,     9,    19,    18,
      9,    10,    20,    19,
     10,    11,    21,    20,
6          - THE NUMBER OF DISPLACEMENTS SET TO ZERO
0,T,,S12   - THE CONSTRAINED COLUMN,THROUGH-THE-THICKNESS POSITION,CONSTRAINED
1,A,,S23                                                          DIRECTION
2,A,,S23
11,A,,S23
12,A,,S31
21,A,,S31
51         - THE TOTAL NUMBER OF MASTER DEGREE OF FREEDOMS
12,I,1,U10 - THE COLUMN NUMBER,THROUGH-THE-THICKNESS LABEL,INTERFACE MATERIAL
             NUMBER,MASTER DOF DIRECTION
12,I,2,U10
12,I,3,U10
12,I,4,U10
12,T,,U10
13,I,1,U10
13,I,2,U10
13,I,3,U10
13,I,4,U10
13,T,,U10
14,I,1,U10
14,I,2,U10
14,I,3,U10
14,I,4,U10
14,T,,U10
15,I,1,U10
15,I,2,U10
15,I,3,U10
15,I,4,U10
15,T,,U10
16,I,1,U10
16,I,2,U10
```

```
16,I,3,U10
16,I,4,U10
16,T,,U10
17,I,1,U10
17,I,2,U10
17,I,3,U10
17,I,4,U10
17,T,,U10
18,I,1,U10
18,I,2,U10
18,I,3,U10
18,I,4,U10
18,T,,U10
19,I,1,U10
19,I,2,U10
19,I,3,U10
19,I,4,U10
19,T,,U10
20,I,1,U10
20,I,2,U10
20,I,3,U10
20,I,4,U10
20,T,,U10
21,I,1,U10
21,I,2,U10
21,I,3,U10
21,I,4,U10
21,T,,U10
1,B,,U20
```

APPENDIX 1-E Example Input Data for STAFLAM (Lug/Pin Contact)

```
EXAMPLE : LUG/PIN STAFLM (CONTACT ANALYSIS) INPUT FILE

THICK COMPOSITE LUG STATIC ANALYSIS
1,0,10 - THE NUMBER OF MASTRE DOF'S/NODE,REACTION PRINTOUT,MAX. NO.OF ITERATIONS
DISPLACEMENT.DAT  - THE DISPLACEMENT DATA STORAGE FILE
2                 - THE NUMBER OF SUBSTRUCTURES
STIFDEF.DAT       - LUG STIFFNESS MATRIX STORAGE FILE FROM FATLAM
50                - THE NUMBER OF NODES IN THIS SUBSTRUCTURE
 1, 2, 3, 4, 5, 6, 7, 8, 9,10  - THE NODES DEFINING THIS SUBSTRUCTURE
11,12,13,14,15,16,17,18,19,20
21,22,23,24,25,26,27,28,29,30
31,32,33,34,35,36,37,38,39,40
41,42,43,44,45,46,47,48,49,50
STPIN.DAT         - PIN STIFFNESS MATRIX STORAGE FILE FROM FATLAM
51,               - THE NUMBER OF NODES IN THIS SUBSTRUCTURE
51,52,53,54,55,56,57,58,59,60  - THE NODES DEFINING THIS SUBSTRUCTURE
61,62,63,64,65,66,67,68,69,70
71,72,73,74,75,76,77,78,79,80
81,82,83,84,85,86,87,88,89,90
91,92,93,94,95,96,97,98,99,100
101
0   - NUMBER OF SPECIFIED DISPLACEMENTS
0   - NUMBER OF COUPLED SET
0   - NUMBER OF CONSTRAINT EQUATIONS
50  - THE NUMBER OF GAP/CONTACT ELEMENTS USED IN THIS MODEL
51,U01,1,U01,100.D6,1,0.  - GAP/CONTACT ELEMENT DEFINITION
52,U01,2,U01,100.D6,1,0.
53,U01,3,U01,100.D6,1,0.
54,U01,4,U01,100.D6,1,0.
55,U01,5,U01,100.D6,1,0.
56,U01,6,U01,100.D6,1,0.
57,U01,7,U01,100.D6,1,0.
58,U01,8,U01,100.D6,1,0.
59,U01,9,U01,100.D6,1,0.
60,U01,10,U01,100.D6,1,0.
61,U01,11,U01,100.D6,1,0.
62,U01,12,U01,100.D6,1,0.
63,U01,13,U01,100.D6,1,0.
64,U01,14,U01,100.D6,1,0.
65,U01,15,U01,100.D6,1,0.
66,U01,16,U01,100.D6,1,0.
67,U01,17,U01,100.D6,1,0.
68,U01,18,U01,100.D6,1,0.
69,U01,19,U01,100.D6,1,0.
70,U01,20,U01,100.D6,1,0.
71,U01,21,U01,100.D6,1,0.
72,U01,22,U01,100.D6,1,0.
73,U01,23,U01,100.D6,1,0.
74,U01,24,U01,100.D6,1,0.
75,U01,25,U01,100.D6,1,0.
76,U01,26,U01,100.D6,1,0.
77,U01,27,U01,100.D6,1,0.
78,U01,28,U01,100.D6,1,0.
79,U01,29,U01,100.D6,1,0.
80,U01,30,U01,100.D6,1,0.
81,U01,31,U01,100.D6,1,0.
82,U01,32,U01,100.D6,1,0.
```

```
83,U01,33,U01,100.D6,1,0.
84,U01,34,U01,100.D6,1,0.
85,U01,35,U01,100.D6,1,0.
86,U01,36,U01,100.D6,1,0.
87,U01,37,U01,100.D6,1,0.
88,U01,38,U01,100.D6,1,0.
89,U01,39,U01,100.D6,1,0.
90,U01,40,U01,100.D6,1,0.
91,U01,41,U01,100.D6,1,0.
92,U01,42,U01,100.D6,1,0.
93,U01,43,U01,100.D6,1,0.
94,U01,44,U01,100.D6,1,0.
95,U01,45,U01,100.D6,1,0.
96,U01,46,U01,100.D6,1,0.
97,U01,47,U01,100.D6,1,0.
98,U01,48,U01,100.D6,1,0.
99,U01,49,U01,100.D6,1,0.
100,U01,50,U01,100.D6,1,0.
1                - THE NUMBER OF SPECIFIED FORCES
101,Q01,10000.  - FORCE APPLIED NODE NUMBER, DIRECTION, FORCE MAGNITUDE
```

EXAMPLE : LUG/PIN FATLAM (FAILURE ANALYSIS) INPUT FILE

```
LUG SUBSTRUCTURE BACK SUBSTITUTION AND FAILURE ANALYSIS
1,0,3,1,0          - NCHECK, NATYPE, NORDER, IMPRNT, IANAL
BACKSUB.DAT        - BACK SUBSTITUTION STORAGE FILE
LAMIDEF.DAT        - LAMINA DEFINITION STORAGE FILE
ELEMDEF.DAT        - ELEMENT DEFINITION STORAGE FILE
DISPLACEMENT.DAT   - THE DISPLACEMENT VECTOR STORAGE FILE
POST.DAT           - POST PROCESSING DATA STORAGE FILE
1 - THE INDEX NUMBER OF SUBSTRUCTURE
0,1,1,0,0,0,1,1 - PRINT-OUT FLAGS
```

Appendix 2-A: Room Temperature (RT) Specimen Data

(See Figure 2-A-1 for Location of Dimensions)

Specimen Data for Co-consolidated Elements - RT Dry

Spec ID	Width (in.)	Thick Loc 1 (in.)	Thick Loc 2 (in.)	Thick Loc 3 (in.)	Thick Loc 4 (in.)	Thick Loc 5 (in.)	Unit Ult Load Drop (lb)	Final Ult Load Drop (lb)	Def @ Final Load (in.)
B-RT-1	1.508	0.075	0.111	0.115			610	630	0.24
B-RT-2	1.509	0.075	0.111	0.114				760	0.21
B-RT-3	1.506	0.075	0.111	0.115				730	0.18
Y45-ET-1	1.500	0.031	0.077	0.078	0.039	0.035		1,330	0.43
Y45-ET-2	1.505	0.041	0.073	0.080	0.038	0.038		1,200	
Y45-ET-3	1.515	0.039	0.076	0.075	0.038	0.036		530	0.11
Y60-ET-1	1.503	0.037	0.072	0.070	0.036	0.039		360	0.21
Y60-ET-2	1.503	0.041	0.074	0.070	0.038	0.036		350	0.21
Y60-ET-3	1.506	0.040	0.074	0.070	0.036	0.036		250	0.17

Reconfiguration Blade, Extra 45° - Y, Induction Welded Data - RT Dry

Spec ID	Width (in.)	Thick Loc 1 (in.)	Thick Loc 2 (in.)	Thick Loc 3 (in.)	Thick Loc 4 (in.)	Thick Loc 5 (in.)	Unit Ult Load Drop (lb)	Final Ult Load Drop (lb)	Def @ Final Load (in.)
RB-ET-1	1.512	0.081	0.114	0.116				685	0.22
RB-ET-2	1.518	0.081	0.112	0.116			680	760	0.22
RB-ET-3	1.516	0.081	0.112	0.117				650	0.24
XY45-ET-1	1.504	0.043	0.071	0.064	0.036	0.036	648	855	0.30
X45-ET-2	1.505	0.038	0.073	0.069	0.035	0.035		755	0.19
X45-ET-3	1.504	0.045	0.071	0.068	0.030	0.031		485	0.14
IY60-ET-1	1.507	0.037	0.085	0.092	0.037	0.035	156	202	0.11
IY60-ET-2	1.507	0.039	0.087	0.087	0.039	0.036		228	0.08
IY60-ET-3	1.507	0.037	0.086	0.087	0.038	0.039		120	0.08

GP24-0420-68-D/tpk

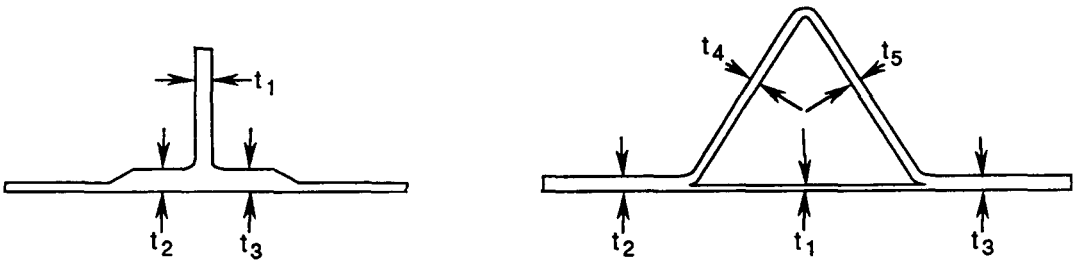

1) w (not shown) is the specimen width at the middle of the specimen (~1.5")
2) All measurements taken at mid-span of specimen (i.e. w/2)
3) t_2 corresponds to the flange marked with the specimen number
4) t_1 taken at center of blade web - or- Y base
5) t_2 & t_3 measured as near to corner radius as possible
6) t_4 & t_5 measured at center of Y sides

GP24-0420-66-D/tpk

Figure 2-A-1. Frame Element Measurement Locations

Appendix 2-B: Elevated Temperature (ET) Specimen Data

(See Figure 2-A-1. for Location of Dimensions)

Specimen Data for Co-consolidated Elements - 250°F Wet

Spec ID	Width (in.)	Thick Loc 1 (in.)	Thick Loc 2 (in.)	Thick Loc 3 (in.)	Thick Loc 4 (in.)	Thick Loc 5 (in.)	Unit Ult Load Drop (lb)	Final Ult Load Drop (lb)	Def @ Final Load (in.)
B-ET-1	1.504	0.075	0.112	0.115			600	700	0.39
B-ET-2	1.506	0.075	0.111	0.115			588	660	0.27
B-ET-3	1.507	0.077	0.112	0.115			612	660	0.31
Y45-ET-1	1.504	0.038	0.078	0.080	0.039	0.039	720	860	0.35
Y45-ET-2	1.510	0.040	0.078	0.078	0.040	0.041		1,200	0.29
Y45-ET-3	1.514	0.035	0.077	0.076	0.040	0.041		1,110	0.31
Y60-ET-1	1.506	0.039	0.070	0.070	0.037	0.034		960	0.24
Y60-ET-2	1.505	0.039	0.069	0.068	0.036	0.035		970	0.20
Y60-ET-3	1.508	0.035	0.070	0.068	0.037	0.035		822	0.19

Reconfiguration Blade, Extra 45° - Y, Induction Welded Data - 250°F Wet

Spec ID	Width (in.)	Thick Loc 1 (in.)	Thick Loc 2 (in.)	Thick Loc 3 (in.)	Thick Loc 4 (in.)	Thick Loc 5 (in.)	Unit Ult Load Drop (lb)	Final Ult Load Drop (lb)	Def @ Final Load (in.)
RB-ET-1	1.512	0.081	0.114	0.116				685	0.22
RB-ET-2	1.518	0.081	0.112	0.116			680	760	0.22
RB-ET-3	1.516	0.081	0.112	0.117				650	0.24
XY45-ET-1	1.504	0.043	0.071	0.064	0.036	0.036	648	855	0.30
X45-ET-2	1.505	0.038	0.073	0.069	0.035	0.035		755	0.19
X45-ET-3	1.504	0.045	0.071	0.068	0.030	0.031		485	0.14
IY60-ET-1	1.507	0.037	0.085	0.092	0.037	0.035	156	202	0.11
IY60-ET-2	1.507	0.039	0.087	0.087	0.039	0.036		228	0.08
IY60-ET-3	1.507	0.037	0.086	0.087	0.038	0.039		120	0.08

GP24-0420-67-D/tpk

APPENDIX 2-C Load/Deflection Data from RT Blade Testing

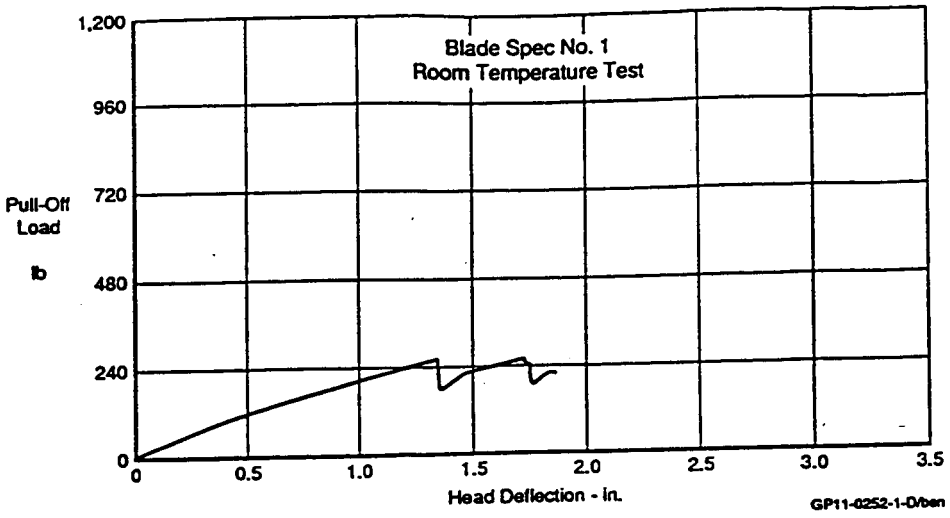

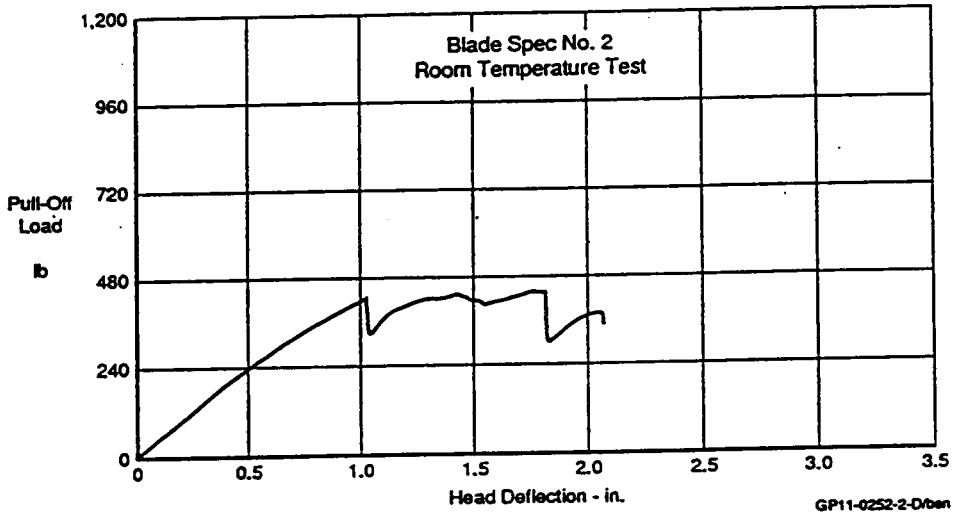

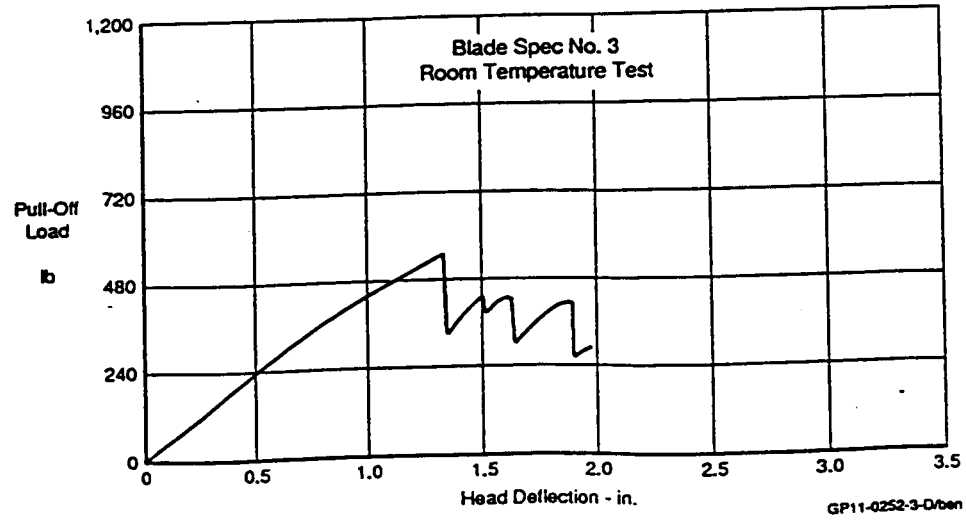

APPENDIX 2-D Load/Deflection Data from RT 60°-Y Testing

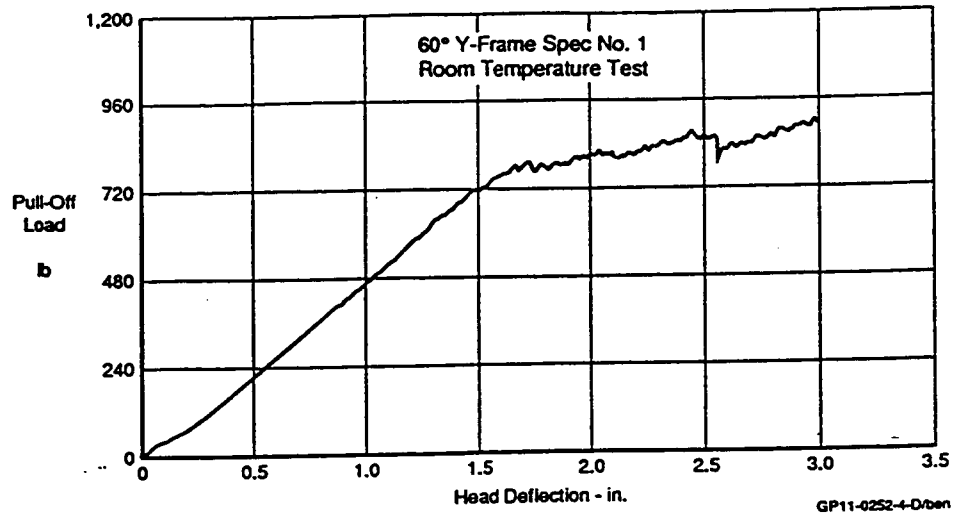

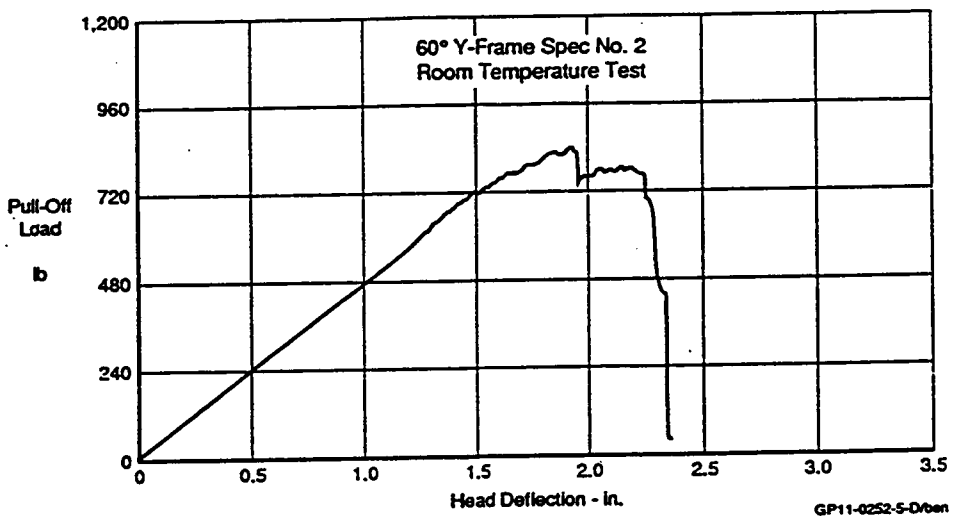

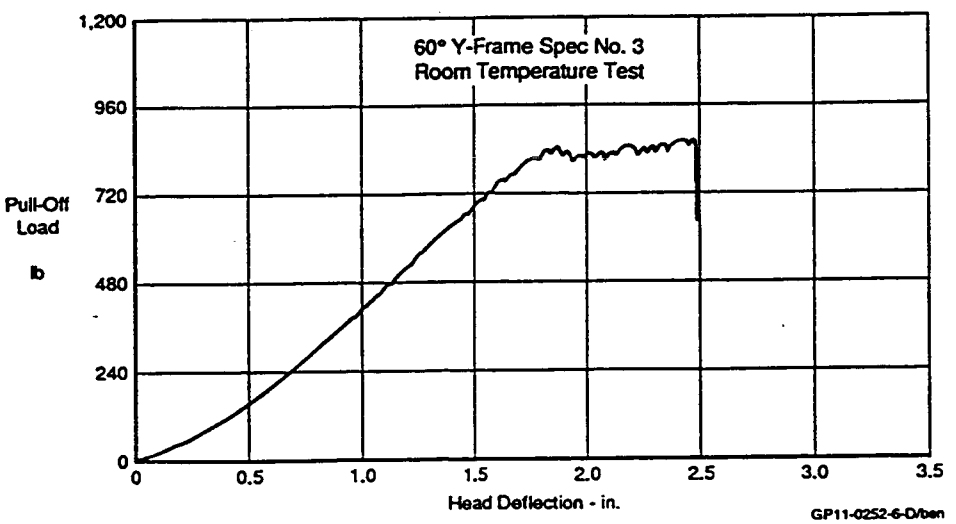

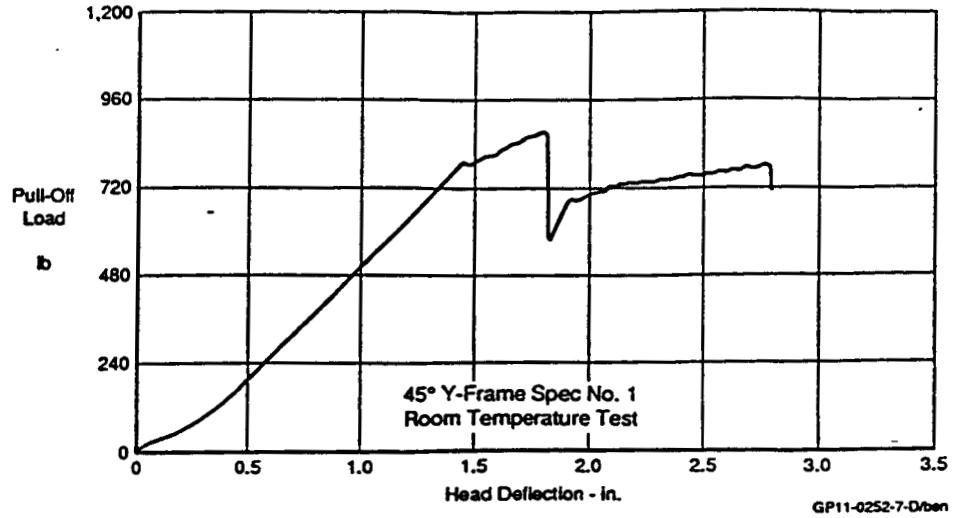
1,200
960
720
480
240
0
Pull-Off Load lb
45° Y-Frame Spec No. 1
Room Temperature Test
0
0.5
1.0
1.5
2.0
2.5
3.0
3.5
Head Deflection - in.
GP11-0252-7-D/ben

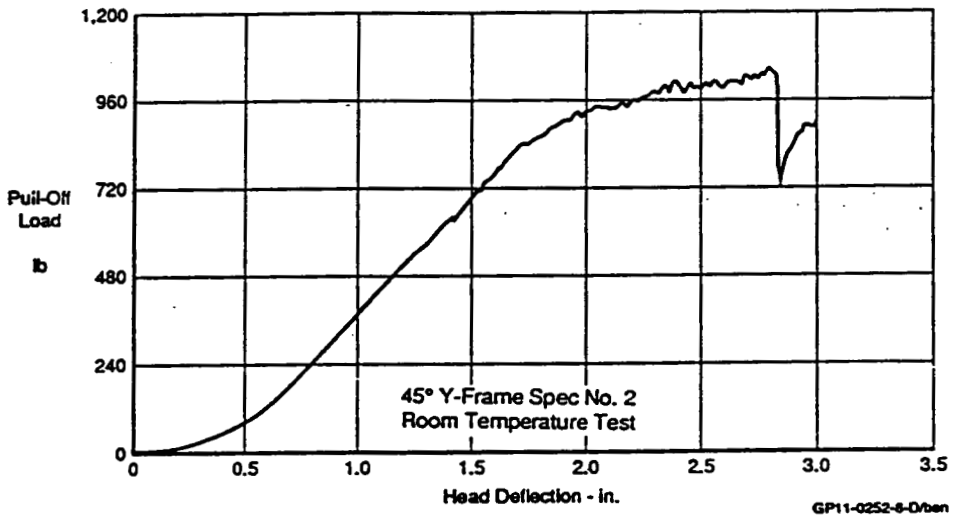
1,200
960
720
480
240
0
Pull-Off Load lb
45° Y-Frame Spec No. 2
Room Temperature Test
0
0.5
1.0
1.5
2.0
2.5
3.0
3.5
Head Deflection - in.
GP11-0252-8-D/ben

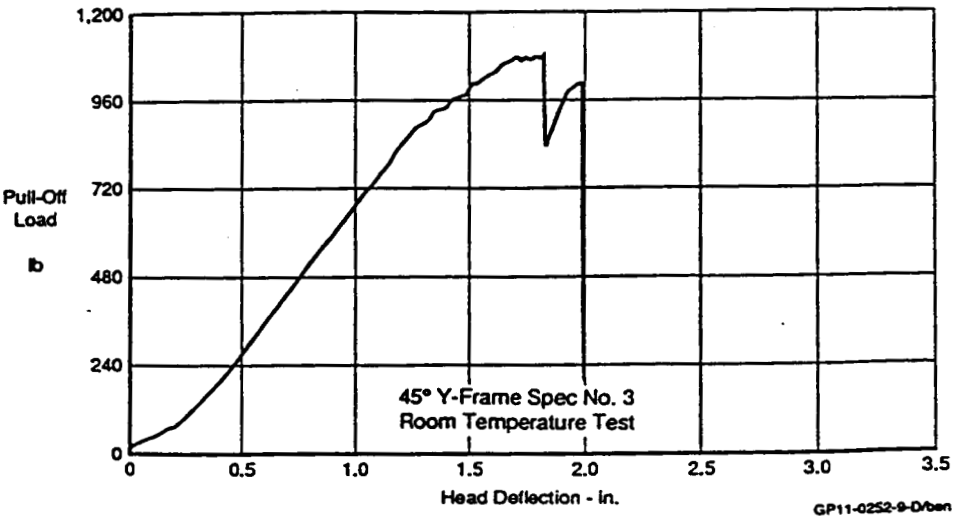
1,200
960
720
480
240
0
Pull-Off Load lb
45° Y-Frame Spec No. 3
Room Temperature Test
0
0.5
1.0
1.5
2.0
2.5
3.0
3.5
Head Deflection - in.
GP11-0252-9-D/ben

APPENDIX 2-F Load/Deflection Data from ET Blade Testing

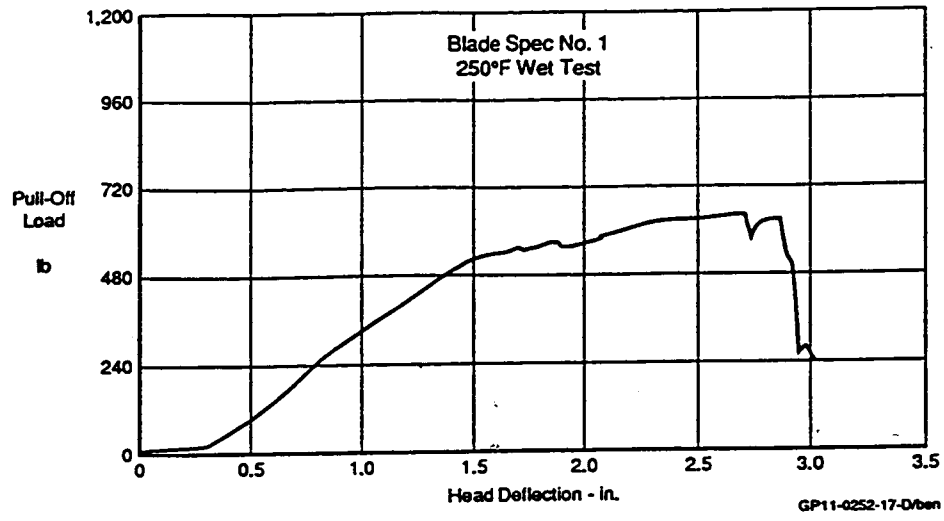

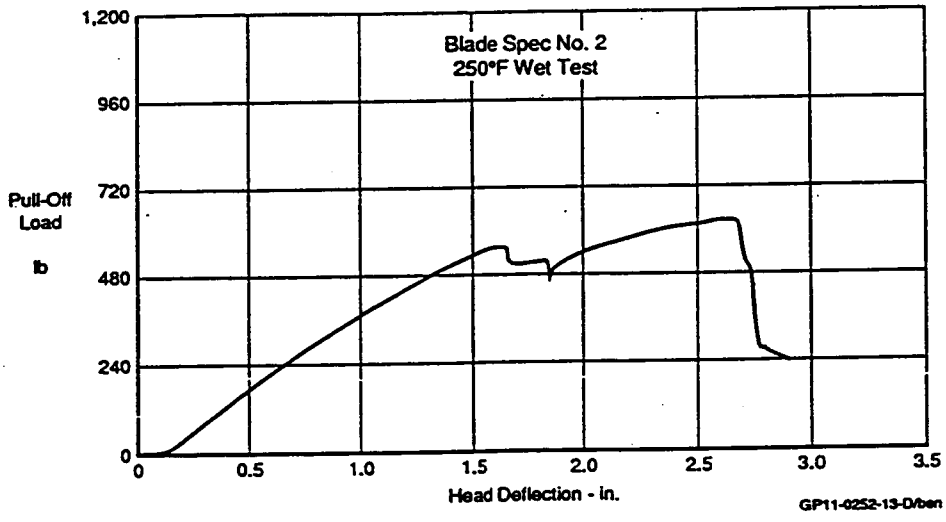

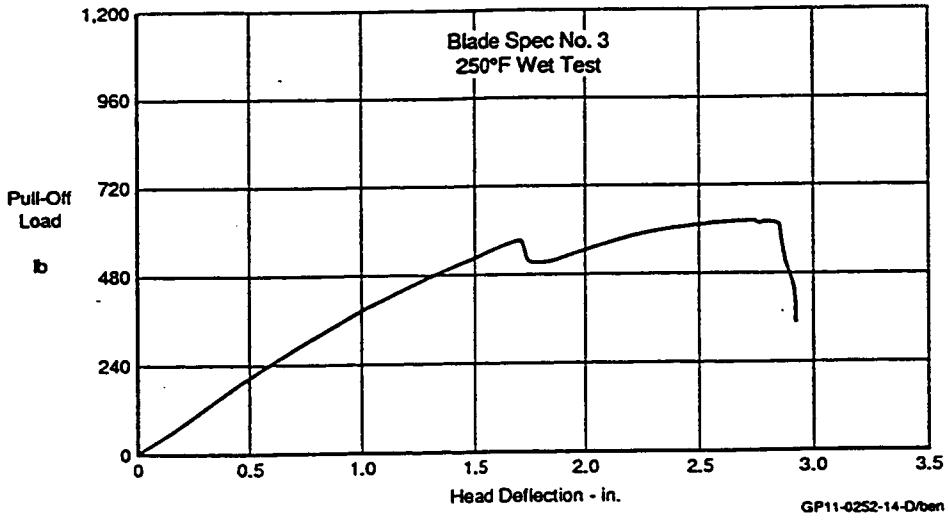

APPENDIX 2-G Load/Deflection Data from ET 60°-Y Testing

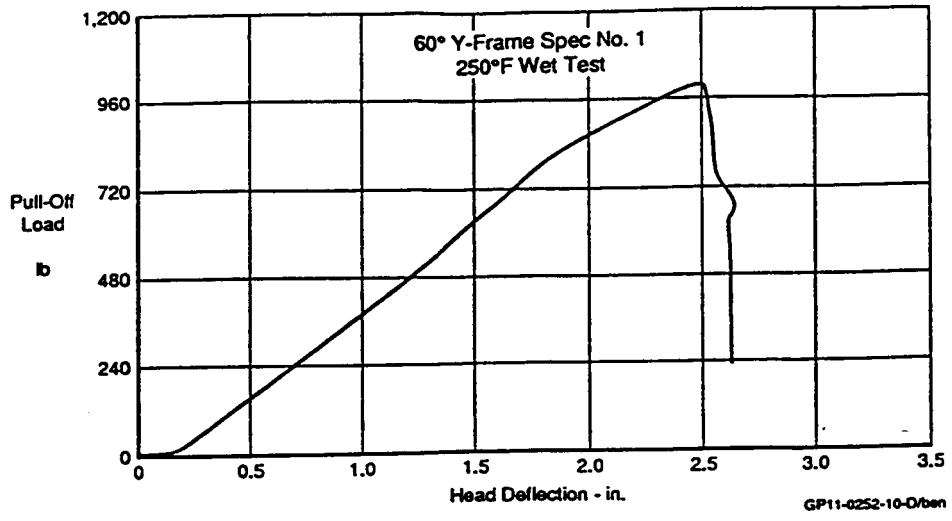

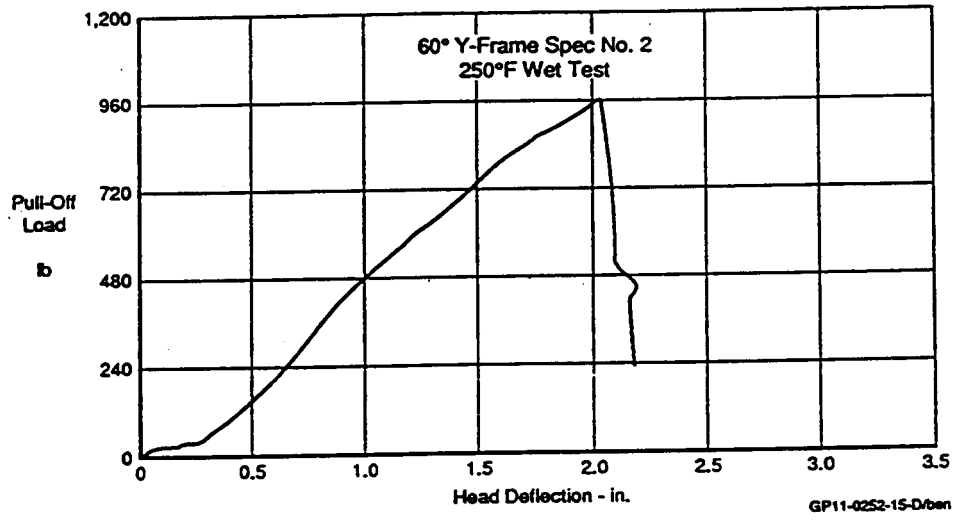

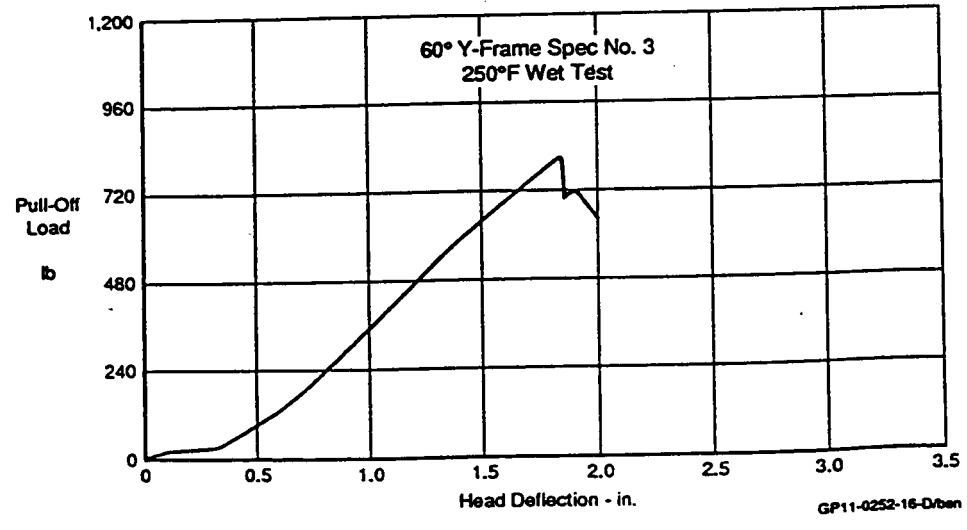

APPENDIX 2-H Load/Deflection Data from ET 45°-Y Testing

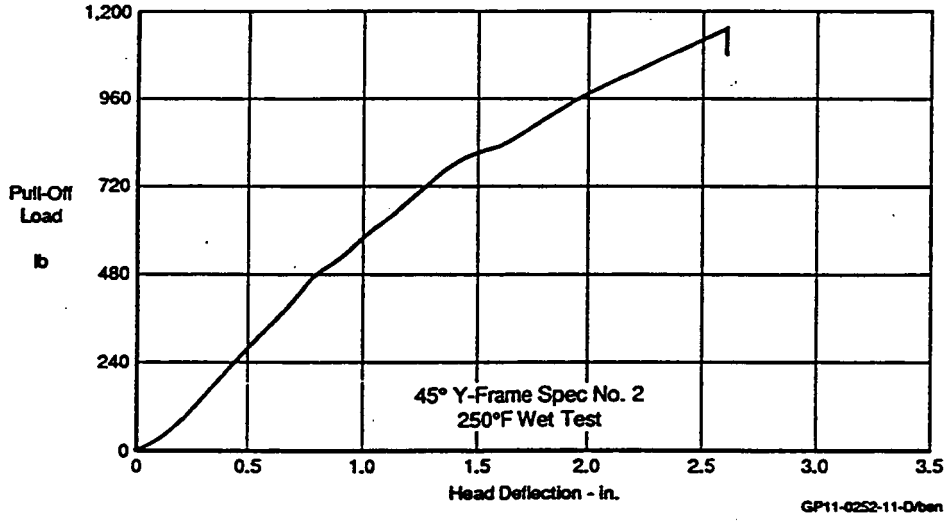

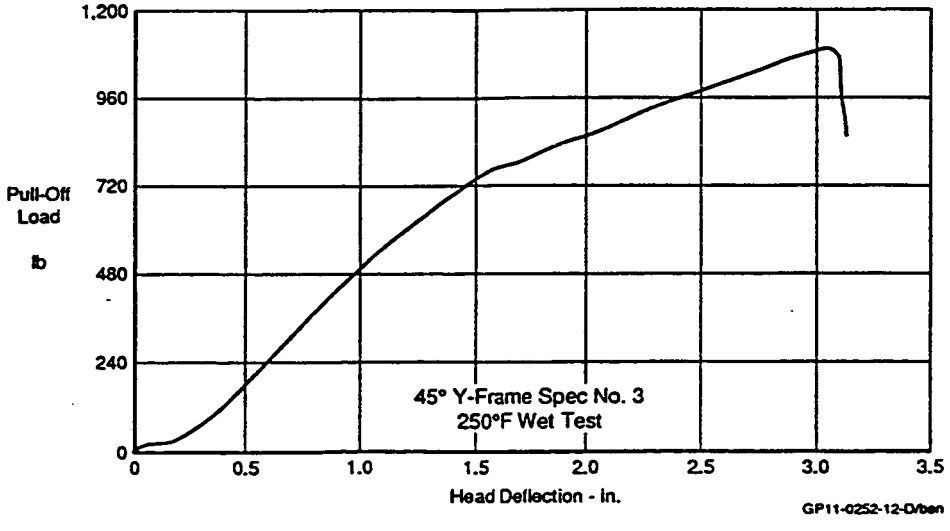

REPORT DOCUMENTATION PAGE

Form Approved
OMB No. 0704-0188

1. AGENCY USE ONLY *(Leave blank)*	2. REPORT DATE	3. REPORT TYPE AND DATES COVERED
	March 1992	Contractor Report April 1989 - April 1991

4. TITLE AND SUBTITLE
Development of Thermoplastic Composite Aircraft Structures

5. FUNDING NUMBERS

6. AUTHOR(S)
M. P. Renieri, S. J. Burpo. L. M. Roundy, S. M. Todd and H. J. Kim

7. PERFORMING ORGANIZATION NAME(S) AND ADDRESS(ES)
McDonnell Aircraft Company
P.O. Box 516
St. Louis, MO 63166-0516

8. PERFORMING ORGANIZATION REPORT NUMBER
NASA CR-189593

9. SPONSORING / MONITORING AGENCY NAME(S) AND ADDRESS(ES)
National Aeronautics ans Space Administration
Langley Research Center
Hampton, VA 23665-5225

10. SPONSORING / MONITORING AGENCY REPORT NUMBER

11. SUPPLEMENTARY NOTES
Langley Technical Monitor: Marvin B. Dow
Final Report

12a. DISTRIBUTION / AVAILABILITY STATEMENT
[redacted]
Subject Category 24

12b. DISTRIBUTION CODE

13. ABSTRACT *(Maximum 200 words)*

Efforts focused on the use of thermoplastic composite materials in the development of structural details associated with an advanced fighter fuselage section with applicability to transport design. In support of these designs, mechanics developments were conducted in two areas. First, a dissipative strain energy approach to material characterization and failure prediction, development at the Naval Research Laboratory, was evaluated as a design/analysis tool. Second, a finite element formulation for thick composites has been developed and incorporated into a lug analysis method which incorporates pin bending effects.

Manufacturing concepts were developed for an upper fuel cell cover. A detailed trade study produced two promising concepts: fiber placement and single-step diaphragm forming. Based on the innovative design/manufacturing concepts for the fuselage section primary structure, elements were designed, fabricated and structurally tested. These elements focused on key issues such as thick composite lugs and low cost forming of fastenerless, stiffener/moldine concepts, Manufacturing techniques included autoclave consolidation, single diaphragm consolidation (SDCC) and roll-forming.

14. SUBJECT TERMS	15. NUMBER OF PAGES 129
	16. PRICE CODE

17. SECURITY CLASSIFICATION OF REPORT	18. SECURITY CLASSIFICATION OF THIS PAGE	19. SECURITY CLASSIFICATION OF ABSTRACT	20. [redacted]
Unclassified	Unclassified		